

**Modellering van complexe EMC-testopstellingen voor de transiëntanalyse
van geïntegreerde schakelingen in de automobiellndustrie**

**Modeling of Complex EMC Test Setups for the Assessment of the Transient Behavior
of Automotive Integrated Circuits**

Niels Lambrecht

Promotoren: prof. dr. ir. D. Vande Ginste, em. prof. dr. ir. D. De Zutter
Proefschrift ingediend tot het behalen van de graad van
Doctor in de ingenieurswetenschappen: elektrotechniek



**UNIVERSITEIT
GENT**

Vakgroep Informatietechnologie
Voorzitter: prof. dr. ir. B. Dhoedt
Faculteit Ingenieurswetenschappen en Architectuur
Academiejaar 2017 - 2018

ISBN 978-94-6355-110-6
NUR 959
Wettelijk depot: D/2018/10.500/28

Modeling of Complex EMC Test Setups for the Assessment of the Transient Behavior of Automotive Integrated Circuits

Niels Lambrecht

Dissertation submitted to obtain the academic degree of
Doctor of Electrical Engineering

Publicly defended at Ghent University on April 30th, 2018

Supervisor:

prof. dr. ir. D. Vande Ginste
Electromagnetics group
Department of Information Technology
Faculty of Engineering and Architecture
Ghent University
Technologiepark-Zwijnaarde 15
B-9052 Ghent, Belgium
<http://emweb.intec.ugent.be>

Supervisor:

em. prof. dr. ir. D. De Zutter
Electromagnetics group
Department of Information Technology
Faculty of Engineering and Architecture
Ghent University
Technologiepark-Zwijnaarde 15
B-9052 Ghent, Belgium
<http://emweb.intec.ugent.be>

Members of the examining board:

em. prof. dr. ir. R. Verhoeven (chairman)
prof. dr. ing. P. Van Torre (secretary)
prof. dr. ir. D. Vande Ginste (supervisor)
em. prof. dr. ir. D. De Zutter (supervisor)
prof. dr. ing. J. Knockaert
prof. dr. ir. N. Stevens
dr. ir. H. Pues
prof. dr. ir. P. Manfredi

Ghent University, Belgium
Ghent University, Belgium
Ghent University, Belgium
Ghent University, Belgium
Ghent University, Belgium
KU Leuven, Belgium
Melexis Technologies N.V., Tessenderlo, Belgium
Politecnico di Torino, Italy

Dankwoord

Deze dissertatie is het resultaat van onderzoek geleverd binnen de onderzoeksgroep Elektromagnetisme aan de universiteit Gent gedurende de periode 2014-2018. Doctoreren is geen vier jaar extra school lopen, zoals velen soms denken. Een doctoraat is het uitvoeren van wetenschappelijk onderzoek binnen een universiteit of in een wetenschappelijke instelling. De resultaten uit dit wetenschappelijk onderzoek werden dan ook gepubliceerd in internationale wetenschappelijke tijdschriften en/of voorgesteld op internationale conferenties.

Om een doctoraat te kunnen beginnen heb je promotoren nodig. Ik prijs mezelf gelukkig dat ik kon promoveren onder de supervisie van Prof.dr.ir. Dries Vande Ginste en em.Prof.dr.ir. Daniël De Zutter. Beiden zijn autoriteiten binnen het domein van Elektromagnetisme. Ik ben hen oprecht dankbaar dat ze me de kans en het vertrouwen gegeven hebben om dit doctoraat te mogen aanvangen. Het onderzoek in dit doctoraat is gebeurd in nauwe samenwerking met Melexis N.V. Ik wil dan ook dr. ir. Hugo Pues bedanken voor de drie jaar lange samenwerking en voor de talloze keren me te komen oppikken aan het pittoreske station van Aarschot.

In vele doctraten is het maatschappelijk en/of wetenschappelijk nut niet helemaal duidelijk voor de buitenwereld. Ik kan echter zeggen dat alles in deze dissertatie van onmiddellijke toepassing was binnen de automobiellindustrie. Het is vrij uitzonderlijk dat het onderzoek van een doctorandus een directe impact heeft op de industrie. Toch is het in dit doctoraat verwezenlijkt. Dit is een gegeven waar ik bijzonder trots op ben.

Gedurende deze vier jaar was het een komen en gaan van doctorandi binnen de onderzoeksgroep Elektromagnetisme. Van al deze mensen wil ik er twee in het bijzonder vermelden. Als collega-radioamateur dank ik Gert-Jan Stockman voor de talrijke radio-experimenten en voor het geduld om me TikZ aan te leren. Verder wil ik Olivier Caytan bedanken. Enerzijds voor de amusante tijd die we hadden als laatstejaarsstudenten burgerlijk ingenieur, anderzijds voor de politieke gesprekken en onze gemeenschappelijke visie. Het was me een waar genoegen. Hiernaast wil ik Joris Van Kerrebrouck vermelden voor de gemeenschappelijke avonturen die we samen beleefd hebben tijdens onze studie. We konden altijd sparren over onze ideeën, bevindingen, maar gelukkig ook over iets anders praten dan alleen de dagelijkse cursussen.

Het belangrijkste wordt bewaard tot het einde. In dit opzicht bedank ik mijn ouders. Mijn moeder dank ik zeer voor de zorgzame taken die ze doorheen mijn hele

leven (en nog steeds) heeft vervult. Mijn vader dank ik uitdrukkelijk, voor zijn onvoorwaardelijke ondersteuning die hij mij gegeven heeft gedurende mijn studies en loopbaan. Verder wil ik mijn twee zussen, Isabel en Ellen, geluk en voorspoed te wensen, zowel op professioneel als op privévlak. Tot slot wens ik mijn neefje Andreas een gelukzalige jeugd en succes in zijn leven toe.

Appels, april 2018
Niels Lambrecht

Technisch sterk, zeker werk!

VT.I. AALST

Inhoudsopgave

Samenvatting	vii
Summary	xi
List of Abbreviations	xv
List of Symbols	xvii
List of Publications	xix
1 Introduction	3
1.1 Context	3
1.2 Motivation	4
1.3 State-of-the-art	6
1.4 Novel Contributions and Overview of the Dissertation	6
2 Efficient Circuit Modeling Technique for the Analysis and Optimization of ISO 10605 Field Coupled Electrostatic Discharge (ESD) Robustness of Nonlinear Devices	11
2.1 Introduction	12
2.2 ISO 10605 Field Coupled ESD Test Circuit Modeling	13
2.3 Measurements and Results	23
2.4 Conclusion	30
3 Modeling Transient Electrical Disturbances by Inductive Coupling for the ISO 7637-3 ICC Test	35
3.1 Introduction	35
3.2 Description of the Inductive Coupling Clamp Test	36
3.3 Modeling of the Inductive Coupling Clamp Test	37
3.4 Validation of the Model Using a Nonlinear DUT	44
3.5 Conclusion	46
4 A Circuit Modeling Technique for the ISO 7637-3 Capacitive Coupling Clamp test	49
4.1 Introduction	49
4.2 Description of the ISO 7637-3 Capacitive Coupling Clamp Test . .	50
4.3 Modeling of the ISO 7637-3 Capacitive Coupling Clamp Test . . .	52
4.4 Modeling of the Test Bench	62
4.5 Validation of the Proposed Model	64
4.6 Conclusion	66

5	Modeling of Contact Bounce in a Transient Electromagnetic Compatibility Test for the Analysis and Optimization of Nonlinear Devices	69
5.1	Introduction	70
5.2	Methodology	70
5.3	Measurements and Results	75
5.4	Conclusion	80
6	Conclusions and Future Work	85
6.1	General Conclusions	85
6.2	Future Work	86
A	Solution of the Multiconductor Transmission Line Equations	91
B	Analysis of the p.u.l. Parameters of the CCC Fixture	97
C	Description of the EFT Pulse According to ISO 7637-3	101

Samenvatting

In de 21^{ste} eeuw wordt de mens omringd door enorm veel elektronische en elektrische apparaten. Niet alleen worden we erdoor omringd, we zijn ook erg afhankelijk geworden van al deze apparaten. Vanuit het perspectief van een elektrotechnisch ingenieur is het verbazingwekkend dat al deze elektronische en elektrische apparaten naast elkaar kunnen functioneren zonder dat ze elkaar voortdurend storen. Toch ervaren we occasioneel dat elektronische en elektrische apparaten met elkaar interfereren. Een voorbeeld is de interferentie tussen een mobiele telefoon en een FM-radio, waar de storing wordt opgevangen door de audiokabel en zich manifesteert als een serie van hoorbare pulsen. Dit soort storing kan vervelend zijn, maar is niet levensbedreigend.

De auto van vandaag zit barstensvol elektronica. Deze elektronica staat in voor het regelen van de vitale functies van je auto. Wanneer in een elektronische module (die bijvoorbeeld je motor controleert) een probleem zou optreden door interferentie, dan kan dit echter wel dramatische gevolgen hebben. Om dit te voorkomen worden alle elektronische en elektrische apparaten uitgebreid getest op hun immuniteit. Met immuniteit bedoelt men het vermogen om correct te blijven functioneren wanneer het apparaat onderworpen wordt aan storingen. Het testen en analyseren van apparaten die onderhevig zijn aan storing behoort tot het domein van “elektromagnetische compatibiliteit”. De testen die men uitvoert om de mogelijke storingen van een apparaat na te bootsen, noemt men “compliancetesten”. Deze staan op hun beurt dan weer beschreven in internationale standaarden waar de fabrikant van elektronische en elektrische apparaten aan moet voldoen, wil men dat hun toestel op de markt te koop wordt aangeboden.

Wanneer elektromagnetische compatibiliteitsproblemen pas ontdekt worden in de compliancefase van het ontwerpproces kunnen de kosten voor het oplossen van deze problemen hoog oplopen. Men wordt dan namelijk opnieuw geconfronteerd met ontwerpkosten, testkosten, fabricagekosten en debugtijd. Dit vertraagt de marktintroductietijd van het product wezenlijk en kan zelfs fataal zijn voor bepaalde ondernemingen. Zodoende is het uiterst belangrijk om de uitkomst van een compliancetest te voorspellen.

In dit doctoraatschrift ligt de focus op het softwarematig simuleren van compliancetesten die gebruikt worden in de automobielin industrie. In de automobielin industrie worden twee types compliancetesten beschouwd. Enerzijds zijn er de radiofrequentie (RF) testen. Dit zijn de testen waarbij men sinusoidale stoorsignalen gebruikt. Men kijkt dan bij welke frequenties en/of vermogen van het stoorsignaal het toestel de vooropgelegde specificaties niet langer behaalt. Deze RF testen werden in het verleden reeds uitgebreid behandeld en onderzocht. Anderzijds vormen de veldgekoppelde transiënttesten de grote uitdaging van vandaag. Het analyseren van deze veldgekoppelde transiënttesten is niet mogelijk met de methoden die

gebruikt werden bij de RF testen. Dit wordt niet enkel veroorzaakt door de aard van de complexe koppelingsmechanismes, maar ook door het grote aantal golfvormen (gaande van trage, omschakelrelais-gebaseerde stoorsignalen tot extreem snelle, elektrostatische ontladingspulsen (electrostatic discharge (ESD))). In dit doctoraat worden er circuitmodellen ontworpen voor de volgende belangrijke veldgekoppelde transiënttesten:

- ultrafast plate-to-wire coupled electrostatic discharge (ESD-Rinne)
- slow magnetic-field coupled immunity (ICC)
- fast electric-field coupled immunity (CCC)
- wideband wire-to-wire coupled immunity (RI-130)

De circuitmodellen kunnen worden gebruikt door een circuitontwerper in zijn/haar traditionele software-gebaseerde ontwerpsomgeving. Dit laat toe het ontwerp te testen qua immuniteit in een *precompliance* fase.

Aangezien de testbanken van de veldgekoppelde transiënttesten bestaan uit zeer lange bundels draden wordt er in dit doctoraat uitvoerig gebruik gemaakt van de transmissielijntheorie. Deze lange bundels draden stellen in deze testen de “kabelboom” (Eng.: wire harness) van het voertuig voor. De kabelboom verbindt de voedingsbron en stuurelektronica van de auto met het te testen apparaat.

Hoofdstuk 1 reikt een algemene inleiding aan inzake de context en doelstellingen van dit werk. In Hoofdstuk 2 bespreken we de ESD-Rinne test. Dit is één van de belangrijkste testen in de automobieliindustrie omdat een ongewenste elektrostatische ontlading in een auto kan leiden tot ernstige schade zowel aan de auto als aan de passagiers in de auto. In dit hoofdstuk wordt een equivalent circuitmodel ontwikkeld dat de ontwerper van elektronische schakelingen reeds vroeg in de ontwerpfase toelaat alle pijnpunten van het elektronisch ontwerp bloot te leggen. Er wordt in dit hoofdstuk speciaal aandacht besteed aan het ESD pistool, die het stoorsignaal genereert. Vervolgens wordt bij het modelleren van de elektrisch grote testbank gebruik gemaakt van de transmissielijntheorie. Het voorgestelde model wordt ten slotte uitgebreid gevalideerd met behulp van metingen. Hoofdstuk 3 behandelt de ICC test. In de ICC test wordt met behulp van een inductieve koppelingsprobe een traag variërend stoorsignaal in een kabelboom gekoppeld. Hoofdstuk 3 geeft een gedetailleerde beschrijving van het koppelingsmechanisme tussen de inductieve probe en de kabelboom. Door de geïnduceerde stoorsignalen op de kabelboom voor te stellen als gedistribueerde spanningsbronnen kunnen we dit model samenvoegen met het transmissielijnmodel dat de elektrisch grote structuur van de testbank in rekening brengt. Dit resulteert in een equivalent circuitmodel dat uitgebreid werd getest door middel van metingen. In Hoofdstuk 4 wordt de CCC test besproken waar men door middel van een capacitieve koppelingsprobe het stoorsignaal in een deel van de kabelboom injecteert. In dit hoofdstuk stellen we een model voor dat zowel gebruik maakt van de klassieke transmissielijntheorie

als van twee concepten die gebruikt worden in het domein van de elektromagnetische afscherming, i.e. *surface transfer impedance* en *surface transfer admittance*. Dit resulteert in een efficiënt en nauwkeurig circuitmodel, wat bevestigd is door metingen. In Hoofdstuk 5 komt de RI-130 test aan bod. Hierbij is in de stoorbron een mechanische relais aanwezig. Dit maakt de test onderhevig aan het “dender-effect”, wat kan beschouwd worden als een stochastisch proces. Dit fenomeen bepaalt in grote mate de amplitude van het stoorsignaal. In dit hoofdstuk wordt een uitgebreide studie van het dendereffect gemaakt waaruit een model is afgeleid dat het slechtst mogelijke scenario voorspelt.

In Hoofdstukken 2-5 werden alle modellen gevalideerd door middel van metingen met een niet-lineair circuit als te testen apparaat, dit om het nut van het gedane wetenschappelijk werk in het bijzonder in de context van de automobielindustrie, te illustreren. Het onderzoek en in het bijzonder de metingen, gebeurden in nauwe samenwerking met Melexis Technologies N.V., Tessenderlo, België, wat de actualiteitswaarde en belang van het onderzoek garandeert.

In het laatste hoofdstuk van dit werk worden de algemene conclusies opgesomd. Daarenboven worden kort enkele suggesties voor verder onderzoek aangereikt, zoals het onderzoeken van de reproduceerbaarheid van de veldgekoppelde transiënttesten. Samenvattend kan gesteld worden dat dit werk een duidelijke beschrijving geeft van koppelingsmechanismen in de belangrijke veldgekoppelde transiënttesten. Daarenboven is er in dit werk ook voor elk van deze veldgekoppelde transiënttesten een zeer efficiënt en nauwkeurig equivalent circuitmodel ontworpen, wat van groot belang is voor de ontwerpsingenieur tijdens het preventief testen van de vooropgelegde specificaties van zijn/haar ontwerp.

Summary

In the 21st century we are surrounded by electronic and electrical systems. Moreover, we are also greatly dependent on those systems in our daily lives. From the point of view of an electrical engineer it is quite surprising that all these electronic and electrical systems function correctly without interfering with each other. Occasionally though, we encounter interference between electronic and electrical systems. An example is the interference between a cell phone and an FM radio, where the interference is picked up by the audio cable and presents itself as a series of audible pulses through the loudspeaker. This interference presents itself as a series of audible noise pulses. Although the audible noise pulses might be rather annoying, they are not harmful.

Today's cars are full of electronic devices. These electronic devices are responsible to control the vital functions of (our) car. In contrast to the example first given, if a problem would occur in one of these electronic devices, this could lead to dramatic consequences. To avoid these situations, all electronic and electrical systems are extensively tested with respect to their immunity. Here, immunity is defined as the ability of an electronic and electrical system to function properly whilst being subjected to all kinds of undesired disturbances. Testing and analyzing the functionality of these systems under these harsh circumstances belongs to the field of "electromagnetic compatibility" (EMC).

The tests that mimic the possible disturbances of a device is called "compliance tests". To predict the outcome of a compliance test, pre-compliance testing is performed. Pre-compliance testing is crucial since compliance tests are expensive and should therefore ideally have to be performed only once. Consequently, potential EMC problems should already have been detected and dealt with before compliance testing. Finding out about EMC problems only in the testing stage of the process can be very expensive for a company in terms of re-design costs, re-testing costs, re-manufacturing costs and debugging time. This will delay the time-to-market substantially and could eventually be lethal for certain enterprises. It is thus of paramount importance to perform pre-compliance testing already during the early design stages of a novel product or system.

In this Ph.D. dissertation, we focus on constructing circuit equivalent models that allow to simulate (pre-)compliance tests during the design phase. In particular, we deal with tests that are used in the automotive industry. In the automotive industry there are two types of compliance tests. On the one hand, during radio frequency (RF) tests, a sinusoidal disturbance signal is injected into the device-under-test (DUT). It is investigated at which frequencies and/or power of the sinusoidal disturbance signal the system (DUT) will go out of its predefined specifications. These RF tests were already thoroughly studied in the past. On the other hand, designers in automotive industry are faced with the novel field-coupled transient immunity

tests. These are the most difficult ones to comply with as they cannot be tackled successfully with existing analysis and design techniques. This is not only due to the complex field coupling mechanisms, but also to the large variety of test waveforms (ranging from slow relay-switching disturbances to ultrafast electrostatic discharge (ESD) events).

In this Ph.D. dissertation we construct equivalent circuit models for the following important field-coupled transient immunity tests:

- ultrafast plate-to-wire coupled electrostatic discharge (ESD-Rinne)
- slow magnetic-field coupled immunity (ICC)
- fast electric-field coupled immunity (CCC)
- wideband wire-to-wire coupled immunity (RI-130)

The equivalent circuit models can be used by a circuit designer, in his/her traditional software design environment, to perform an immunity test in a pre-compliance phase. All the aforementioned test setups consist of a very large wire bundle, which represents the wire harness of a car, connecting the supply and control unit with the DUT. To take these electrically long wires into account we will make extensive use of transmission line theory.

The first chapter presents a general introduction about the context and objectives of this work. In Chapter 2 we discuss the ESD-Rinne test. This is one of the most important tests in the automotive industry, because an unwanted electrostatic discharge can lead to significant damage to a car and to the persons inside. In this chapter we develop an equivalent circuit model for the ESD-Rinne test. Special attention is devoted to the ESD gun, since this device generates the disturbance signal. Furthermore, the electrical large test bench setup is modeled by means of transmission line theory. Finally, the model is extensively validated by comparison with measurements. Chapter 3 addresses the ICC test. Here, a slowly varying disturbance signal is injected in the wire harness, via an inductive coupling probe. By modeling the coupling mechanism as distributed voltage sources, we can easily combine it with transmission line theory, again taking the electrically large test setup into account. This results in an equivalent circuit model of the ICC test, which is extensively validated by means of measurements. Chapter 4 focuses on the CCC test in which a capacitive coupling clamp is used to inject a disturbance signal into the wire harness. Instead of applying the traditional approach, where the capacitive coupling clamp is modeled as a single capacitor, we propose a new model by combining the classical transmission line theory with two electromagnetic shielding concepts i.e. surface transfer impedance and surface transfer admittance. It is shown that the proposed model is highly efficient and accurate for the case of the CCC test, which is again confirmed by measurements. The compliance test discussed in Chapter 5 is the RI-130 test. Here, a mechanical relay is present in the disturbance generator. Hence, the test is influenced by contact bounce, which

is considered as a stochastic process. This phenomenon determines the key features of the disturbance signal, such as the amplitude. In Chapter 5 we present and validate an equivalent circuit model that predicts the worst case scenario of the RI-130 test.

All models proposed in Chapters 2-5 are tested using a nonlinear device under test. This demonstrates the appositeness of the circuit models for the designer in the automotive industry. The research and in particular the measurements, were performed in close cooperation with Melexis Technologies N.V., Tessenderlo, Belgium, guaranteeing their state-of-the-art importance.

The final chapter describes the overall conclusions drawn from the research presented in this dissertation. Additionally, suggestions are made for further research, such as the investigation of the reproducibility of the field-coupled transient test. In summary, this dissertation gives a clear description of and insight into the couplings mechanism in important field-coupled transient immunity tests. Moreover, in this dissertation, an accurate and fast equivalent circuit model is constructed for each of these tests, which is of great value for EMC-aware design in the automotive industry.

List of Abbreviations

ADS	Keysight's Advanced Design System
BCI	Bulk Current Injection
BJT	Bipolar junction transistors
CCC	Capacitive Coupled Clamp
CRT	Cathode ray tubes
DPI	Direct Power Injection
DUT	Device Under Test
EFT	Electrical Fast Transient
EM	Electromagnetic
EMC	Electromagnetic Compatibility
EMI	Electromagnetic Interference
ESD	Electrostatic Discharge
FCC	Federal Communications Commission
FCP	Field Coupled Plane
FDTD	Finite-Difference Time-Domain
IC	Integrated Circuit
ICC	Inductive Current Clamp
MTL	Multiconductor Transmission Line
NC	normal-closed
PC	Polynomial Chaos
p.u.l.	per-unit-of-length
RF	Radio Frequency
TL	Transmission Line
VM	Vehicle Manufacturers
VR	Voltage Regulator

List of Symbols

$ \cdot $	Absolute value
f	Frequency
ω	Angular frequency
N_p	Number of turns of the primary winding
L_p	Inductance of the primary winding
L_{ii}	Self-inductance
M_{ip}	Mutual inductance between the primary winding and the i-the winding
$R(\omega)$	Reluctance of the ferrite core
$Z_{in}(\omega)$	Input impedance
V_{ZS}	Voltage across self-inductor
I_{ZS}	Current across self-inductor
Z_t	Surface transfer impedance
Y_t	Surface transfer admittance
Z_i	Impedance of the internal transmission line
Y_i	Admittance of the internal transmission line
Z_e	Impedance of the external transmission line
Y_e	Admittance of the external transmission line
V_i	Voltage along the internal transmission line
I_i	Current along the internal transmission line
V_e	Voltage along the external transmission line
I_e	Current along the external transmission line
k_i	Propagation factor of the internal transmission line
k_e	Propagation factor of the external transmission line
β_i	Imaginary part of the propagation factor of the internal transmission line
β_e	Imaginary part of the propagation factor of the external transmission line
V_{FT}	Voltage source term
I_{FT}	Current source term
V_s	Distributed voltage sources along the transmission line
I_s	Distributed current sources along the transmission line
$Z_{C,i}$	Characteristic impedance of the internal transmission line
$Z_{C,e}$	Characteristic impedance of the external transmission line
A	Matrix A

List of Publications

Articles published in International Journals

- N. Lambrecht, C. Gazda, H. Pues, D. De Zutter, and D. Vande Ginste, "Efficient Circuit Modeling Technique for the Analysis and Optimization of ISO 10605 Field Coupled Electrostatic Discharge (ESD) Robustness of Nonlinear Devices," *IEEE Transactions on Electromagnetic Compatibility*, vol. 58, no. 4, pp. 971 - 980, 2016.
- N. Lambrecht, H. Pues, D. De Zutter, and D. Vande Ginste, "Modeling of Contact Bounce in a Transient Electromagnetic Compatibility Test for the Analysis and Optimization of Nonlinear Devices," *IEEE Transactions on Electromagnetic Compatibility*, vol. 59, no. 2, pp. 541 - 544, 2017.
- N. Lambrecht, H. Pues, D. De Zutter, and D. Vande Ginste, "A Circuit Modeling Technique for the ISO 7637-3 Capacitive Coupling Clamp Test," *IEEE Transactions on Electromagnetic Compatibility*, vol. 60, no. 4, pp. 858-865, 2018.

Article to Appear in International Journal

- R. Medico, N. Lambrecht, H. Pues, D. Vande Ginste, D. Deschrijver, T. Dhaene, and D. Spina, "Machine Learning-based Error Detection in Transient Susceptibility Tests," *IEEE Transactions on Electromagnetic Compatibility*, accepted for publication on March 28th, 2018

Articles published in Conference Proceedings

- N. Lambrecht, H. Pues, D. De Zutter, and D. Vande Ginste, "Circuit Modeling of the ISO 10605 Field Coupled Electrostatic Discharge Test to Design Robust Automotive Integrated Circuits," in *The 11th International Workshop on Electromagnetic Compatibility of Integrated Circuits (EMC Compo 2017)*, Saint Petersburg, Russia, 4-8 July 2017, pp. 141-145.
- N. Lambrecht, H. Pues, D. De Zutter, and D. Vande Ginste, "Modeling Transient Electrical Disturbances by Inductive Coupling for the ISO 7637-3 ICC Test," in *EMC Europe 2017*, Angers, France, 4-8 Sept. 2017, pp. 75-77.

**MODELING OF COMPLEX EMC TEST SETUPS FOR THE
ASSESSMENT OF THE TRANSIENT BEHAVIOR OF
AUTOMOTIVE INTEGRATED CIRCUITS**

1

Introduction

1.1 Context

The amount of state-of-the-art electrical and electronic systems that are present in our 21st century society, is enormous. Nowadays, we are all hugely dependent on electronic devices and systems during our daily activities, for our comfort, and for our general well-being. All these electronic systems will interfere with each other. We call this phenomenon *electromagnetic interference* (EMI).

One of the earliest examples of (undesired) EMI was reported during the 1930s [1]. At that time, more and more cars were being used. During the same period the first commercial television sets, based on cathode ray tubes (CRT), were sold. If it would not have been for the United States' Federal Communications Commission (FCC), televisions would not have become a commercial success, the reason being EMI. Indeed, as all cars used spark plugs, a lot of electromagnetic (EM) noise was created. This noise was picked up by the television sets, who suffered from the interference that manifested itself by jittering the image on the screen every time a car passed by. So, who's fault was this? The car manufacturers, who designed a product that emitted too much EM noise? Or the designers of the CRTs, who came up with a product that was far too susceptible to this noise? The FCC had to put forward some rules, allowing for the car and the television to coexist in harmony. From this example it is clear that we need to make our novel electronic products immune to undesired disturbance sources. The field which studies this immunity behavior is called electromagnetic compatibility (EMC).

Despite decades of efforts and progress made in this domain, many EMC failures are still being reported in literature, ranging from merely annoying instances to situations with life-threatening consequences (Fig. 1.1). For example, all readers will probably have experienced the interference between a cell phone and an FM radio receiver, presenting itself as a series of audible noise pulses. Although the

sound might be rather annoying, this is not harmful. A more dangerous situation, described in literature [2], concerns the malfunctioning of a car that was equipped with a novel microprocessor to control the fuel consumption. Signals from a FM transmitter were coupled onto the electrical wiring in the car and disturbed the processor such that the car engine shuts down. Also in the automotive context, improper airbag deployment was reported [3] and sudden unintended acceleration was reported in cars from Toyota due to EMI. More recently, Uber was suspended from autonomous vehicle testing as a fatal crash occurred due to an unquestionable failure.

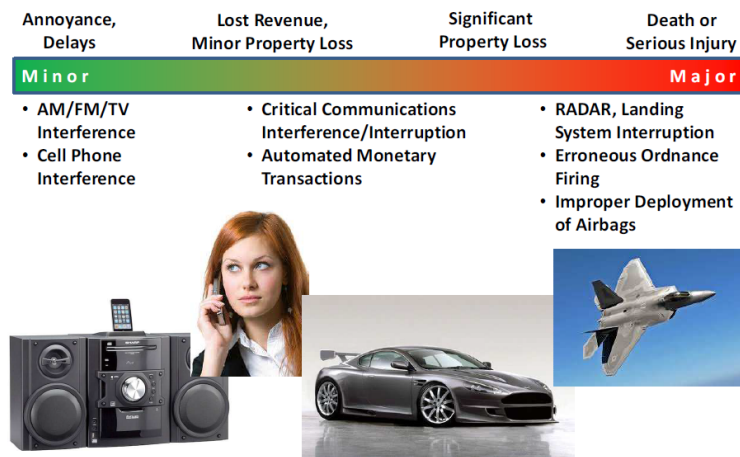


Figure 1.1: Overview of EMC non-compliance.

1.2 Motivation

The last example in the previous section brings us to the focus of this work, i.e. the study of EMC in an automotive context. Modern cars contain a large variety of electrical/electronic modules. In recent years, due to the growing number and complexity of the electrical/electronic modules, the risk of novel and unexpected EMC problems at vehicle level keeps increasing. To minimize this risk, the vehicle manufacturers (VMs) are imposing EMC specifications at module level that are regularly extended and made more strict to take into account the changing EMC environment on board of cars as well as new disturbance mechanisms [4]–[6]. These are then translated in the so-called compliance tests.

If a VM wants to sell his/her product then he/she has to fulfill all the EMC requirements, and pass the corresponding compliance tests. In case of a failed compliance test, e.g., when immunity requirements are not met, the product is rejected and cannot be used or sold. This entails huge consequences for project timelines and budgets. Debugging, re-design, re-manufacturing and re-testing are very costly

and disturb the time-to-market schedule. To avoid these situations, pre-compliance testing can be performed. In pre-compliance testing, a full compliance lab is mimicked in measurement or simulation. Assuming an efficient model could be developed to predict the actual outcome of a compliance test, this would allow the designer to use it early in the design phase of a product. The advantage of performing pre-compliance testing in the early design phase is that EMC problems are much easier to fix when caught early on. The goal is thus to predict and solve all potential EMC problems before tape-out, prototyping and, especially, production, in order to arrive at a so-called “first-time-right design”.

In this Ph.D. dissertation, we devise pre-compliance tests in a simulation environment with applications for automotive industry. In particular, the novel field-coupled transient tests, as these are the most difficult ones to comply with and since they cannot be tackled successfully with existing analysis and design techniques. This is not only due to the complex field-coupled (i.e. non-conducted) coupling mechanisms, but also to the large variety of test waveforms (ranging from slow relay-switching disturbances to ultrafast electrostatic discharge (ESD) events).

Currently, the following field-coupled transient tests are of interest in the automotive industry:

- ultrafast plate-to-wire coupled electrostatic discharge (ESD-Rinne) [7]–[9]
- slow magnetic-field coupled immunity (ICC) [10]
- fast electric-field coupled immunity (CCC) [10]–[13]
- wideband wire-to-wire coupled immunity (RI 130) [14]
- slow and fast capacitively coupled immunity (DCC) [10]

The ultrafast plate-to-wire coupled ESD test is made such that it simulates an electrostatic discharge into a vehicle’s electrical system, based on the human ESD model, as sensitive electrical devices can be adversely affected by energy either conductively coupled or radiated from electrostatic discharges.

The slow magnetic-field coupled immunity (ICC) test, simulates the case when slow transient pulses are inductively coupled to the wire harness of a vehicle. These slow transient pulses mimic typical disturbances that occur as a result of an interruption of circuits with an inductive load, such as a radiator fan motor, air conditioning compressor clutch, etc.

The fast electric-field coupled immunity (CCC) test is a broadband EMC test targeting fast transient pulses, that typically occur as a result of switching processes. Here the coupling occurs along a large piece of the wire harness.

The function of the wideband wire-to-wire coupled immunity (RI 130) test is to simulate a device-under-test (DUT) exposed to coupled transient electromagnetic disturbances created from switch contact arching and contact bounce.

The slow and fast capacitively coupled immunity (DCC) test, is also a broadband

EMC test where in contrast to the CCC test, both slow and fast pulses are injected into the wire harness. Here, the slow transient pulses mimic transient pulses which occur as a result of breaking the circuit to larger inductive loads, such as a radiator fan motor, air conditioning compressor clutch, etc. The manner of injecting the disturbance signal in this test, is by connecting a transient generator via a capacitor to one wire of the wire harness at 50 mm of the DUT. The values of the capacitors are defined in [10].

1.3 State-of-the-art

Today, the above mentioned novel transient immunity requirements are starting to become the biggest EMC challenge for the automotive business. This challenge is still increasing as the VMs are extending these requirements and making them more severe. The challenge/threat mainly stems from the difficulty to retrieve the exact failure mechanisms due to the complex field-coupling mechanisms.

Due to these difficulties, the current design approaches to meet these new requirements (either trial-and-error or approximate measurement-based modeling) do not really work, and a new systematic and accurate design methodology is needed to make first-time-right designs. In literature, some techniques are exposed that make use of full-wave simulations [15]–[18]. However these methods do not give insight in the coupling mechanism of the EMC test. Moreover, these kind of simulations takes a lot of time since the above mentioned field-coupled transient EMC tests are electrically very large. The hybrid full-wave/circuit model presented in [19] was one step in the right direction, but still suffers from lack of insight. Also models were made purely based on measurements [20]–[22]. In this latter case, the model should be generated and measured again when even a very small adjustment is made to the test setup, making this approach costly and time-consuming.

1.4 Novel Contributions and Overview of the Dissertation

To overcome all the above mentioned issues, we propose a full circuit equivalent model of the following field-coupled transient EMC tests: ESD-Rinne, ICC, CCC and RI-130¹. By making circuit models, the whole machinery of circuit simulators becomes available. Hence, the proposed models are easy to use for circuit designers when they want to test their design very early in the design phase.

In Chapter 2 an in-depth analysis of the plate-to-wire coupled electrostatic discharge test (ESD-Rinne) is given. Here, the test bench itself consists of a large copper plate, which acts as a ground plane, and a field coupling plane (FCP) (see

¹As the DCC is a rather simple test, constructing a circuit model is pretty straightforward and hence, not discussed in this work.

Fig. 2.1 on page 14). The FCP is basically a rectangular piece of copper, supported by foam. The wire harness lays on top of the FCP. On one side, the FCP is left open. On the other side, the FCP has a wider section that supports the DUT and then a tapering section connected to the ground plane. The ground strap of the ESD gun is also connected to this point. During the test, ESD pulses of which the waveform is specified in the IEC-61000-4-2 standard [9], are injected in the FCP and the behavior of the DUT is observed.

We observe that the FCP behaves as a transmission line which is shorted at one end and open at the other. When injecting the ESD current, waves will travel to both ends, will be reflected there and all (reflected) contributions eventually create disturbances in the DUT. Here, the dominant differential mode contribution stems from the asymmetry introduced by the load box. The load box, which is typically present in automotive EMC test setups, mimicks equipment such as the control unit of the car. We propose a multiconductor transmission line (MTL) model that takes the inductive and capacitive coupling plus all delays from the FCP to the wire harness into account. Moreover, we include the inductance and transmission line effects of the large ground strap of the ESD gun. Although one would expect that there would be a significant radiation stemming from the large loop made by the ground strap, our model shows that the dominant disturbances come from the crosstalk in the wire harness.

In Chapter 3, we focus on the modeling of the slow magnetic-field coupled immunity (ICC) test (Fig. 3.1 on page 37). We present an equivalent circuit of the injection clamp plus the long wire harness by making use of the transmission line theory.

In Chapter 4, we made an equivalent circuit model of the fast electric-field coupled immunity (CCC) test (Fig. 4.1 on page 51) again by making use of transmission line theory. However, in this chapter, we adapted the transmission line theory. To model the capacitive coupled clamp, we consider it as two transmission lines that are coupled by means of a surface transfer impedance and a surface transfer admittance. Using distributed voltage- and current sources, we transform this complex fixture in an equivalent circuit model.

In Chapter 5, we deal with the wideband wire-to-wire coupled immunity test (RI-130) (Fig. 5.1 on page 71). The mechanical relay in the transient generator of this test setup results in noise contribution stemming from contact bounce. This contact bounce should be considered as a stochastic phenomenon, rendering brute-force simulations intractable, even with a fast circuit model. To overcome this issue, we present a worst case scenario derived from a statistical study of the relay.

In this Ph.D. dissertation all the proposed equivalent circuit models are validated with measurement using a nonlinear device as DUT. This is needed as, in automotive applications, all the DUTs are also nonlinear devices. In all the field-coupled transient tests we apply transmission line theory, although many researchers are tempted to use solely capacitive- or inductive coupling. Depending on the impedance of the devices that terminate the wire harness, the dominant coupling can be ca-

capacitive (high impedance) or inductive (low impedance). Owing to the use of transmission line theory, however, we do not need to take the DUT into account when modeling the test bench. Hence, our proposed models are more generally applicable. The research and in particular the measurements, were performed in close cooperation with Melexis Technologies N.V., Tessenderlo, Belgium, guaranteeing their state-of-the art importance. The presented circuit models will be adopted by this company's chip designers.

References

- [1] C. R. Paul, *Introduction to Electromagnetic Compatibility*, 2nd ed. Hoboken, NJ07030: John Wiley and Sons, Inc., 2006.
- [2] D. Vande Ginste, “Circuit and EMC Concepts”, Ghent University, unpublished syllabus, 2014-2015.
- [3] K. Couturier and H. Tabuchi, *The Airbag in Your Car Could Explode. This is What You Should Do About it*. The New York Times, 29 dec. 2016.
- [4] EMC-CS-2009.1, *Electromagnetic Compatibility Specification for Electrical/electronic Components and Subsystems*, Ford General Specification Electrical/electronic, 2010.
- [5] GMW3097, *General Specification for Electrical/electronic Components and Subsystems*, *Electromagnetic Compatibility GM Worldwide Engineering Standard*, General Specification, 2012.
- [6] TL81000, *Electromagnetic Compatibility of Automotive Electronic Components*, Volkswagen Group Standard, 2014.
- [7] DC-10614 *EMC Performance Requirements - Components*, 2005.
- [8] ISO 10605 *Road Vehicles Test Methods for Electrical Disturbances from Electrostatic Discharge*, 2008.
- [9] IEC 61000-4-2 Ed. 2.0 *Electromagnetic Compatibility (EMC) Part 4-2, Testing and Measurement Techniques Electrostatic Discharge Immunity Test*, 2008.
- [10] ISO 7637-3 *Road Vehicles, Electrical Disturbances from Conduction and Coupling, Part 3, Electrical Transient Transmission by Capacitive and Inductive Coupling via Lines Other than Supply Lines*, 2014.
- [11] IEC 61000-4-4, *Testing and Measurement Techniques - Electrical Fast Transient/Burst Immunity Test*, IEC, 2012.
- [12] F. D. Martzloff and T. F. Leedy, “Electrical Fast Transient Tests: Applications and Limitations”, in *Conference Record of the IEEE Industry Applications Society Annual Meeting*, San Diego, CA, USA, USA, 1989, 1625–1632 vol.2.
- [13] B. Cormier and W. Boxleitner, “Electrical Fast Transient (EFT) Testing-an Overview”, in *IEEE 1991 International Symposium on Electromagnetic Compatibility*, Cherry Hill, NJ, USA, USA, 1991, pp. 291–296.
- [14] FMC1278, *Electromagnetic Compatibility Specification for Electrical and Electronic Components and Subsystems*, www.fordemc.com/docs/download/FMC1278.pdf, Ford, Oct. 2016.

- [15] M. Rizvi and J. L. Vetri, "ESD Source Modeling in FDTD", in *Proceedings of IEEE Symposium on Electromagnetic Compatibility*, Chicago, IL, USA, 1994, pp. 77–82.
- [16] K. Wang, D. Pommerenke, and R. Chundru, "Numerical Modeling of ESD-Simulators", vol. 1, Minneapolis, MN, USA, 2002, pp. 93–98.
- [17] K. Wang, D. Pommerenke, R. Chundru, T. Van Doren, J. Drewniak, and A. Shashindranath, "Numerical Modeling of Electrostatic Discharge Generators", *IEEE Transactions on Electromagnetic Compatibility*, vol. 45, no. 2, pp. 258–271, 2003.
- [18] S. Caniggia, E. Dudenhoefter, and F. Maradei, "Full-Wave Investigation of EFT Injection Clamp Calibration Setup", in *2010 IEEE International Symposium on Electromagnetic Compatibility*, Fort Lauderdale, FL, USA, 2010, pp. 602–607.
- [19] T. Takada, T. Sekine, and H. Asai, "Hybrid Simulation of ESD Events by SPICE-like and Finite-Difference Time-Domain Methods", *2013 IEEE Electrical Design of Advanced Packaging Systems Symposium (EDAPS)*, 2013.
- [20] J. Koo, Q. Cai, G. Muchaidze, A. Martwick, K. Wang, and D. Pommerenke, "Frequency-Domain Measurement Method for the Analysis of ESD Generators and Coupling", *IEEE Transactions on Electromagnetic Compatibility*, vol. 49, no. 3, pp. 504–511, 2007.
- [21] D. C. Smith, "An Investigation into the Performance of the IEC 1000-4-4 Capacitive Clamp", in *1996 Proceedings Electrical Overstress/Electrostatic Discharge Symposium*, Orlando, FL, USA, 1996, pp. 223–226.
- [22] S. Radman, I. Bacic, and K. Malaric, "Capacitive Coupling Clamp", in *2008 16th International Conference on Software, Telecommunications and Computer Networks*, Split, Croatia, 2008, pp. 75–79.

2

Efficient Circuit Modeling Technique for the Analysis and Optimization of ISO 10605 Field Coupled Electrostatic Discharge (ESD) Robustness of Nonlinear Devices

Based on “Efficient Circuit Modeling Technique for the Analysis and Optimization of ISO 10605 Field Coupled Electrostatic Discharge (ESD) Robustness of Nonlinear Devices,” N. Lambrecht, C. Gazda, H. Pues, D. De Zutter, and D. Vande Ginste, *IEEE Transactions on Electromagnetic Compatibility*, vol. 58, no. 4, pp. 971 - 980, 2016.

★ ★ ★

In this chapter, we propose a circuit modeling technique for the ISO 10605 field coupled electrostatic discharge (ESD) test, often used in the automotive sector. First, a novel circuit model of the ESD gun is proposed. Second, a circuit model is developed for the ISO 10605 field coupled ESD test bench and concatenated with models for the load box and the device under test (DUT). To validate the advocated models, a nonlinear DUT is simulated, manufactured and measured under the ISO 10605 field coupled ESD test conditions. Furthermore, it is shown that the circuit model can be used to efficiently optimize the design of the DUT, making it more robust against ESD disturbances. The optimized DUT design was again manufactured and measured, validating the simulated results.

2.1 Introduction

Electrostatic discharge (ESD) causes failure and damage of electronic equipment. Especially in the automotive sector, the ESD test is a very important transient Electromagnetic Compatibility (EMC) test, because charge easily builds up on a moving vehicle. A typical EMC test that simulates the possible ESD disturbances on a vehicle level very well, is introduced for automotive ESD testing in Rev. B of DaimlerChrysler standard DC-10614 [1] and in an informative annex of ISO 10605 [2]. This ISO 10605 field coupled ESD test was created to obtain an ESD test setup that produces repeatable test results and for which a good correlation between the vehicle level ESD test and the real world environment is obtained.

For designers of electronic circuits and equipment, it is of the utmost importance that during the pre-compliance phase, i.e., early in the design phase, the EMC behavior of their novel devices and systems can be predicted efficiently. This avoids expensive iterations in later stages of the design cycle, costly and time consuming measurements and troubleshooting and hence, it reduces time to market, leading to a more cost-effective development. To accomplish this, modeling of EMC tests has become indispensable. However, there are many different types of EMC tests and almost every EMC test has to be modeled in a different way. Typical examples of narrowband (i.e. non-transient) EMC tests — of interest for automotive applications — are the Direct Power Injection (DPI) and the Bulk Current Injection (BCI) test. The DPI test [3] is used to determine an IC's susceptibility against disturbance frequencies up to 3 GHz. In [4], an EM/circuit co-design technique is proposed for the analysis and design of reliable DPI tests of ICs. The BCI test [5] is another susceptibility test, taking the influence of (shielded) cables and bundles of wires, present in automotive and avionics applications, into account. A lot of literature on the modeling of BCI tests is available, e.g. [6], [7], [8], [9]. The modeling typically consists of two parts: (i) the modeling of the injection clamp and (ii) the modeling of the wire harness itself.

Whereas the DPI and BCI test are narrowband susceptibility tests, more and more attention is devoted to broadband transient tests, of which the ISO 10605 field

coupled ESD test is an important example. In [10], a behavioral model for an 18 MHz D flip-flop is built after which this model is used in the simulation of an ESD stress test following ISO 10605, and validated via comparison with measurements. Whereas in [10], the ESD test setup itself described in the ISO 10605 standard, was simulated leveraging commercially available full-wave tools, in this chapter, we focus on a fast and reliable circuit modeling technique of the entire test setup. As circuit simulators are powerful design tools, able to deal with active nonlinear components and easily integrated with advanced optimization and troubleshooting techniques, our circuit modeling approach allows for a rapid analysis of the DUT and its subsequent optimization. However, due to the electrically large dimensions and the broad spectrum of the transient signals, constructing such a circuit model is not straightforward. The goals put forward in this chapter are:

- the development of an accurate equivalent circuit model of the ESD gun.
- the development of an accurate equivalent circuit model of the electrically large test bench described in the ISO 10605 field coupled ESD test (see Fig. 2.1).
- to study the effects of the test and validate the advocated circuit models via measurements, using a nonlinear DUT.

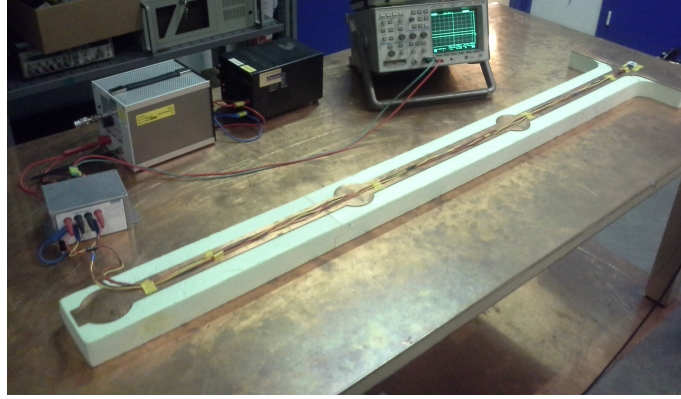
The remainder of this chapter is organized as follows. In Section 2.2, the circuit modeling techniques for each part of the ISO 10605 field coupled ESD test setup are explained and partially validated. Section 2.3 deals with the validation of these models, via comparison with measurements. Finally, some concluding remarks are formulated in Section 2.4.

2.2 ISO 10605 Field Coupled ESD Test Circuit Modeling

In this section, we discuss the circuit modeling of the entire ESD test setup. Equivalent circuits for its subparts are constructed and then concatenated. It is of great importance that every part is modeled accurately, as the quality of the overall simulation results depends on the precision of the model for each subpart. In order to assess the quality of the models, we verify the equivalent circuits by means of measurements.

2.2.1 Description of the ISO 10605 field coupled ESD test

The methodology described in this chapter might be more generally applicable, but as the ISO 10605 field coupled ESD test is gaining importance, it is the focus of this chapter and we start with its rigorous description. The test setup comprises



(a)



(b)

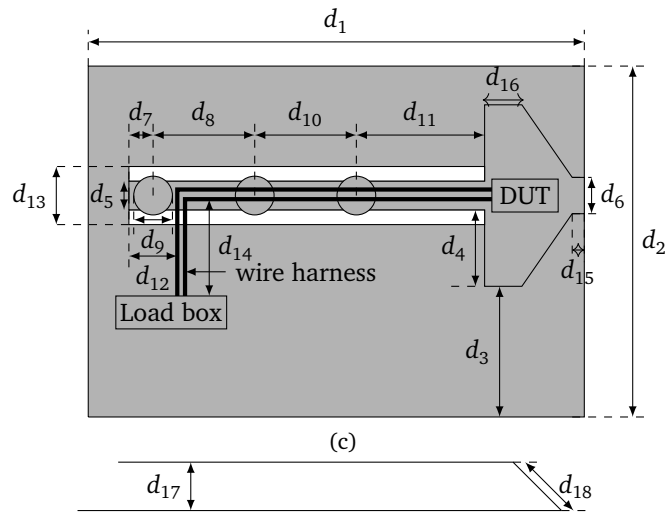


Figure 2.1: (a) top view (b) side view (c) sketch top view (see Table 2.1 for dimensions) (d) sketch side view (see Table 2.1 for dimensions)

Table 2.1: Dimensions of the test bench.

Dimension	Value	Dimension	Value
d_1	2 m	d_2	1 m
d_3	0.54 m	d_4	155 mm
d_5	40 mm	d_6	80 mm
d_7	50 mm	d_8	500 mm
d_9	80 mm	d_{10}	500 mm
d_{11}	500 mm	d_{12}	110 mm
d_{13}	120 mm	d_{14}	340 mm
d_{15}	30 mm	d_{16}	160 mm
d_{17}	50 mm	d_{18}	112 mm

a wire harness connecting a DUT with a load simulator (aka load box), an ESD gun connected to a pulse generator, and a test bench (Fig. 2.1 and Table 2.1). The test bench itself consists of a large copper plate, which acts as a ground plane, and a field coupling plane (FCP). The FCP is basically a rectangular piece of copper with a length of 1550 mm and a width of 40 mm, supported by foam with a thickness of 50 mm. It also contains three so-called circular-shaped islands with a radius of 40 mm, spaced 500 mm apart. The wire harness lays on top of the FCP. On one side, the FCP is left open. On the other side, the FCP has a wider section (width= 350 mm, length= 160 mm) that supports the DUT and then a tapering section connected to the ground plane. The ground strap of the ESD gun is also connected to this point. During the test, ESD pulses of which the waveform is specified in the IEC-61000-4-2 standard [11] (see Fig. 2.2), are injected subsequently at each of the three islands, and the behavior of the DUT is observed. In this chapter we use a 330 pF/ 330 Ω body model, this to illustrate the most severe scenario, which corresponds to a discharge of a human body through a metallic part (e.g., tool, key, ring) and where the signal is injected inside the vehicle.

2.2.2 Modeling of the ESD gun

The ESD gun, generating the interference signal, is one of the key components of the test. In essence, it is an inhomogeneous device with small, intricate geometric details. A great deal of attention has been devoted to the modeling of ESD guns. A first, simple human-body model is mimicked by an RC-circuit where a capacitor C_s is charged by a high voltage, and then discharged through a discharge resistor R_1 . The capacitor C_s in series with the resistor R_1 corresponds to the capacitance and skin resistance of the human body respectively (Fig. 2.3). However, as shown below (Fig. 2.7), this circuit cannot accurately reproduce the waveform of the ESD gun. A more accurate way to model the inhomogeneous device creating its transient response via a discharge process, is by means of finite-difference time-domain (FDTD) simulations. This full-wave approach allows reproducing the response of the device in the time domain [12]–[14]. As full-wave simulators typ-

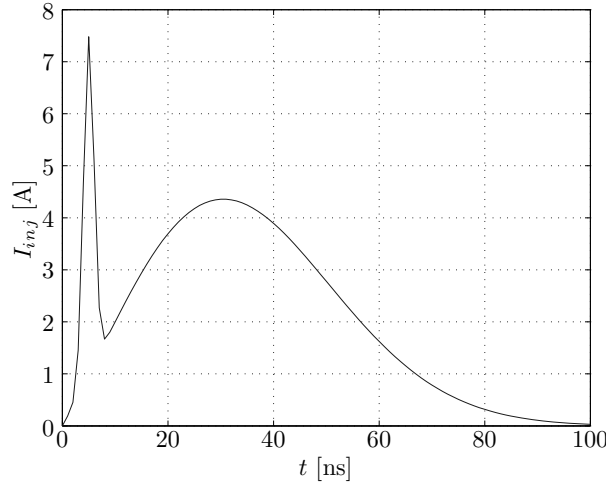


Figure 2.2: IEC-61000-4-2 ESD current waveform with its characteristic two peaks.

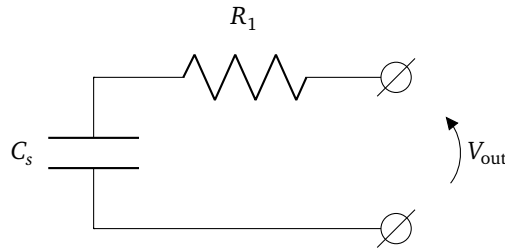


Figure 2.3: A simple ESD generator circuit, representing a human-body model.

ically consume a lot of CPU time, an alternative way is to construct circuit models that mimic the ESD gun's behavior. In [15], a hybrid full-wave/circuit model was proposed, and a circuit model based on frequency-domain measurements was presented in [16]. Another technique is advocated in [17], [18], where the circuit model is based on parameters related to the materials the ESD generator is made of, RC circuits, parasitic elements, the discharge tip and the return path. However, in the ESD test that we are dealing with here, there is a much longer return path than is foreseen in the intended applications of [17], [18]. The return path is called the ground strap (see Fig. 2.4) and it is necessary to model its influence accurately.

In the ISO 10605 field coupled ESD test, the ESD pulse is injected at the three islands whereas one end of the ground strap remains fixed to the copper plate. Hence, the shape of the ground strap is different for the three injection islands, as sketched in Fig. 2.4. This change in geometry leads to a different electrical be-

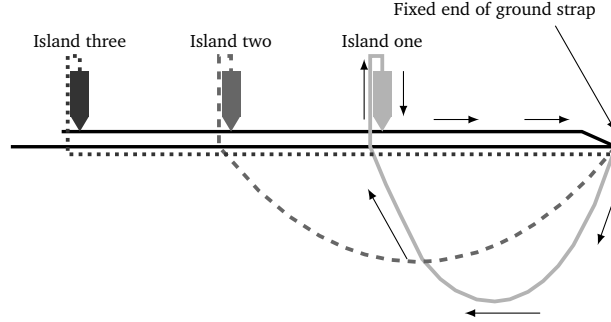


Figure 2.4: Different shapes of the ground strap when injecting at different islands. The arrows indicate the current flow in the loop when injecting at island one (see Table 2.2 for corresponding loop inductances).

havior. The ground strap forms a large loop when we inject at island one, i.e. the island closest to the DUT. This loop introduces extra inductance. The value of the inductance clearly depends on the shape of the ground strap and thus on the island at which we inject. Consequently, we propose a novel circuit equivalent, inspired by [17], [18], but with some crucial refinements. Fig. 2.5 depicts the final equivalent circuit model for the ESD gun. We have introduced an extra inductance L_1 in series with a transmission line TL_1 in order to accurately account for the (varying) loop inductance and the electrical length of the ground strap. In time-domain simulations, this electrical length leads to a delay that is now accurately mimicked. We calculated the self-inductance of the loop for each island by numerical integration of the Neuman formula [19]. From these calculations, we obtained the values presented in Table 2.2. The values for the delay and characteristic impedance of TL_1 are obtained by carefully estimating these values based on time-domain measurements. Adding transmission line TL_1 in series with inductor L_1 to the model leads to a better timing and value of the typical second maximum that characterizes the ESD pulse (Fig. 2.2). Another novel item in our circuit model is the second transmission line TL_2 that takes the interconnection of the pulse generator to the ESD gun and the internal interconnections of the ESD gun itself into account. Here again, the appropriate values for the delay and characteristic impedance for TL_2 are chosen by carefully estimating these values based on time-domain measurements. This transmission line is able to model oscillations appearing in the tail of a non-ideal ESD current waveform (as presented below in Fig. 2.7).

The new model of the ESD gun is now validated by measurements. These measurements are performed by injecting an ESD pulse into a large copper ground plane, placing a current probe around the tip of the ESD gun, as sketched in Fig. 2.6. In this test setup, the ground strap forms a loop with an inductance $L_1 = 1\mu\text{H}$. The injected current I_{inj} , picked up by the probe, is measured and also modeled with the equivalent circuit of Fig. 2.5. As depicted in Fig. 2.7, we see that the

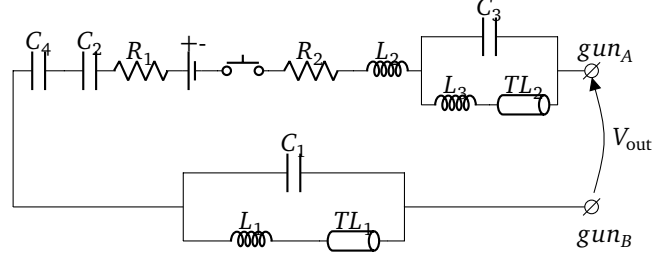


Figure 2.5: The proposed equivalent-circuit model of the ESD gun (see Tables 2.2 and 2.3 for the circuit element values).

Table 2.2: Inductance L_1 for the three injection islands (see Figs. 2.4 and 2.5).

Injection island	Loop inductance
Island one	$2.25 \mu\text{H}$
Island two	$2.48 \mu\text{H}$
Island three	$1.56 \mu\text{H}$

Table 2.3: Component values of the equivalent ESD gun circuit (Fig. 2.5).

Component	Value	Component	Value
R_1	330Ω	R_2	100Ω
C_1	12 pF	C_2	330 pF
C_3	2 pF	C_4	110 pF
TL_1, Z_c	80Ω	TL_2, Z_c	30Ω
TL_1, delay	19 ns	TL_2, delay	10 ns
L_2	200 nH	L_3	50 nH

simulation (black solid line), leveraging the novel circuit model, gives a good approximation of the measured waveform (black dashed line) of the ESD current, whereas the simple model of Fig. 2.3 (grey solid line) clearly cannot capture all pertinent behavior. A zoom on the first 100 ns of the ESD pulse is included in the inset of Fig. 2.7.

2.2.3 Modeling of the Test Bench

The second important part of the ISO 10605 field coupled ESD test is the test bench itself. To avoid time-consuming full-wave simulations and given the relatively small cross-sectional dimensions, we propose a multiconductor transmission line (MTL) approach [20] to model the test bench. Here, it is assumed that the ground plane is an equipotential plane and the slight nonuniformity of the FCP caused by the three islands, is ignored. The tapered section of the FCP is modeled via a staircase approach, i.e. by concatenation of three pieces of uniform TLs.

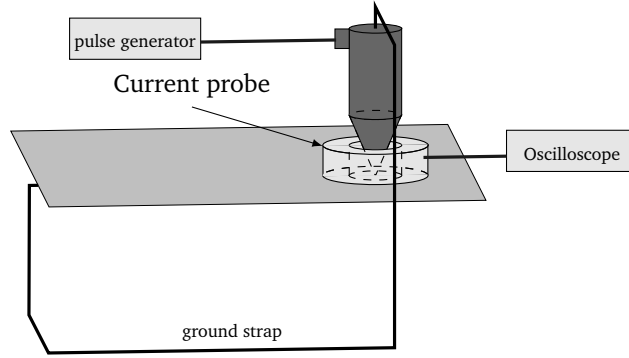


Figure 2.6: Sketch of the test setup for measuring the ESD current and validating the proposed circuit of Fig. 2.5.

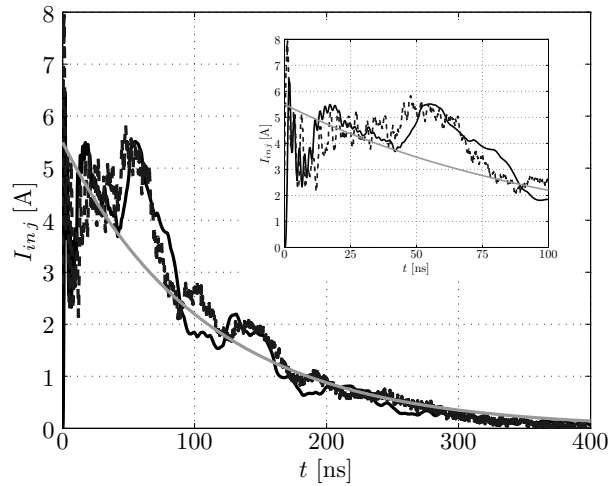


Figure 2.7: Transient response of the ESD current in the case setup of Fig. 2.6 with a large ground strap loop of $1\ \mu\text{H}$ and an ESD pulse of $2\ \text{kV}$ (simulation: black solid line; measurement: black dashed line; RC model: grey solid line).

The approximated version of the test bench is depicted in Fig. 2.8 with dimensions given in Table 2.4, allowing to model it with the reference technique described in [21] and [22], namely as a cascade of uniform MTL sections. Similarly as in [21] and [22], the per-unit-of-length (p.u.l.) parameters of the MTL sections are computed using the quasi-TM technique described in [23].

Without loss of generality but for conciseness, we consider a wire harness consisting of two wires. The corresponding equivalent cascaded MTL circuit is shown in Fig. 2.9. The injection of the ESD current with the ESD gun in this MTLs model is

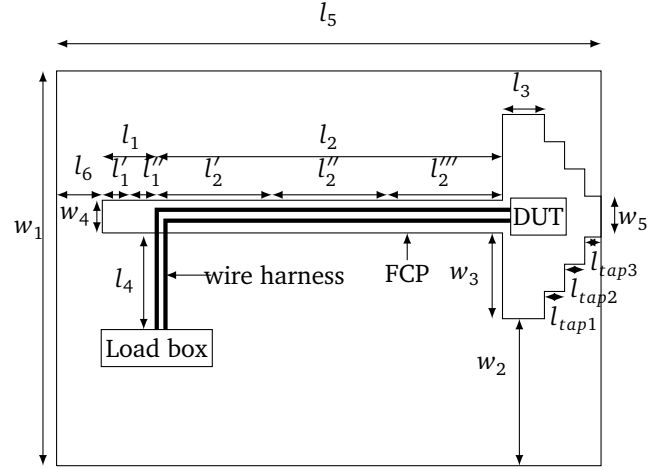


Figure 2.8: Top view of the approximated test bench. The geometrical parameters are given in Table 2.4.

Table 2.4: Dimensions of the simplified test bench.

Dimension	Value	Dimension	Value
l_1	0.11 m	l'_1	0.06 m
l''_1	0.05 m	l_2	1.45 m
l'_2	0.45 m	l''_2	0.5 m
l'''_2	0.5 m	l_3	0.16 m
l_4	0.34 m	l_5	2 m
l_6	0.168 m	w_1	1 m
w_2	0.54 m	w_3	0.155 m
w_4	0.04 m	w_5	0.08 m
l_{tap1}	0.037 m	l_{tap2}	0.037 m
l_{tap3}	0.037 m		

carried out as depicted in Fig. 2.10, where the connections gun_A and gun_B in this figure correspond to the ones of Fig. 2.5. When injecting at island one the current source is placed between transmission line l'''_2 and l'_2 , for injecting at island two the current source is placed between l''_2 and l'_2 (as depicted in Fig. 2.10) and for injecting at island three the current source is placed between transmission lines l''_1 and l'_1 .

2.2.4 Load box and DUT

The load box and the DUT are connected to the two ends of the wire harness. Here, the loadbox (or load simulator) mimicks equipment that is also present in

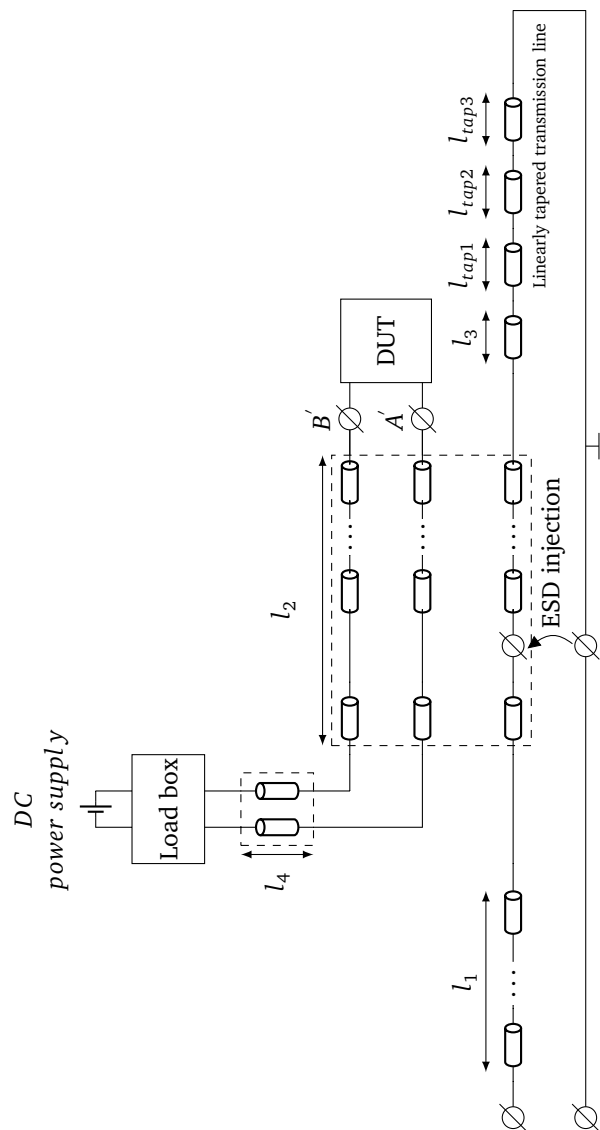


Figure 2.9: The ISO 10605 field coupled ESD test bench modeled with MTLs. (ESD injection details can be seen in Fig. 2.10.)

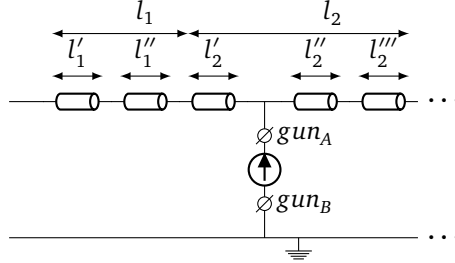


Figure 2.10: Injection of ESD current into the circuit model at island two.

a car and controls the DUT. Such equipment can be, e.g., a CPU. In an EMC test setup we represent this equipment by a passive impedance network, which can be different in various applications. This is always described in the EMC test plan. So, it simply suffices to measure the S-parameters of the load box once and use these S-parameters in the circuit simulator, e.g., by constructing a macromodel of the measured S-parameters from which a circuit model is synthesized. Details are not discussed here, as this has been the topic of a large body of literature (e.g., [24]–[26]). For the 2-wire setup, as used in this chapter, we measured the S-parameters up to 4 GHz and we directly fed the S-parameter data into the ADS circuit simulator of Keysight Technologies together with our circuit models for the ESD test bench and the ESD gun. This measurement up to 4 GHz is sufficient as the spectral component at 1 GHz are 60 dB weaker than the dominant spectral components (Fig. 2.11). At the other end of the wire harness, the DUT is connected. The two-terminal nonlinear DUT considered here, is described further in Section 2.3.

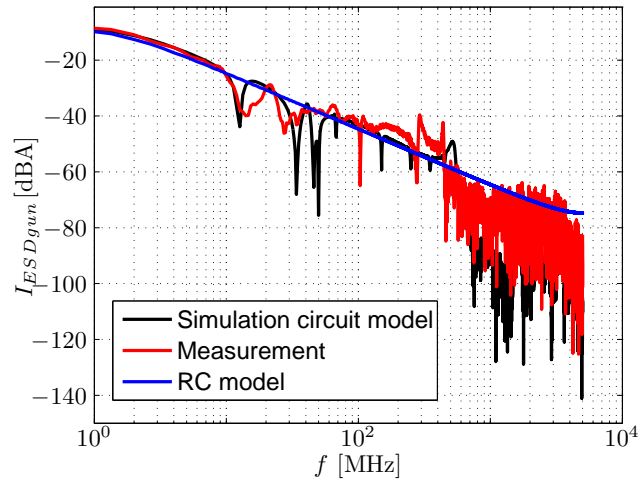


Figure 2.11: Spectrum of ESD current waveform.

Having these circuit models we can observe that the FCP behaves as a transmission line which is shorted at one end and open at the other. When injecting the ESD current, waves will travel to both ends, will be reflected there and all (reflected) contributions eventually create disturbances in the DUT. Here, the dominant differential mode contribution stems from the asymmetry introduced by the load box. With our MTL model we take the inductive and capacitive coupling plus all delays from the FCP to the wire harness into account. Moreover, by inserting the inductance due to the large ground strap of the ESD gun and the appropriate transmission lines we also include all the delays and the inductive effect of the ESD gun.

2.3 Measurements and Results

To validate and illustrate the appositeness of the circuit model, we apply it to (the optimization of) a nonlinear DUT, being a negative-resistance oscillator with an ESD protection circuit. All the measurements in this section were performed by injecting an ESD pulse of 500 V, 1 kV and 2 kV at $t = 500$ ns, to study the nonlinear behavior of the oscillator.

2.3.1 Description of the DUT

A negative resistance oscillator [27] is an active circuit that has a complex input impedance with a negative real part at its port, this to compensate the losses of its components, and hence, to ensure a stable oscillation. The oscillation frequency is set by tuning the input impedance (including the imaginary part) with a matching network at the load. Here, to serve as a nonlinear DUT, such an oscillator is designed and manufactured on an FR4 substrate (thickness of 1.5 mm, $\epsilon_r = 4.6$ and $\tan \delta = 0.01$). A bipolar junction transistor (BJT), i.e., the BFR92A by NXP Semiconductors, is used as the active element. Table 2.5, together with Fig. 2.12, depicts the oscillator that produces a ground tone at 145 MHz with a power of 2.5 dBm (109,5 dB μ V) for a supply voltage of 4.5 V and a load of 50 Ω . For clarity of the schematic, we left out all the parasitics. However, during simulations, all parasitics were included, based on the model or datasheet provided by the vendor. The spectrum of the undisturbed oscillator is shown in Fig. 2.13.

Further, at the DUT's power supply, i.e. between nodes A and B in Fig. 2.12, we place ESD protection diodes to limit the voltage across the transistor, such that it will not get damaged during the ESD test. This ESD clamping circuit is shown in Fig. 2.14, where ESD5V3L1U unidirectional diodes, from Infineon Technologies, are used. Nodes A and B of the ESD clamping circuit are connected to the corresponding nodes A and B of the oscillator, shown in Fig. 2.12. Nodes A' and B' are connected to the wire harness.

The ESD protection diodes have a clamping voltage of 10 V. Hence, they will limit the voltage of the ESD disturbance between points A and B. When clamping occurs,

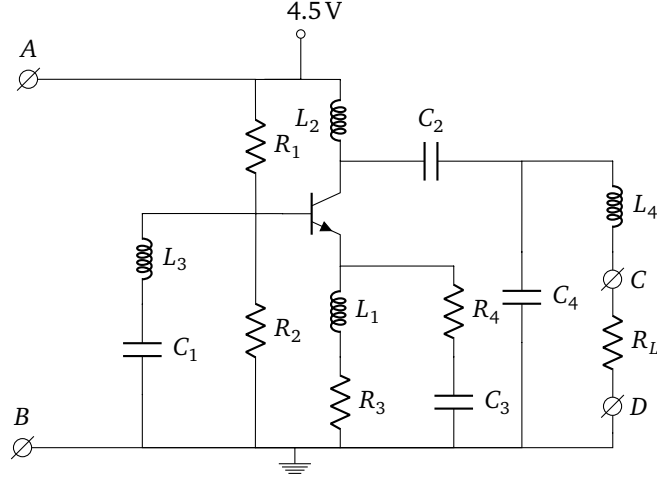


Figure 2.12: Schematic of the oscillator (see Table 2.5 for values of the components).

Table 2.5: Component values of the oscillator of Fig. 2.12.

Component	Value	Component	Value
L_1	360 nH	L_2	360 nH
L_3	180 nH	L_4	27 nH
R_1	10 k Ω	R_2	4.7 k Ω
R_3	100 Ω	R_4	3.6 Ω
R_L	50 Ω	C_1	1 nF
C_2	10 pF	C_3	30 pF
C_4	3.6 pF		

signals will be reflected by the DUT, which will in turn lead to ringing. This ringing will be present in the entire setup (including the DUT), and it will disturb the output signal of the oscillator.

2.3.2 Validation results

In this section we show the results of the ESD test, performed on the DUT of Section 2.3.1, when injecting at island two. In particular, the measured and simulated voltage across the 50 Ω load R_L , between nodes C and D of Fig. 2.12, is given. Besides the expected voltage peaks at the time of injection, we also notice beating in the output signal of the oscillator, even long after the ESD disturbance is removed. As the correspondence between simulation and measurement are hard to appreciate from Fig. 2.15 and to better assess the lasting influence of the ESD at late time, in Fig. 2.16, we show the spectrum of the output signal obtained after a Fourier

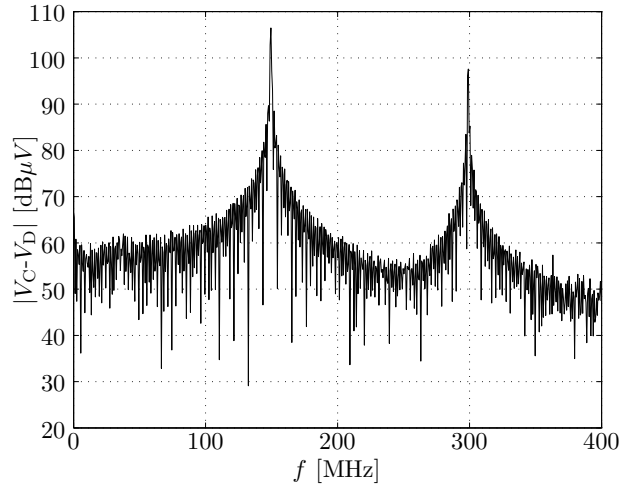


Figure 2.13: Spectrum of the oscillator (undisturbed).

transformation of the transient signal between $1.1\ \mu\text{s}$ and $1.7\ \mu\text{s}$ when injection of 500V was applied. At $t = 1.1\ \mu\text{s}$ the ESD pulse has already died out completely and what is left in the output signal is the lasting effect of this pulse. We notice spectral peaks at 145 MHz and 290 MHz (first harmonic) as expected for a normally functioning oscillator. However a strong unwanted spectral component at 17 MHz, causing the beating (see Fig. 2.15), is observed in the measured data and correctly predicted by the simulation. The 17 MHz peak is due to the reflections at the ESD diodes, including its parasitics. The slight shift in the simulation results for the extra spectral component at 17 MHz is caused by the imperfect nonlinear model of the ESD protection diodes, as provided by the supplier. Further note that the spectral peaks at 145 MHz and 290 MHz are also correctly predicted by our circuit model. It is of course clear that one cannot expect the circuit model data to exactly correspond with the measurements in every detail of the spectrum, but as demonstrated in Fig. 2.16, the circuit model predicts all salient features of the output signal.

When increasing the ESD disturbance voltage from 500V to 1 kV, the magnitude of the unwanted peak at 17 MHz increases by 8 dB. In case of injecting with a disturbance voltage of 2 kV, this magnitude further increases with another 2 dB (as depicted in Fig. 2.17). This clearly shows the nonlinear behavior of the DUT.

As an extra validation of the test bench and the ESD gun model, we performed a measurement of the voltage between nodes A and B (see Fig. 2.18). Here, one can also clearly see the clamping of the ESD protection diodes.

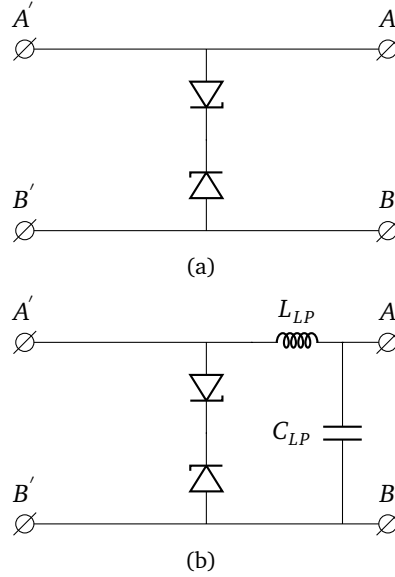


Figure 2.14: ESD protection circuits. (a) Traditional ESD protection circuit, (b) ESD protection circuit with low pass filter.

2.3.3 Application example

To make the active DUT more ESD robust, a possible solution could be to put a second-order Butterworth filter in series with the ESD protection circuit, as depicted in Fig. 2.14. As we want to keep the additional components, and hence their values L_{LP} and C_{LP} as small as possible, we are confronted with the following optimization problem:

$$\begin{aligned}
 &\text{minimize} && L_{LP} > 0, C_{LP} > 0 \\
 &\text{subject to} && |V_C - V_D| < 70 \text{ dB}\mu\text{V} \\
 &&& \text{for } 0 \text{ MHz} < f < 50 \text{ MHz}
 \end{aligned}$$

This optimization problem is solved with the optimization type gradient embedded in the ADS circuit simulation of Keysight Technologies. Leveraging our novel equivalent circuit model, the complete optimization process only took 50 s of CPU time and yielded the following values: $L_{LP} = 504.851 \text{ nH}$ and $C_{LP} = 14.9035 \text{ nF}$. To manufacture the optimized oscillator, the following commercially available values were selected: $L_{LP} = 560 \text{ nH}$ and $C_{LP} = 15 \text{ nF}$. Adding this filter leads to a great improvement of the design, making it more ESD robust. Indeed, from Figs. 2.19 and 2.20 we observe a more cleanly oscillating signal, without additional spectral components at lower frequencies. This leads to a faster recovery

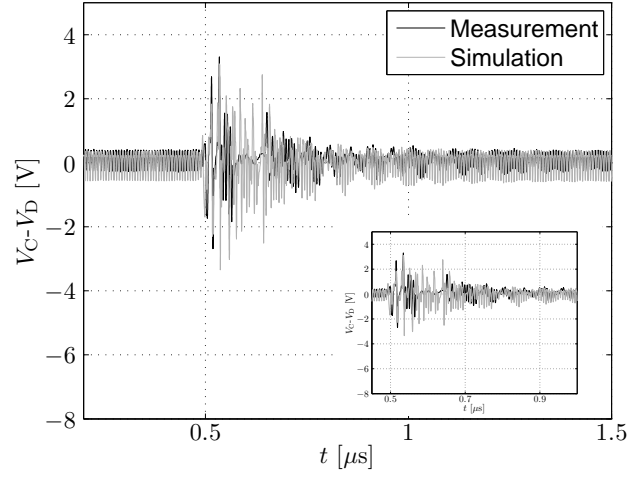


Figure 2.15: Disturbance at the output voltage of the 145 MHz oscillator when injecting at island two with an ESD pulse of 1 kV at $t = 500$ ns (measurement: black solid; simulation: grey solid line). A zoom on the first $1 \mu\text{s}$ is included in the inset.

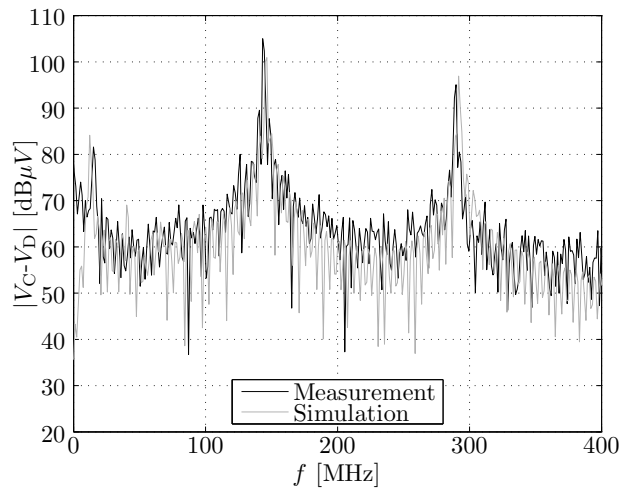
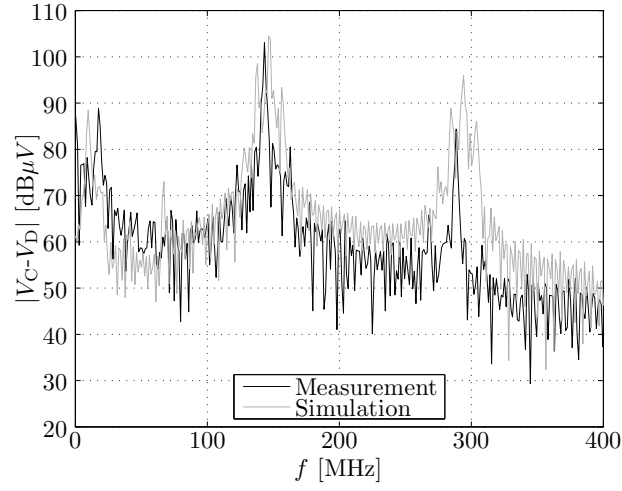
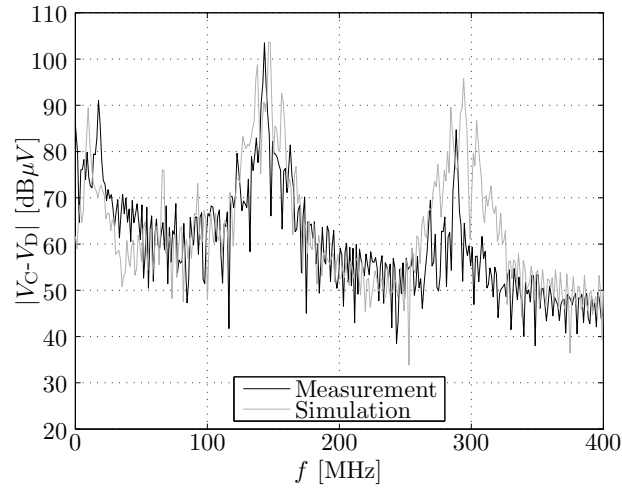


Figure 2.16: Disturbance of a 145 MHz oscillator when injecting at island two with an ESD pulse of 500 V. The FFT is taken between $1.1 \mu\text{s}$ and $1.7 \mu\text{s}$.

time of the oscillator after the ESD pulse is removed. Moreover, we also notice that the maximum peak voltage in this situation is much lower than in the case



(a)



(b)

Figure 2.17: Disturbance of a 145 MHz oscillator when injecting at island two with an ESD pulse of 1 kV (a) and in the case of an ESD pulse of 2 kV (b). In both cases the FFT is taken between 1.1 μ s and 1.7 μ s.

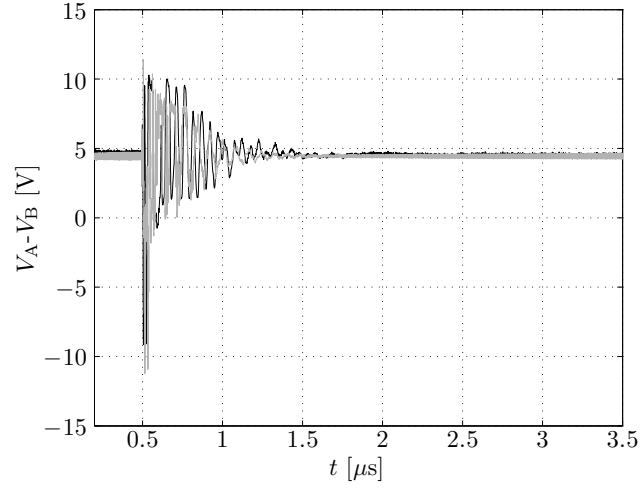


Figure 2.18: Disturbance of the voltage between the oscillator's nodes A and B when injecting at island two with an ESD pulse of 1 kV at $t = 500$ ns (measurement: black solid; simulation: grey solid line).

without the low-pass filter, which also adds to the immunity of the circuit.

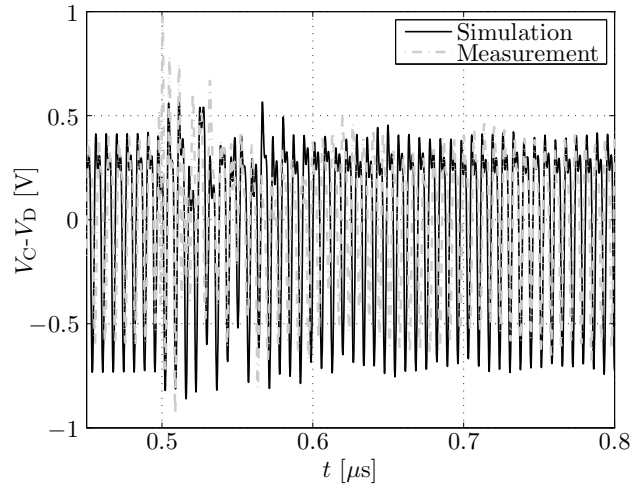


Figure 2.19: Measurement of the disturbance of a 145 MHz oscillator with low-pass filter when injecting at island two with an ESD pulse of 500 V.

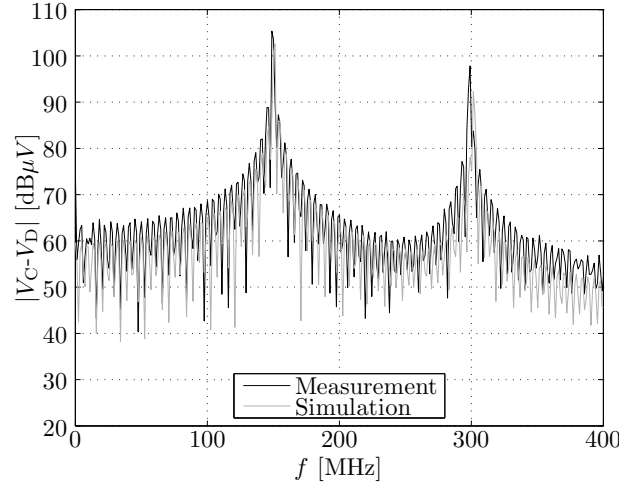


Figure 2.20: Disturbance of a 145 MHz oscillator with a low-pass filter in the protection circuit, by injecting at island two with an ESD pulse of 500 V. The FFT is taken between 1.1 μ s and 1.7 μ s.

2.4 Conclusion

In this chapter, we have presented a circuit model strategy for the entire ISO 10605 field coupled ESD test setup. Novel circuit models for the ESD gun and the test bench were concatenated with pertinent equivalent circuits of the load box and the DUT. The model, which was extensively validated by means of measurements, allows to efficiently and accurately predict the behavior of the DUT in the pre-compliance phase. As an example, a nonlinear DUT i.e. a negative-resistance oscillator with ESD protection diodes, was investigated. Additionally, we demonstrated that our proposed circuit model may be advantageously used for the optimization of DUTs, making them more immune against ESD disturbances. It can be concluded that the advanced approach is useful to effectively troubleshoot and solve problems using the ISO 10605 field coupled ESD testing.

References

- [1] *DC-10614 EMC Performance Requirements - Components*, 2005.
- [2] *ISO 10605 Road Vehicles Test Methods for Electrical Disturbances from Electrostatic Discharge*, 2008.
- [3] *IEC 62132-4, Integrated Circuits, Measurement of Electromagnetic Immunity, 150 kHz to 1 GHz Part 4 Direct RF Power Injection Method*, ed. 1.0, February 2006. IEC.
- [4] D. Vande Ginste, D. De Zutter, H. Rogier, and H. Poes, "Efficient Analysis and Design Strategies for Radio Frequency Boards Dedicated to Integrity Monitoring of Integrated Circuits Using an Electromagnetic Circuit Co-Design Technique", *IET Science, Measurement & Technology*, vol. 4, no. 5, pp. 268–277, 2010.
- [5] *ISO 11452-4, Road Vehicles, Component Test Methods for Electrical Disturbances from Narrowband Radiated Electromagnetic Energy Part 4, Bulk Current Injection (BCI)*, 2005.
- [6] A. Orlandi, "Circuit Model for Bulk Current Injection Test on Shielded Coaxial Cables", *IEEE Transactions on Electromagnetic Compatibility*, vol. 45, no. 4, pp. 602–615, 2003.
- [7] A. Orlandi, G. Antonini, and R. M. Rizzi, "Equivalent Circuit Model of a Bundle of Cables for Bulk Current Injection (BCI) Test", *IEEE Transactions on Electromagnetic Compatibility*, vol. 48, no. 4, pp. 701–713, 2006.
- [8] F. Grassi, F. Marliani, and S. A. Pignari, "Circuit Modeling of Injection Probes for Bulk Current Injection", *IEEE Transactions on Electromagnetic Compatibility*, vol. 49, no. 3, pp. 563–576, 2007.
- [9] A. Durier, H. Poes, D. Vande Ginste, M. Chernobryvko, C. Gazda, and H. Rogier, "Novel Modeling Strategy for a BCI Set-Up Applied in an Automotive Application: An Industrial Way to Use EM Simulation Tools to Help Hardware and ASIC Designers to Improve Their Designs for Immunity Tests", Dubrovnik, Croatia, 2011, pp. 41–46.
- [10] G. Shen, S. Yang, V. V. Khilkevich, D. J. Pommerenke, H. L. Aichele, D. R. Eichel, and C. Keller, "ESD Immunity Prediction of D Flip-Flop in the ISO 10605 Standard Using a Behavioral Modeling Methodology", *IEEE Trans. Electromagn. Compat.*, vol. 57, no. 4, pp. 651–659, 2015.
- [11] *IEC 61000-4-2 Ed. 2.0 Electromagnetic Compatibility (EMC) Part 4-2, Testing and Measurement Techniques Electrostatic Discharge Immunity Test*, 2008.

- [12] M. Rizvi and J. L. Vetri, "ESD Source Modeling in FDTD", in *Proceedings of IEEE Symposium on Electromagnetic Compatibility*, Chicago, IL, USA, 1994, pp. 77–82.
- [13] K. Wang, D. Pommerenke, and R. Chundru, "Numerical Modeling of ESD-Simulators", vol. 1, Minneapolis, MN, USA, 2002, pp. 93–98.
- [14] K. Wang, D. Pommerenke, R. Chundru, T. Van Doren, J. Drewniak, and A. Shashindranath, "Numerical Modeling of Electrostatic Discharge Generators", *IEEE Transactions on Electromagnetic Compatibility*, vol. 45, no. 2, pp. 258–271, 2003.
- [15] T. Takada, T. Sekine, and H. Asai, "Hybrid Simulation of ESD Events by SPICE-like and Finite-Difference Time-Domain Methods", *2013 IEEE Electrical Design of Advanced Packaging Systems Symposium (EDAPS)*, 2013.
- [16] J. Koo, Q. Cai, G. Muchaidze, A. Martwick, K. Wang, and D. Pommerenke, "Frequency-Domain Measurement Method for the Analysis of ESD Generators and Coupling", *IEEE Transactions on Electromagnetic Compatibility*, vol. 49, no. 3, pp. 504–511, 2007.
- [17] H. Tanaka, O. Fujiwara, and Y. Yamanaka, "A Circuit Approach to Simulate Discharge Current Injected in Contact With an ESD-Gun", in *Proc. 3rd International Symposium on Electromagnetic Compatibility*, Beijing, China, 2002, pp. 486–489.
- [18] T. Sekine, H. Asai, and J. S. Lee, "Unified Circuit Modeling Technique for the Simulation of Electrostatic Discharge (ESD) Injected by an ESD Generator", *IEEE International Symposium on Electromagnetic Compatibility*, 2012.
- [19] R. Dengler, "Self Inductance of a Wire Loop as a Curve Integral", Cornell university library, Tech. Rep., 2013.
- [20] C. R. Paul, *Analysis of Multiconductor Transmission Lines*. J. Wiley and Sons, New York and Sons, New York, 1994.
- [21] M. Chernobryvko, D. Vande Ginste, and D. De Zutter, "A Two-Step Perturbation Technique for Nonuniform Single and Differential Lines", *IEEE Transactions on Microwave Theory and Techniques*, vol. 61, no. 5, pp. 1758–1767, 2013.
- [22] M. Chernobryvko, D. De Zutter, and D. Vande Ginste, "Nonuniform Multiconductor Transmission Line Analysis by a Two-Step Perturbation Technique", *IEEE Transactions on Components, Packaging and Manufacturing Technology*, vol. 4, no. 11, pp. 1838–1846, 2014.
- [23] T. Demeester and D. De Zutter, "Quasi-TM Transmission Line Parameters of Coupled Lossy Lines Based on the Dirichlet to Neumann Boundary Operator", *IEEE Transactions on Microwave Theory and Techniques*, vol. 56, no. 7, pp. 1649–1660, 2008.

- [24] S. Grivet-Talocia and M. Bandinu, “Improving the Convergence of Vector Fitting for Equivalent Circuit Extraction from Noisy Frequency Responses”, *IEEE Transactions on Electromagnetic Compatibility*, vol. 48, no. 1, pp. 104–120, 2006.
- [25] G. Antonini, “SPICE Equivalent Circuits of Frequency-Domain Responses”, *IEEE Transactions on Electromagnetic Compatibility*, vol. 45, no. 3, pp. 502–512, 2003.
- [26] D. Deschrijver, B. Haegeman, and T. Dhaene, “Orthonormal Vector Fitting: A Robust Macromodeling Tool for Rational Approximation of Frequency Domain Responses”, *IEEE Transactions on Advanced Packaging*, vol. 30, no. 2, pp. 216–225, 2007.
- [27] F. Ellinger, *Radio Frequency Integrated Circuits and Technologies*. Springer Science and Business Media, 2008.

3

Modeling Transient Electrical Disturbances by Inductive Coupling for the ISO 7637-3 ICC Test

Based on “Modeling Transient Electrical Disturbances by Inductive Coupling for the ISO 7637-3 ICC Test,” N. Lambrecht, H. Pues, D. De Zutter, and D. Vande Ginste, in *EMC Europe 2017*, Angers, France, 4-8 Sept. 2017, pp. 75–77.

★ ★ ★

In this chapter, we model the inductive current clamp (ICC) method described in the ISO 7637-3 standard, where we apply a broadband transient signal as disturbance. To validate the advocated model, a nonlinear device under test (DUT) is simulated, manufactured and measured under the ISO 7637-3 standard test conditions. Furthermore, it is shown that the proposed model can be used to study the DUT's immunity.

3.1 Introduction

For designers of electronic circuits and equipment, it is of utmost importance that, early in the design phase, the electromagnetic compatibility (EMC) behavior of their novel devices and systems can be efficiently predicted. This avoids expensive iterations in later stages of the design cycle, costly and time consuming measurements and troubleshooting and hence, it reduces time to market of the products,

leading to more cost effective development. To accomplish this, modeling of EMC tests has become indispensable. The EMC test discussed in this chapter is the inductively coupling clamp method (ICC). In contrast to the bulk current injection test (BCI) [1]–[5], which is a narrowband EMC test, the ICC test is a broadband EMC test where slow transient pulses are inductively coupled to the wire harness that connects the load simulator to the device under test (DUT). The slow transient pulses mimic typical disturbances that occur as a result of an interruption of circuits with an inductive load, such as a radiator fan motor, air conditioning compressor clutch, etc. These slow transient pulses are described in [6].

In this chapter, we propose a circuit equivalent model for the ISO 7637-3 ICC test, which is capable to deal with transient pulses as described in [6]. In the automotive industry, the aforementioned test is used for testing active sensor IC's. Hence, we will demonstrate that the presented model is able to deal with active nonlinear components and can easily be integrated with advanced optimization and troubleshooting techniques. The method is thoroughly validated by means of measurements and its appositeness for rapid EMC analysis of the DUT, here, by way of example, being a low drop-out voltage regulator (VR), is shown.

The remainder of this chapter is organized as follows. In Section 3.2, a thorough description of the ICC test is given. The modeling techniques for the inductive coupling clamp and ICC test bench are explained in Section 3.3. Section 3.4 deals with the validation of the developed circuit model, via comparison with measurements using a nonlinear active DUT. Finally, some concluding remarks are formulated in Section 3.5.

3.2 Description of the Inductive Coupling Clamp Test

The default ICC test setup is depicted in Fig. 3.1. The test bench itself consists of a large metal plate, which acts as a ground plane. The coupling circuit consists of an ICC that contains all signal lines except for the ground wire (see also Fig. 3.4). Both the DUT and the wire harness are placed on a non-conductive, low relative permittivity material ($\epsilon_r \leq 1.4$), at (50 ± 5) mm above the ground plane. The length of the wire harness is (1700 ± 300) mm. The center of the ICC is placed at (150 ± 50) mm from the connector of the DUT. The transient pulses generated by the transient pulses generator are the slow transient pulses depicted in Fig. 3.2. A negative transient pulse may be realized by switching the generator output connection. A transient pulse is typically described by a double-exponential pulse (3.1) with parameters α , β and U_0 as follows.

$$v_s(t) = U_0 (e^{-\alpha t} - e^{-\beta t}). \quad (3.1)$$

The transformation to the physical parameters such as rise time t_r , pulse width t_d and maximum amplitude U_s , as shown in Fig. 3.2, into the parameters α , β and U_0 is given in [7] and these relations are used in this chapter. A more detailed

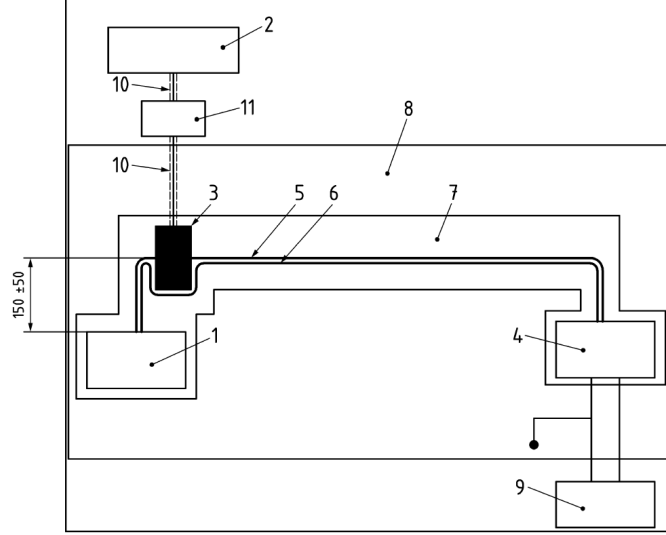


Figure 3.1: The default ISO 7637-3 inductive coupling clamp test setup [6], where 1=DUT, 2=transient pulses generator, 3=inductive coupling clamp (ICC), 4=load simulator, 5=test harness, 6=ground wire, 7=insulation, 8=ground plane, 9=power supply, 10=50Ω coaxial cable and 11=matching network (optional).

description of these parameters is found in appendix C

In [6] different test levels are defined to apply in the ICC test. In this chapter, we will test our examples at test level III, as this test level is sufficient to cause disturbance of the DUT and to prevent damage of the voltage probe. This test level is adjusted in a calibration setup as depicted in Fig. 3.3, so that the measured voltage peak = 5 V, measured pulse duration = $7 \mu s \pm 30\%$ and measured rise time = $\leq 1.2 \mu s$. To meet these requirements, we had to set $U_S = 14 V$ and the internal resistor of the generator, $R_i = 10 \Omega$, but no matching network was necessary thanks to the well adapted frequency characteristics of our injection probe. The rise time of $v_s(t)$ is defined in ISO 7637-3 as $1 \mu s$ and the time duration of $v_s(t)$ is defined as $50 \mu s$.

3.3 Modeling of the Inductive Coupling Clamp Test

In this section, circuit models for the coupling clamp and test bench are presented. When validating these models in Section 3.4 for a non-linear DUT, all necessary circuit models are imported into Keysight's Advanced Design System (ADS). The time-domain circuit solver of ADS allows for the easy combination of classical lumped element circuits; active circuitry; parts of circuits specified by S-parameters and

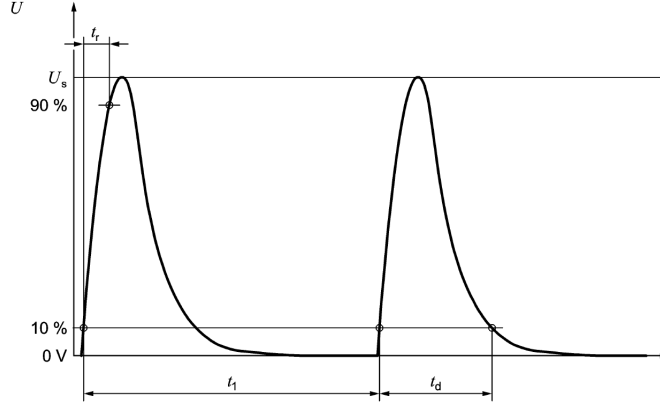


Figure 3.2: Slow transient pulse Positive 2a [6].

multiconductor transmission lines characterized by their per-unit-of-length resistance, inductance, conductance and capacitance parameters (i.e. RLGC-models). Such an RLGC-model is used for the workbench (see below). Of course, other solvers such as HSPICE can be used as well.

3.3.1 Modeling of the inductive coupling clamp

This section deals with the model of the ICC probe shown in Fig. 3.4. From this, a schematic diagram was made, inspired by [1], which is depicted in Fig. 3.5. Here, the coupling between the ICC clamp and wires 1 to N is represented by the mutual coupling inductances M_{1p} to M_{Np} . The N-connector of the ICC clamp is taken into account by means of L_N and C_N . Parameters C_{W1} and L_{W1} denote the total capacitance and inductance of the ICC clamp itself. The inductance of the ICC probe is named L_p . This inductance is frequency dependent as the windings of L_p are wound around the ferrite core of the ICC clamp. Due to the presence of the ferrite core, the complex frequency-dependent, self-inductances $L_p(\omega)$, $L_{ii}(\omega)$ and mutual inductances $M_{ip}(\omega)$ can be expressed as functions of the reluctance of the ferrite core $R(\omega)$ as [1], [8]:

$$L_p(\omega) = \frac{N_p^2}{R(\omega)} \quad (3.2)$$

$$L_{ii}(\omega) = \frac{1}{R(\omega)} + L_{id} \quad (3.3)$$

$$M_{ip}(\omega) = \frac{N_p}{R(\omega)} \quad (3.4)$$

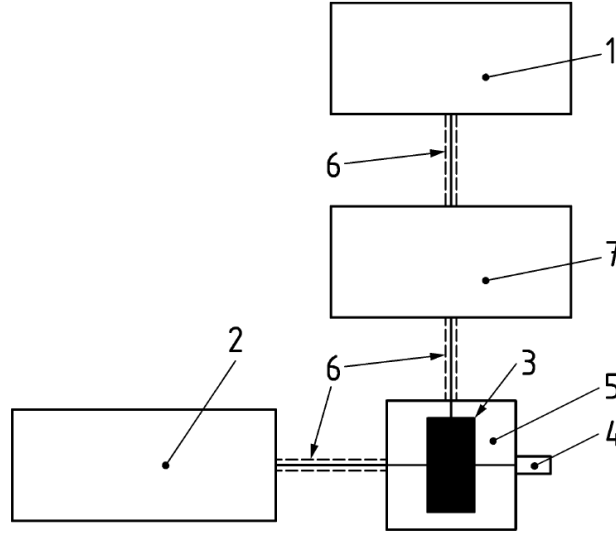


Figure 3.3: Set-up for transient pulses level adjustment [6], where 1=transient pulse generator, 2=high impedance oscilloscope, 3=inductive coupling clamp (ICC), 4=short circuit, 5=calibration fixture, 6=50 Ω coaxial cable, 7=matching network (optional).

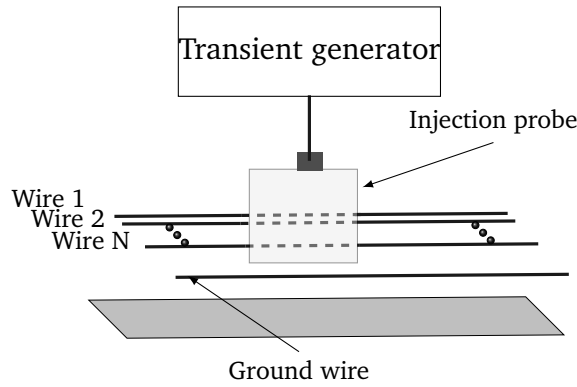


Figure 3.4: Inductive coupling clamp with multi-conductor transmission line.

where N_p denotes the number of turns of the primary winding and L_{id} is the total self-inductance of the wire with respect to the inner surface of the ferrite core. Estimation of the reluctance $R(\omega)$ requires the knowledge of the relative permeability of the ferrite core. This is obtained by measuring the probe input impedance $Z_{in}(\omega)$ in absence of the secondary circuit. By equating this measured impedance with the expression of the probe input impedance derived from the circuit model

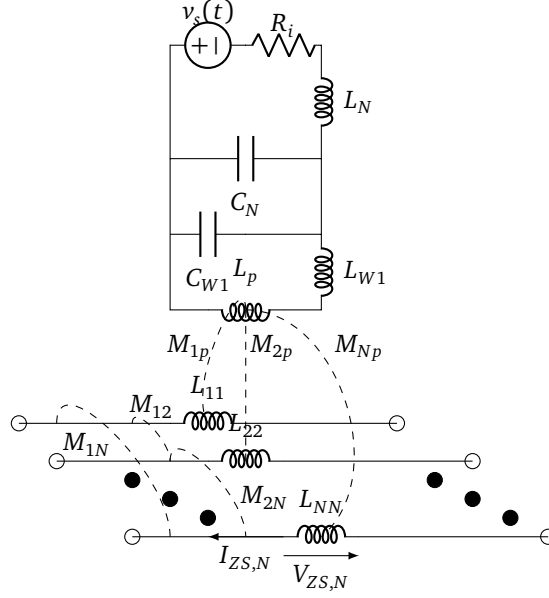


Figure 3.5: Schematic view of the injection probe with $C_N = 4$ pF, $L_N = 3$ nH, $C_{W1} = 1.7$ pF, $L_{W1} = 32.5$ nH.

in Fig. 3.5 (in absence of the secondary circuit), the following expression for the complex self-inductance $L_p(\omega)$ is obtained [1]:

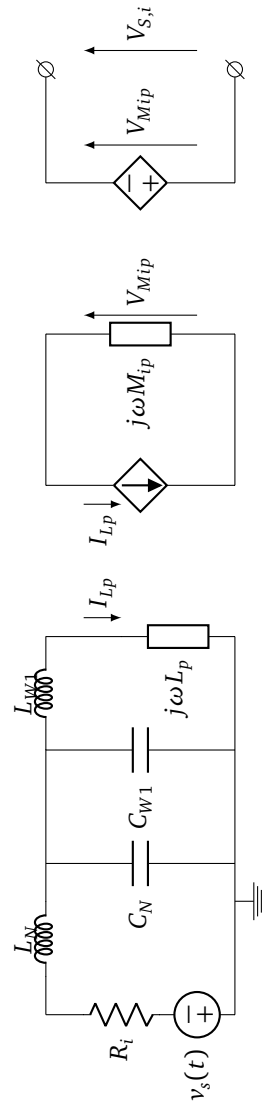
$$L_p(\omega) = \frac{1}{D} (Z_{in}(\omega) - j\omega(L_N + L_{W1}) - \omega^2 L_{W1} (C_N + C_{W1}) [Z_{in}(\omega) - j\omega L_N]), \quad (3.5)$$

where

$$D = j\omega(1 + j\omega(C_N + C_{W1})[-Z_{in}(\omega) + j\omega L_N]). \quad (3.6)$$

The frequency behavior of the reluctance of the magnetic core $R(\omega)$ is then recovered via (3.2), and consequently, the self- and mutual inductances L_{ii} and M_{ip} are obtained via (3.3) and (3.4). The mutual inductance between the wires M_{ij} and total self-inductance of the wire with respect to the inner surface of the ferrite core L_{id} are obtained by using the technique described in [9].

From Fig. 3.5, the coupling between the probe and the multi-wire transmission line is written as

Figure 3.6: Equivalent schematic of the induced voltage $V_{S,i}$ in the wire.

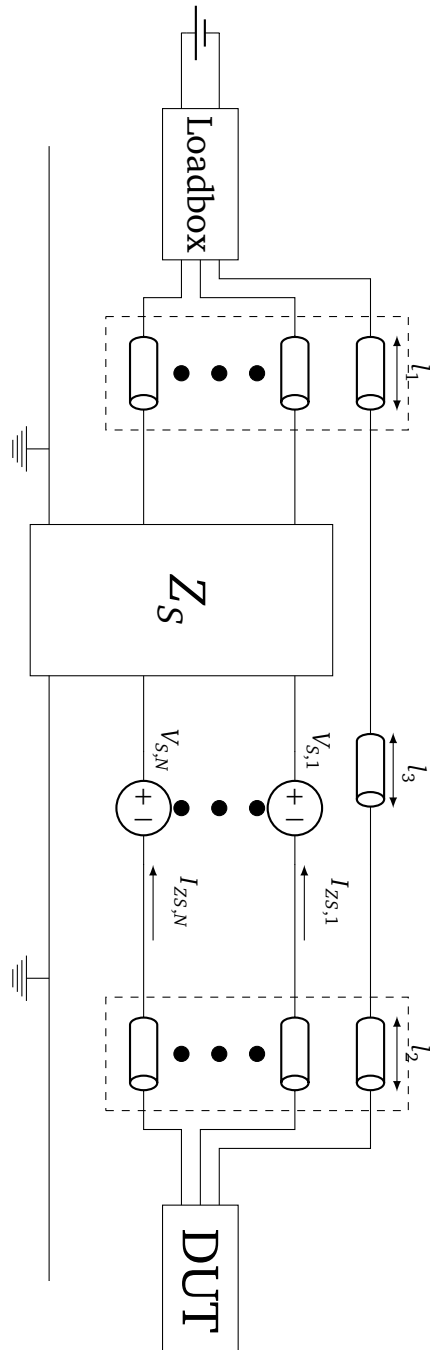


Figure 3.7: Proposed model of the ISO 7637-3 inductive coupling clamp test.

$$\begin{aligned}
V_{ZS,1} &= j\omega(L_{11}I_{ZS,1} - M_{12}I_{ZS,2} - \cdots - M_{1N}I_{ZS,N}) \\
&\quad - j\omega M_{1p}I_{Lp} \\
V_{ZS,2} &= j\omega(-M_{12}I_{ZS,1} + L_{22}I_{ZS,2} - \cdots - M_{2N}I_{ZS,N}) \\
&\quad - j\omega M_{2p}I_{Lp} \\
&\vdots \\
V_{ZS,N} &= j\omega(-M_{1N}I_{ZS,1} + M_{2N}I_{ZS,2} - \cdots - L_{NN}I_{ZS,N}) \\
&\quad - j\omega M_{2p}I_{Lp}
\end{aligned}$$

where $V_{ZS,i}$ is the voltage across self-inductor L_{ii} , $I_{ZS,i}$ is the current through L_{ii} and I_{Lp} is the current through L_p . This is rewritten in matrix form as

$$\mathbf{V}_{ZS} = \mathbf{Z}_S \mathbf{I}_{ZS} - \mathbf{V}_S \quad (3.7)$$

with $\mathbf{I}_{ZS} = [I_{ZS,1}, \dots, I_{ZS,N}]^T$, $\mathbf{V}_{ZS} = [V_{ZS,1}, \dots, V_{ZS,N}]^T$ and $\mathbf{V}_S = [V_{S,1}, \dots, V_{S,N}]^T$, and where

$$V_{S,i} = j\omega M_{ip}I_{Lp}, \quad (3.8)$$

$$Z_{S,ii} = j\omega L_{ii}, \quad i = j \quad (3.9)$$

$$Z_{S,ij} = -j\omega M_{ij}, \quad i \neq j. \quad (3.10)$$

Hence, we model the inductive current clamp as an impedance matrix in series with a voltage source at every wire that is clamped by the ICC. Here, the equivalent circuit model of the voltage source $V_{S,i}$, i.e. at the i th wire, is depicted in Fig. 3.6.

3.3.2 Modeling of the test bench

To take the long wire harness into account, we model it as a multiconductor transmission line (MTL). Thereto, we apply the same method as in [10]. The corresponding equivalent circuit is shown in Fig. 3.7, where $l_1=1.48$ m, $l_2=0.15$ m and $l_3=0.07$ m. In the ICC test, the ground wire of the DUT is typically not included in the ICC clamp and runs next to it (see Fig. 3.7). The load box and the DUT are connected to the two ends of the wire harness. The load box is a passive impedance,

readily characterized by means of S-parameter measurements or simulations, and it is described in the EMC test plan. At the other end of the wire harness, the DUT is connected. The nonlinear DUT considered here, is described further in Section 3.4. In Fig. 3.7, we represent the model of the ICC clamp with its impedance matrix and its equivalent series voltage sources at every wire that is clamped by the ICC clamp.

3.4 Validation of the Model Using a Nonlinear DUT

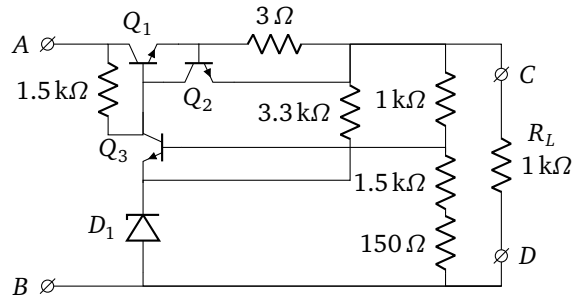


Figure 3.8: Schematic of the controlled series VR.

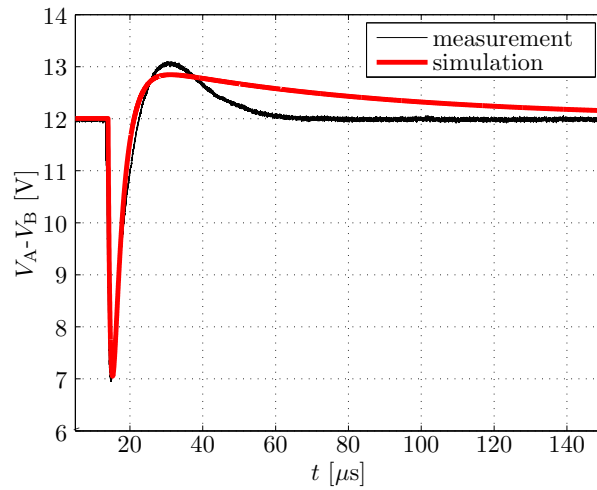


Figure 3.9: Disturbance voltage between nodes A and B when injecting a slow transient pulse for a 12 V system of test level III as defined in [6].

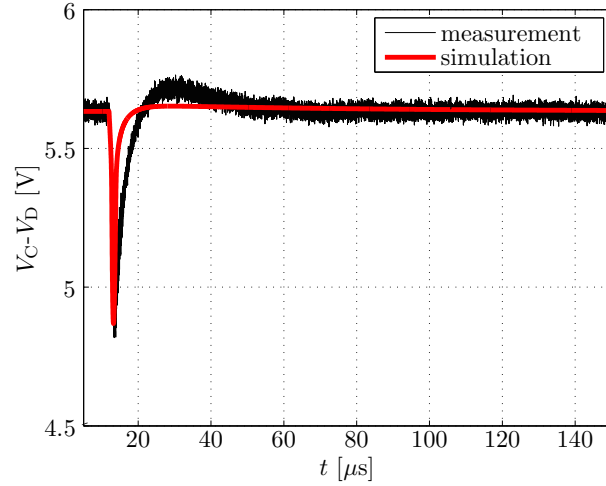


Figure 3.10: Disturbance voltage between nodes C and D when injecting a slow transient pulse for a 12 V system of test level III as defined in [6].

To validate and illustrate the appositeness of our proposed model, we apply it to a nonlinear DUT and compare it with measurements. The DUT is a low drop-out voltage regulator (VR) (from 12 V to 5 V) with schematic shown in Fig. 4.11. This DUT was also used in [11] to validate the modeling of the RI-130 test [12]. We choose to use a voltage regulator as DUT here and in the following chapters, as a voltage regulator is a very common used device in the automotive sector. This because the 13.8 V voltage of a car battery is not pretty unstable. For this case, the ground wire from the load box to node B of the DUT is not included in the clamp and the wires connecting the load box to node A and C are both included in the ICC clamp. So, we have $N=2$ wires included in the clamp and one next to it.

To validate, we perform a measurement of the voltages between nodes A and B and between nodes C and D . Here, we inject a slow transient pulse for a 12 V system of test level III as defined in [6]. Readers interested in more details on the modelling of real world multiconductor cables can find more details in [13].

Obviously, one cannot expect the circuit model data to exactly correspond with the measurements, as our model of the DUT has limited accuracy. Still, as clearly demonstrated in Figs. 3.9 and 3.10, the proposed model predicts all salient features of the output signal, and in particular the magnitude of the disturbance's main peak is accurately modeled. This is of critical importance and it allows the circuit designer to analyze the immunity of his/her circuit during the design phase.

3.5 Conclusion

In this chapter, we modeled the ISO 7637-3 ICC test and made a circuit equivalent model for it, capable of dealing with transient signals as described in [6]. The proposed model, which was validated by means of measurements, allows to efficiently and accurately predict the behavior of the DUT during the design phase. As an example of a nonlinear DUT, a voltage regulator was used.

References

- [1] F. Grassi, F. Marliani, and S. A. Pignari, "Circuit Modeling of Injection Probes for Bulk Current Injection", *IEEE Transactions on Electromagnetic Compatibility*, vol. 49, no. 3, pp. 563–576, 2007.
- [2] A. Orlandi, "Circuit Model for Bulk Current Injection Test on Shielded Coaxial Cables", *IEEE Transactions on Electromagnetic Compatibility*, vol. 45, no. 4, pp. 602–615, 2003.
- [3] A. Orlandi, G. Antonini, and R. M. Rizzi, "Equivalent Circuit Model of a Bundle of Cables for Bulk Current Injection (BCI) Test", *IEEE Transactions on Electromagnetic Compatibility*, vol. 48, no. 4, pp. 701–713, 2006.
- [4] A. Durier, H. Pues, D. Vande Ginste, M. Chernobryvko, C. Gazda, and H. Rogier, "Novel Modeling Strategy for a BCI Set-Up Applied in an Automotive Application: An Industrial Way to Use EM Simulation Tools to Help Hardware and ASIC Designers to Improve their Designs for Immunity Tests", in *2011 8th Workshop on Electromagnetic Compatibility of Integrated Circuits*, Dubrovnik, Croatia, 2011, pp. 41–46.
- [5] F. Grassi, G. Spadacini, and S. A. Pignari, "Time-Domain Response of Bulk Current Injection Probes to Impulsive Stress Waveforms", in *2015 IEEE International Symposium on Electromagnetic Compatibility (EMC)*, Dresden, Germany, 2015, pp. 843–848.
- [6] *ISO 7637-3 Road Vehicles, Electrical Disturbances from Conduction and Coupling, Part 3, Electrical Transient Transmission by Capacitive and Inductive Coupling via Lines Other than Supply Lines*, 2014.
- [7] M. Magdowski and R. Vick, "Estimation of the Mathematical Parameters of Double-Exponential Pulses Using the Nelder-Mead Algorithm", *IEEE Transactions on Electromagnetic Compatibility*, vol. 52, no. 4, pp. 1060–1062, 2010.
- [8] E. C. Snelling, *Soft Ferrites, Properties and Applications*. London: Illife Books, 1969.
- [9] T. Demeester and D. De Zutter, "Quasi-TM Transmission Line Parameters of Coupled Lossy Lines Based on the Dirichlet to Neumann Boundary Operator", *IEEE Transactions on Microwave Theory and Techniques*, vol. 56, no. 7, pp. 1649–1660, 2008.
- [10] N. Lambrecht, C. Gazda, H. Pues, D. De Zutter, and D. Vande Ginste, "Efficient Circuit Modeling Technique for the Analysis and Optimization of ISO 10605 Field Coupled Electrostatic Discharge (ESD) Robustness of Nonlinear Devices", *IEEE Transactions on Electromagnetic Compatibility*, vol. 58, no. 4, pp. 971–980, 2016.

- [11] N. Lambrecht, H. Pues, D. De Zutter, and D. Vande Ginste, “Modeling of Contact Bounce in a Transient Electromagnetic Compatibility Test for the Analysis and Optimization of Nonlinear Devices”, *IEEE Transactions on Electromagnetic Compatibility*, pp. 1–4, 2016.
- [12] *FMC1278, Electromagnetic Compatibility Specification for Electrical and Electronic Components and Subsystems*, www.fordemc.com/docs/download/FMC1278.pdf, Ford, Oct. 2016.
- [13] P. Manfredi, D. De Zutter, and D. Vande Ginste, “Analysis of Nonuniform Transmission Lines With an Iterative and Adaptive Perturbation Technique”, *IEEE Transactions on Electromagnetic Compatibility*, vol. 58, no. 3, pp. 859–867, 2016.

4

A Circuit Modeling Technique for the ISO 7637-3 Capacitive Coupling Clamp Test

Based on “A Circuit Modeling Technique for the ISO 7637-3 Capacitive Coupling Clamp Test,” N. Lambrecht, H. Pues, D. De Zutter, and D. Vande Ginste, *IEEE Transactions on Electromagnetic Compatibility*, vol. 60, no. 4, pp. 858-865, 2018.

★ ★ ★

In this chapter, we propose a transmission line modeling technique for the ISO 7637-3 Capacitive Coupling Clamp (CCC) test. Besides modeling the test bench, special attention is devoted to the capacitive coupling clamp itself, for which an equivalent circuit is constructed based on the concept of surface transfer impedance and surface transfer admittance. The overall model is validated by means of measurements using a nonlinear circuit as device-under-test (DUT), as such demonstrating the appositeness to mimick the CCC test in simulations during the design phase.

4.1 Introduction

Electrical fast transient (EFT) disturbances represent one of the most serious threats to the operation of electronic systems. The electromagnetic (EM) energy resulting from an EFT event easily couples to cables connected to electronic equipment. Consequently, voltage pulses appear at the electronic system's ports, adversely affecting signal integrity and causing operation upsets. These effects are expected to become worse due to the continuous miniaturization trend in Integrated Circuits

(IC) manufacturing and the resulting reduction of power supply voltages that are making electronic systems even more vulnerable.

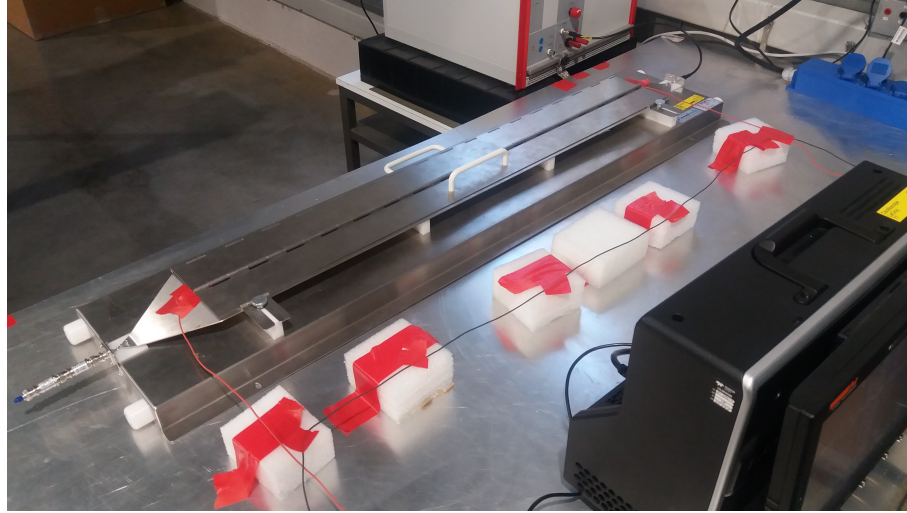
Recognizing the importance of EFTs for designers, whose aim is to achieve electromagnetic compatibility (EMC) of equipment, international standards — such as the International Electrotechnical Commission (IEC) 61000-4-4 — have been developed to provide test methods for the characterization of electronic system immunity to fast transient disturbances [1]–[3]. Such immunity tests are usually performed when the first prototype is ready or even just before production and, in case of failures, equipment reworking and redesign results in additional costs and delays. The EMC test discussed in this chapter is the ISO 7637-3 capacitive coupling clamp method [4]. The CCC test is a broadband EMC test suitable for coupling fast transient pulses, which typically occur as a result of switching processes. A first method to model the ISO 7637-3 capacitive coupling clamp is given in [5], [6], where its properties are measured and characterized by making use of a vector network analyzer. Another technique to model the injection clamp is via a full-wave approach [7] to allow reproducing the response of the device in the time domain. As full-wave simulators typically consume a lot of CPU time, an alternative way is to construct circuit models that mimic the behavior of the injection clamp [8]–[10]. However, these models were solely based on calculating mutual inductances and capacitances and do not fully encompass all transmission line effects.

In this chapter, we propose an efficient technique, using transmission line theory and the concept of surface transfer impedance and surface transfer admittance, to model the capacitive coupling clamp as well as the CCC test bench. The proposed circuit equivalent of the CCC test setup is validated by means of measurements, leveraging a nonlinear circuit as device-under-test (DUT). As such, the appropriateness to mimic the CCC test in simulations during the design phase of susceptible equipment is demonstrated.

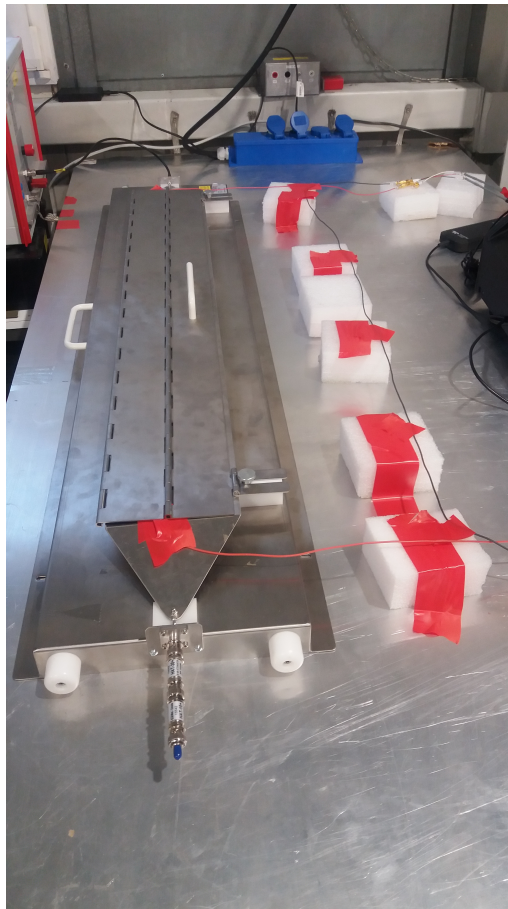
The remainder of this chapter is organized as follows. In Section 4.2, a thorough description of the CCC test is given. The modeling technique for the capacitive coupling clamp is explained in Section 4.3. The model of the CCC test bench is explained in Section 4.4. Section 4.5 deals with the validation of the developed circuit model, via comparison with measurements using a nonlinear active DUT. Finally, some concluding remarks are formulated in Section 4.6.

4.2 Description of the ISO 7637-3 Capacitive Coupling Clamp Test

The ISO 7637-3 capacitive coupling clamp test uses an injection clamp (see Fig. 4.1), which is a mechanical test fixture consisting of two metallic plates connected to each other, placed above a ground plane. As is depicted in Fig. 4.2, the wires under test are located inside the coupling clamp, i.e. between the two plates, while the other wires of the wire harness are placed at least 100 mm away from the coupling



(a)



(b)

Figure 4.1: ISO 7637-3 capacitive coupling clamp test setup. (a) Top view, (b) Side view

test fixture at a height of 50 mm above the ground plane. As in other module-level automotive EMC tests, the wire harness connects the DUT (at a height of 50 mm above the ground plane) with a load simulator (load box). The test is performed with a total harness length of 1700 mm.

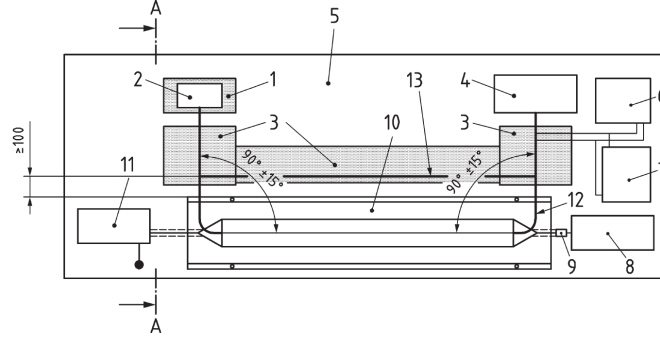


Figure 4.2: The default ISO 7637-3 capacitive coupling clamp test setup [4], where 1=insulation support, 2=DUT, 3=insulation support for test harness, 4=load simulator, 5=ground plane, 6=power supply, 7=battery, 8=oscilloscope (50Ω), 9=50Ω, 10=CCC and 11=transient pulses generator, 12=lines to be tested, 13=lines not to be tested.

An EFT generator introduces a predefined disturbance via the coupling clamp. The EFT pulse is depicted in Fig. 4.3 and is described by a traditional double-exponential pulse (4.1) where the parameters α , β and U_0 determine its shape:

$$v_s(t) = U_0 (e^{-\alpha t} - e^{-\beta t}). \quad (4.1)$$

In practice, the physical parameters such as rise time t_r , pulse width t_d and maximum amplitude U_s , indicated in Fig. 4.3, can be easily related to α , β and U_0 [11]. A more detailed description of these parameters is found in appendix C. In [4] different test levels are defined to apply in the CCC test. In this chapter, we will test with the pulse 3b shown in Fig. 4.3 at level III, as this test level is sufficient to cause disturbance of the DUT and to prevent damage of the voltage probe. This test level corresponds to the following parameter values: $U_s = 60 V$, $t_r = 5 ns$, $t_d = 0.15 \mu s$, $t_1 = 100 \mu s$, $t_4 = 10 ms$ and $t_5 = 90 ms$. These parameters correspond to $\alpha = 5.06 \cdot 10^6 Hz$, $\beta = 3.806 \cdot 10^8 Hz$ and $U_0 = 64.45$.

4.3 Modeling of the ISO 7637-3 Capacitive Coupling Clamp Test

4.3.1 Transmission line model of the injection clamp

In our model we consider the injection via the coupling clamp as a shielding problem, i.e., we look at the clamp as if it is shielding the wire harness inside it. In-

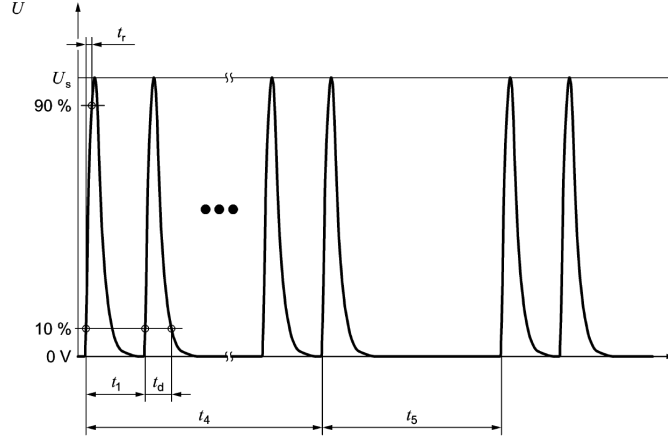


Figure 4.3: Fast transient pulse 3b [4].

spired by [12], we analyze the coupling of the field that is present between the outer surface of the clamp and the ground plane to the wire harness, by describing the problem with the help of two distinct transmission lines (TLs), i.e., an external TL and an internal TL (see Fig. 4.4). Here, the external TL consists of the ground plane and the outer surface of the clamp. This *external* line has a current I_e flowing on the exterior of the clamp and the ground plane acts as return path. This external line also has a voltage difference V_e between the exterior of the clamp and the ground plane. The internal line consists of the wire harness and the interior part of the clamp. This internal line has a current I_i flowing on the wire harness, and the internal surface of the shield acts as return path. There is also a voltage difference V_i between the wire harness and the internal surface of the shield. As discussed below, the coupling between these two TLs occurs via the surface transfer impedance Z_t and the surface transfer admittance Y_t . In this chapter, for notational conciseness, we consider a wire harness of two wires, where one wire runs inside the injection clamp and the other one runs next to it. The theory described in this chapter can however be generalized to $N > 2$ wires.

Although the cross-section of the CCC fixture has approximately a triangular shape, in this chapter, we approximate it by a rectangular cross-section (see Fig. 4.4). As the height of the opening (1 mm) is much smaller than the width of the fixture (14 cm), this approximation will have little influence on the accuracy of the model, and it expedites the simulations.

Calculation of the TLs' parameters

We start our analysis by considering the CCC as a multiconductor TL (MTL) where all voltages are defined with respect to the ground plane (Fig. 4.5). This MTL is governed by the following Telegrapher's equations:

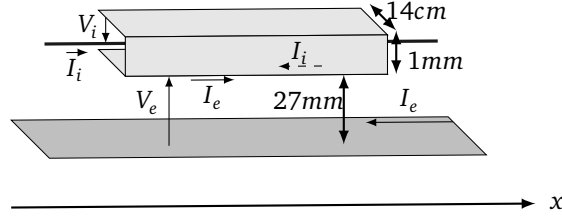


Figure 4.4: Inner and external transmission line model of the capacitive coupling clamp.

$$\frac{d}{dx} \begin{bmatrix} V_1 \\ V_2 \end{bmatrix} + \begin{bmatrix} Z_{11} & Z_{12} \\ Z_{21} & Z_{22} \end{bmatrix} \begin{bmatrix} I_1 \\ I_2 \end{bmatrix} = 0 \quad (4.2)$$

$$\frac{d}{dx} \begin{bmatrix} I_1 \\ I_2 \end{bmatrix} + \begin{bmatrix} Y_{11} & Y_{12} \\ Y_{21} & Y_{22} \end{bmatrix} \begin{bmatrix} V_1 \\ V_2 \end{bmatrix} = 0 \quad (4.3)$$

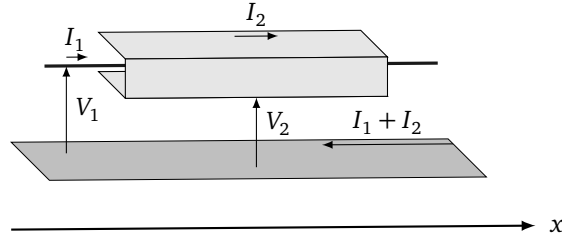


Figure 4.5: Multiconductor transmission line model of the capacitive coupling clamp.

By making use of the technique proposed in [13], we easily obtain the per-unit-length (p.u.l.) parameters, being the impedance and admittance matrices' elements Z_{ij} and Y_{ij} ($i, j=1,2$). Note that, given reciprocity, $Z_{12} = Z_{21}$ and $Y_{12} = Y_{21}$. Next, we relate the MTL of Fig. 4.5 to the situation depicted in Fig. 4.4, consisting of two distinct TLs. The internal and external TL are described by the following equations [14]:

$$\frac{d}{dx} \begin{bmatrix} V_i \\ I_i \end{bmatrix} + \begin{bmatrix} 0 & Z_i \\ Y_i & 0 \end{bmatrix} \begin{bmatrix} V_i \\ I_i \end{bmatrix} = \begin{bmatrix} 0 & Z_t \\ -Y_t & 0 \end{bmatrix} \begin{bmatrix} V_e \\ I_e \end{bmatrix} \quad (4.4)$$

$$\frac{d}{dx} \begin{bmatrix} V_e \\ I_e \end{bmatrix} + \begin{bmatrix} 0 & Z_e \\ Y_e & 0 \end{bmatrix} \begin{bmatrix} V_e \\ I_e \end{bmatrix} = \begin{bmatrix} 0 & Z_t \\ -Y_t & 0 \end{bmatrix} \begin{bmatrix} V_i \\ I_i \end{bmatrix} \quad (4.5)$$

and the coupling between the two is provided by the surface transfer impedance Z_t and the surface transfer admittance Y_t . As Fig. 4.4 on the one hand and Fig. 4.5

Table 4.1: p.u.l. parameters of CCC fixture

f [MHz]	$C_{11} \left[\frac{\text{pF}}{\text{m}} \right]$	$C_{12} \left[\frac{\text{pF}}{\text{m}} \right]$	$C_{22} \left[\frac{\text{pF}}{\text{m}} \right]$	$L_{11} \left[\frac{\text{nH}}{\text{m}} \right]$	$L_{12} \left[\frac{\text{nH}}{\text{m}} \right]$	$L_{22} \left[\frac{\text{nH}}{\text{m}} \right]$	$R_{11} \left[\frac{\text{m}\Omega}{\text{m}} \right]$	$R_{12} \left[\frac{\text{m}\Omega}{\text{m}} \right]$	$R_{22} \left[\frac{\text{m}\Omega}{\text{m}} \right]$
1	35.6	-35.6	99.3	505.2	175.1	175.1	128.1	2.9	2.9
10	35.6	-35.6	99.3	492.6	174.7	174.7	380.9	9.2	9.2
30	35.6	-35.6	99.3	490.2	174.7	174.7	651.7	15.8	15.8
60	35.6	-35.6	99.3	489.2	174.7	174.7	917.0	22.3	22.3
100	35.6	-35.6	99.3	488.6	174.6	174.6	1174.0	28.6	28.6

on the other hand describe the same system, the following relations are readily obtained

$$V_1 = V_i + V_e \quad (4.6a)$$

$$V_2 = V_e \quad (4.6b)$$

$$I_1 = I_i \quad (4.6c)$$

$$I_2 = I_e - I_i \quad (4.6d)$$

Substitution of (4.6) into (4.2) and (4.3) and identification with (4.4) and (4.5) yields

$$Z_t = Z_{22} - Z_{12} \quad (4.7a)$$

$$Y_t = Y_{11} + Y_{12} \quad (4.7b)$$

$$Z_i = Z_{22} + Z_{11} - 2Z_{12} \quad (4.7c)$$

$$Y_i = Y_{11} \quad (4.7d)$$

$$Z_e = Z_{22} \quad (4.7e)$$

$$Y_e = Y_{11} + 2Y_{21} + Y_{22} \quad (4.7f)$$

Hence, by looking at the injection clamp as an MTL (Fig. 4.5) and calculating its p.u.l. parameters, we can easily deduce the sought-for surface transfer impedance Z_t , the surface transfer admittance Y_t and the p.u.l. impedances Z_i and Z_e and admittances Y_i and Y_e of the internal and external TL respectively. Note that these p.u.l. impedances and admittances can be written as $Z_i = R_i + j\omega L_i$, $Y_i = G_i + j\omega C_i$ and $Z_e = R_e + j\omega L_e$, $Y_e = G_e + j\omega C_e$, with ω the angular frequency, R_i and R_e the p.u.l. resistances, L_i and L_e the p.u.l. inductances, G_i and G_e the p.u.l. conductances and C_i and C_e the p.u.l. capacitances of the internal and external TL respectively. For illustration we give the p.u.l. parameters of the CCC fixture up to 100 MHz (see Table 4.1). This frequency range is sufficient as the bandwidth of the signal is only about $\frac{1}{\pi 5\text{ns}} = 63.6\text{Hz}$. In our model, the small dielectric losses are neglected. It is also noticed that, up to the numerical precision of the simulations, $C_{11} = -C_{12}$ and $L_{12} = L_{22}$, which is due to the fact that conductor 1 is nearly entirely enclosed by conductor 2. For a more in depth study of the p.u.l. parameters of the CCC fixture, see appendix B. In what follows, we will use the 'weak coupling assumption' [15], neglecting the coupling of the internal TL to the external TL. This amounts to putting Z_t and Y_t to zero in (4.5) while retaining the coupling terms in (4.4).

4.3.2 The external TL

The external TL (as shown in Fig. 4.6) is given by the exterior of the clamp and the ground plane.

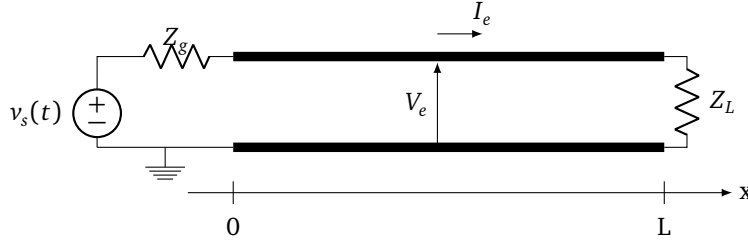


Figure 4.6: Schematic of the external TL.

In time-harmonic regime and adopting the weak coupling assumption, we obtain the following equations

$$\frac{dV_e(x)}{dx} = -Z_e I_e(x), \quad (4.8)$$

$$\frac{dI_e(x)}{dx} = -Y_e V_e(x), \quad (4.9)$$

And hence,

$$V_e(x) = Ae^{-k_e x} + Be^{k_e x}, \quad (4.10)$$

$$I_e(x) = \frac{1}{Z_{C,e}} (Ae^{-k_e x} - Be^{k_e x}), \quad (4.11)$$

with

$$Z_{C,e} = \sqrt{\frac{Z_e}{Y_e}}, \quad (4.12)$$

$$k_e = \sqrt{Z_e Y_e}. \quad (4.13)$$

The square roots in (4.12) and (4.13) are defined such that $\Im(k_e) > 0$ and $\Re(k_e) > 0$. The clamp, its far-end load Z_L , and the EFT source resistor Z_g are specified in the standards such that $Z_{C,e} = Z_g = Z_L = 50\Omega$. Hence, given this matching, $B = 0$ in (4.10) and (4.11) and $A = \frac{v_s(s)}{2}$, with $s = j\omega$, i.e. the frequency-domain equivalent of $v_s(t)$ (4.1).

4.3.3 The internal TL

To solve the internal TL we use the *chain parameter matrix* (CPM) formulation [15]. See appendix A for a brief explanation of the chain parameter matrix. This leads to the following equations

$$\begin{bmatrix} V_i(L) \\ I_i(L) \end{bmatrix} = \Phi(L) \begin{bmatrix} V_i(0) \\ I_i(0) \end{bmatrix} + \begin{bmatrix} V_{FT} \\ I_{FT} \end{bmatrix} \quad (4.14)$$

$\Phi(L)$ is the 2×2 chain parameter matrix (since we assume that only one wire runs into the injection clamp).

$$\Phi(L) = \begin{bmatrix} \frac{1}{2}(e^{k_i L} + e^{-k_i L}) & -Z_{C,i} \frac{1}{2}(e^{k_i L} - e^{-k_i L}) \\ \frac{-1}{Z_{C,i}} \frac{1}{2}(e^{k_i L} - e^{-k_i L}) & \frac{1}{2}(e^{k_i L} + e^{-k_i L}) \end{bmatrix} \quad (4.15)$$

Here, $k_i = \sqrt{Z_i Y_i}$ and $Z_{C,i} = \sqrt{\frac{Z_i}{Y_i}}$. V_{FT} and I_{FT} are the equivalent source terms at the end of the transmission line, given by

$$\begin{bmatrix} V_{FT} \\ I_{FT} \end{bmatrix} = \int_0^L \Phi(L - \tau) \begin{bmatrix} V_d(\tau) \\ I_d(\tau) \end{bmatrix} d\tau \quad (4.16)$$

where V_d and I_d are distributed voltage and current sources along the line. In our case, these distributed sources appear because of the coupling of the external TL to the internal TL by means of the transfer surface impedance and transfer surface admittance, as follows:

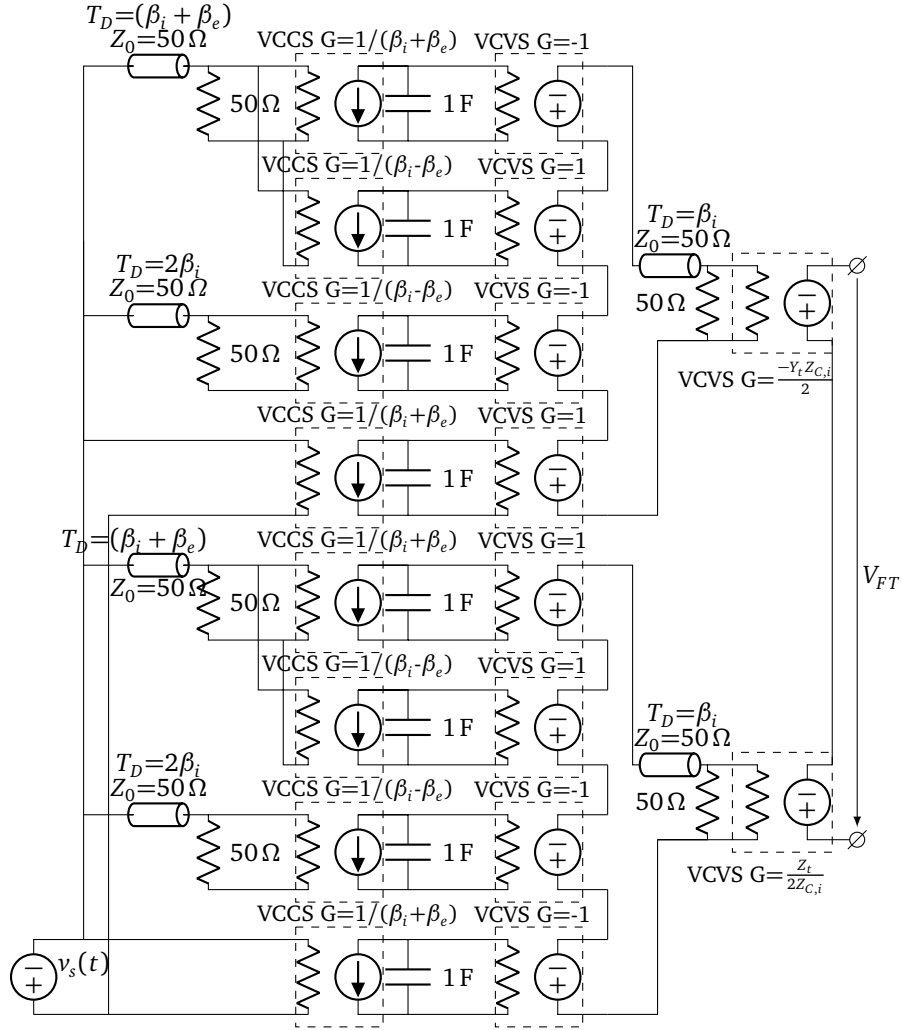
$$V_d(\tau) = Z_t I_e(\tau), \quad (4.17)$$

$$I_d(\tau) = -Y_t V_e(\tau). \quad (4.18)$$

The source terms V_{FT} and I_{FT} are expressed as:

$$\begin{aligned} V_{FT} &= \int_0^L \Phi_{11}(L - \tau) \frac{Z_t}{Z_{C,e}} V_e(\tau) d\tau \\ &\quad - \int_0^L \Phi_{12}(L - \tau) Y_t V_e(\tau) d\tau \end{aligned} \quad (4.19)$$

$$\begin{aligned} I_{FT} &= \int_0^L \Phi_{21}(L - \tau) \frac{Z_t}{Z_{C,e}} V_e(\tau) d\tau \\ &\quad - \int_0^L \Phi_{22}(L - \tau) Y_t V_e(\tau) d\tau \end{aligned} \quad (4.20)$$

Figure 4.7: Circuit model of the equivalent voltage source V_{FT} (4.23).

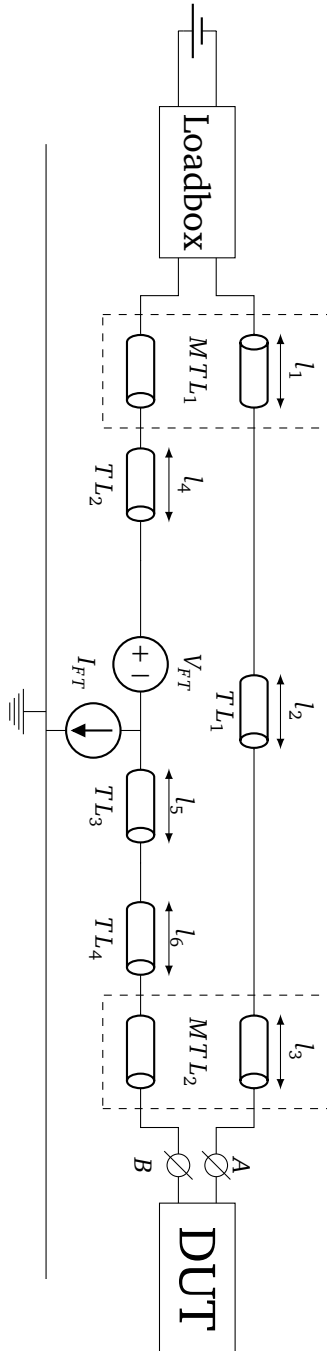


Figure 4.8: Transmission line Modeling of the ISO 7637-3 Capacitive Coupling Clamp test bench (See Table 4.2).

4.3.4 Circuit model of the equivalent source terms V_{FT} and I_{FT}

In the ISO 7637-3 [4] a *transient* signal is injected and measured at the DUT end of the CCC. In (4.19) and (4.20) we obtained an expression for the source terms V_{FT} and I_{FT} in the frequency domain. Hence, using these expressions would make it necessary to take the Fourier transformation of the injected disturbance signal, apply (4.19) and (4.20) and take the inverse Fourier transform of the result. This not only causes overhead but would also result in the occurrence of the Gibbs phenomenon due to the fast pulses. Even more importantly, this would also imply that nonlinear DUTs cannot be assessed. These issues are solved by reformulating (4.19) and (4.20) in the Laplace domain and by constructing a circuit equivalent that allows rapid transient analysis in any commercial circuit solver. Transforming (4.19) and (4.20) to the Laplace domain ($s = j\omega$), neglecting the very small losses, yields:

$$V_{FT}(s) = \int_0^L \frac{1}{2} (e^{s\beta_i(L-\tau)} + e^{-s\beta_i(L-\tau)}) e^{-s\beta_e\tau} \frac{Z_t}{Z_{C,e}} d\tau - \int_0^L -Z_{C,i} \frac{1}{2} (e^{s\beta_i(L-\tau)} - e^{-s\beta_i(L-\tau)}) Y_t e^{-s\beta_e\tau} d\tau \quad (4.21)$$

$$I_{FT}(s) = \int_0^L \frac{1}{2} (e^{s\beta_i(L-\tau)} - e^{-s\beta_i(L-\tau)}) \frac{Z_t}{Z_{C,e}} e^{-s\beta_e\tau} d\tau - \int_0^L \frac{1}{2} (e^{s\beta_i(L-\tau)} + e^{-s\beta_i(L-\tau)}) Y_t e^{-s\beta_e\tau} d\tau \quad (4.22)$$

Analytically performing the integration of (4.21) and (4.22), the following closed form is obtained for $V_{FT}(s)$ and $I_{FT}(s)$:

$$V_{FT}(s) e^{-s\beta_i L} = \frac{-Z_{C,i} Y_t v_s(s)}{2} \left[\frac{e^{-s(\beta_i+\beta_e)L} - 1}{s(\beta_i + \beta_e)} + \frac{e^{-s(\beta_i+\beta_e)L} - e^{-2s\beta_i L}}{s(\beta_i - \beta_e)} \right] + \frac{Z_t v_s(s)}{2Z_{C,i}} \left[\frac{e^{-s(\beta_i+\beta_e)L} - 1}{-s(\beta_i + \beta_e)} + \frac{e^{-s(\beta_i+\beta_e)L} - e^{-2s\beta_i L}}{s(\beta_i - \beta_e)} \right] \quad (4.23)$$

$$\begin{aligned}
I_{FT}(s)e^{-s\beta_i L} = & \frac{-v_s(s)Y_t}{2} \left[\frac{1 - e^{-s(\beta_i + \beta_e)L}}{s(\beta_i + \beta_e)} \right. \\
& + \left. \frac{e^{-s(\beta_i + \beta_e)L} - e^{-2s\beta_i L}}{s(\beta_i - \beta_e)} \right] \\
& + \frac{Z_t v_s(s)}{2(Z_{C,i})^2} \left[\frac{e^{-s(\beta_i + \beta_e)L} - 1}{s(\beta_i + \beta_e)} \right. \\
& + \left. \frac{e^{-s(\beta_i + \beta_e)L} - e^{-2s\beta_i L}}{s(\beta_i - \beta_e)} \right]
\end{aligned} \tag{4.24}$$

with $L = 1$ m, $\beta_i = \sqrt{L_i C_i}$ and $\beta_e = \sqrt{L_e C_e}$. From (4.23) and (4.24) we construct an equivalent circuit using the following Laplace domain - time-domain correspondences, $V(s)e^{-sT} \Leftrightarrow v(t - T)$ and $\frac{V(s)}{s} \Leftrightarrow \int_0^t v(t)dt$. In (4.23) and (4.24), the right-hand side and left-hand side is multiplied by a retardation operator $e^{-s\beta_i L}$. This is needed to eliminate advancing time operators $e^{+s\beta_i L}$ that appear in the right-hand sides of (4.23) and (4.24) during the integration. This retardation operator can be implemented by a simple TL model to take the delay into account. The equivalent circuit model of (4.23) is depicted in Fig. 4.7, a similar circuit for I_{FT} can be deduced from (4.24). From Fig. 4.7 it can be seen that the delay factors are modeled by a transmission line terminated by its characteristic impedance while the scaling factors are included in the voltage-controlled-current-sources (VCCS). The integration factor $1/s$ is modeled by taking a current source loaded with a capacitor of 1 F. The integrated voltage is then measured across this capacitor. This is done for every term in (4.23). Summation is obtained by placing all the voltage-controlled-voltage-sources (VCVS) in series, where an extra delay line with $T_D = \beta_i$ takes the retardation operator $e^{-s\beta_i L}$ into account.

4.4 Modeling of the Test Bench

Using the circuit equivalents of (4.23) and (4.24), we can now construct an equivalent circuit model of the entire ISO 7637-3 CCC test setup (Fig. 4.8). The CCC injection clamp that encompasses the victim wire is represented by TL_3 with propagation factor k_i and characteristic impedance $Z_{C,i}$ and voltage source V_{FT} and current source I_{FT} . TL_1 represents the wire that is placed (at least) 100 mm away from the coupling test fixture and at a height of 50 mm above the ground plane. TL_2 and TL_4 represent the parts of the victim wire outside the clamp and not running alongside the wire represented by TL_1 . MTL_1 and MTL_2 represent the two parts of the wire harness where the wires run next to each other, connected to the load box and DUT respectively. To model this wire harness as a multiconductor transmission line (MTL), we applied the same method as in [16]. The load box and the DUT are connected to the two ends of the wire harness. The load box is a

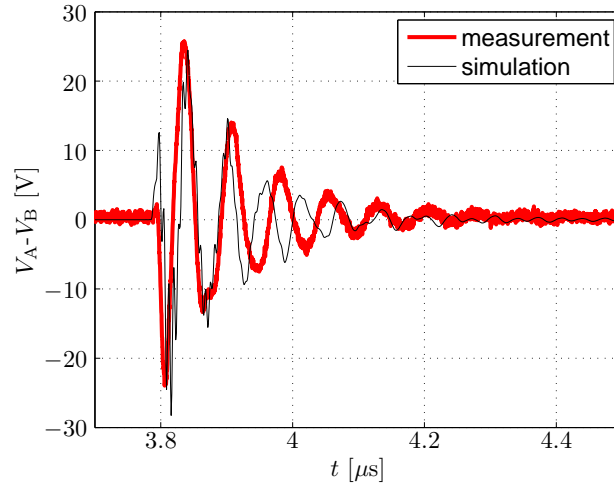
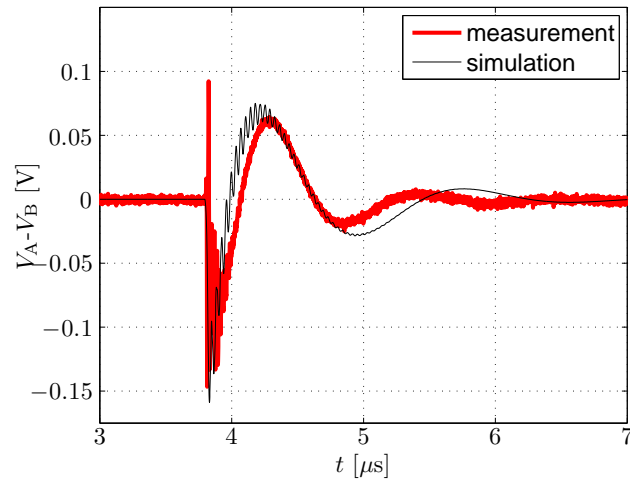
Figure 4.9: Voltage across the 10 k Ω resistor DUT.

Figure 4.10: Voltage across a 100 nF capacitor DUT.

Table 4.2: Dimensions of the transmission line model of the ISO 7637-3 Capacitive Coupling Clamp test bench

Dimension	Value	Dimension	Value
l_1	0.4 m	l_3	0.4 m
l_2	1.0 m	l_4	0.1 m
l_5	1.0 m	l_6	0.1 m

passive impedance, readily characterized by means of S-parameter measurements or simulations, and it is described in the EMC test plan. At the other end of the wire harness, the DUT is connected. The two-terminal nonlinear and passive DUTs considered here, are described further in Section 4.5.

4.5 Validation of the Proposed Model

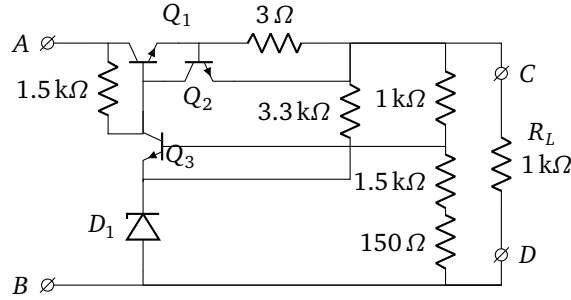


Figure 4.11: Schematic of the controlled series VR.

To validate and illustrate the appropriateness of our proposed model, we use passive and nonlinear DUTs. We measure the voltages at the DUTs and compare this with the simulation result of our model.

4.5.1 Passive DUT

As passive DUTs we use a $10\text{ k}\Omega$ resistor and a 100 nF capacitor, representing DUTs with a high input impedance and a capacitance input stage respectively. The purpose of these passive DUTs is to validate the proposed model of the test setup without having to deal with a potential inaccurate model of the DUT. The voltage across the resistor is depicted in Fig. 4.9. Fig. 4.10 shows the voltage across the capacitor. As can be seen, our model accurately predicts the peak amplitude of the signal waveform and its envelope. Also, there is a good correspondence concerning the ringing frequency between simulations and measurements. E.g., for the $10\text{ k}\Omega$ DUT (Fig. 4.9), in measurement we have a ringing frequency of 13.7 MHz , while in simulation 16.1 MHz , is observed.

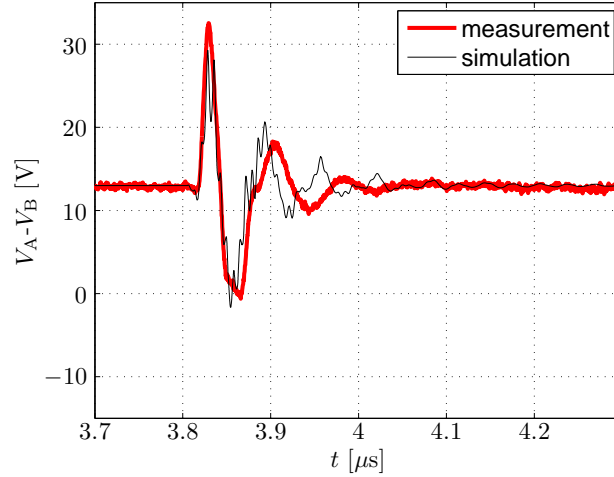


Figure 4.12: Input voltage of the VR when we inject a fast transient pulse 3b level II.

4.5.2 Nonlinear DUT

As an example of a nonlinear DUT, a low drop-out voltage regulator (VR) with schematic shown in Fig. 4.11 is selected. This DUT was also used in [17] to validate the RI-130 test model [18]. To validate our capacitive coupling clamp test model, we measure the voltage at the input of the VR, i.e., between nodes A and B, during the test when we inject a fast transient pulse 3b level II. The result is shown in Fig. 4.12. We also observe the waveform between nodes C and D, shown in Fig. 4.13. Similar as for the passive DUTs and owing to imperfections of the test setup, the ringing frequency is not exactly the same when comparing simulations with measurements. Additionally, we cannot expect the circuit model data to correspond exactly with the measurements, as the model of the DUT itself also has limited accuracy. Nonetheless, as clearly demonstrated, the proposed model predicts all salient features of the output signal and input signal of the VR, and in particular the magnitude of the disturbance peaks and the duration of the disturbance is accurately modeled. This is of critical importance and it allows the circuit designer to analyze the immunity of his/her circuit during the design phase. It is important to mention that the CPU time to run the simulation is only 4.83 s on a workstation equipped with a i7-4770 CPU at 3.40 GHz with 32 GB RAM, which demonstrates the efficiency of the circuit modeling approach.

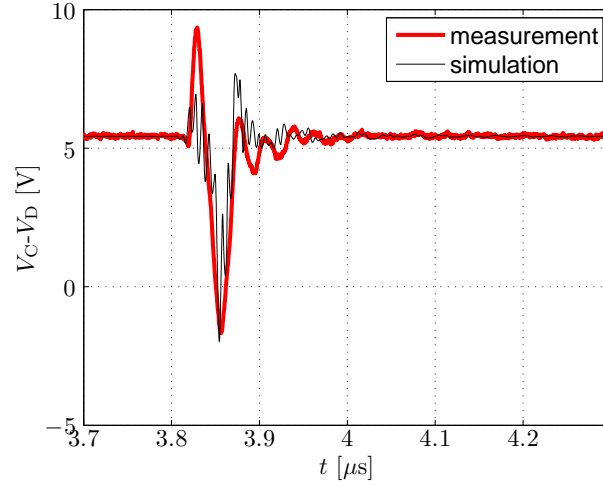


Figure 4.13: Output voltage of the VR when we inject a fast transient pulse 3b level II.

4.6 Conclusion

In this chapter, we have proposed a circuit modeling technique for the ISO 7637-3 Capacitive Coupling Clamp test. Special attention has been devoted to the modeling of the capacitive coupling clamp where the concept of the surface transfer impedance and surface transfer admittance was leveraged. The overall model was validated by means of measurements using a nonlinear VR as DUT. Good accuracy and efficiency was demonstrated. Consequently, the equivalent model can be used to assess the immunity of novel circuits and devices in their design phase.

References

- [1] *IEC 61000-4-4, Testing and Measurement Techniques - Electrical Fast Transient/Burst Immunity Test*, IEC, 2012.
- [2] F. D. Martzloff and T. F. Leedy, "Electrical Fast Transient Tests: Applications and Limitations", in *Conference Record of the IEEE Industry Applications Society Annual Meeting*, San Diego, CA, USA, USA, 1989, 1625–1632 vol.2.
- [3] B. Cormier and W. Boxleitner, "Electrical Fast Transient (EFT) Testing-an Overview", in *IEEE 1991 International Symposium on Electromagnetic Compatibility*, Cherry Hill, NJ, USA, USA, 1991, pp. 291–296.
- [4] *ISO 7637-3 Road Vehicles, Electrical Disturbances from Conduction and Coupling, Part 3, Electrical Transient Transmission by Capacitive and Inductive Coupling via Lines Other than Supply Lines*, 2014.
- [5] D. C. Smith, "An Investigation into the Performance of the IEC 1000-4-4 Capacitive Clamp", in *1996 Proceedings Electrical Overstress/Electrostatic Discharge Symposium*, Orlando, FL, USA, 1996, pp. 223–226.
- [6] S. Radman, I. Bacic, and K. Malaric, "Capacitive Coupling Clamp", in *2008 16th International Conference on Software, Telecommunications and Computer Networks*, Split, Croatia, 2008, pp. 75–79.
- [7] S. Caniggia, E. Dudenhoeffer, and F. Maradei, "Full-Wave Investigation of EFT Injection Clamp Calibration Setup", in *2010 IEEE International Symposium on Electromagnetic Compatibility*, Fort Lauderdale, FL, USA, 2010, pp. 602–607.
- [8] F. Musolino and F. Fiori, "Modeling the IEC 61000-4-4 EFT Injection Clamp", *IEEE Transactions on Electromagnetic Compatibility*, vol. 50, no. 4, pp. 869–875, 2008.
- [9] J. Hallon and M. Bittera, "Directivity of Capacitive Clamp for EFT Pulses Injection", in *2014 24th International Conference Radioelektronika*, Bratislava, Slovakia, 2014, pp. 1–4.
- [10] S. Bauer, B. Deutschmann, and G. Winkler, "Prediction of the Robustness of Integrated Circuits Against EFT/BURST", in *2015 IEEE International Symposium on Electromagnetic Compatibility (EMC)*, Dresden, Germany, 2015, pp. 45–49.
- [11] M. Magdowski and R. Vick, "Estimation of the Mathematical Parameters of Double-Exponential Pulses Using the Nelder-Mead Algorithm", *IEEE Transactions on Electromagnetic Compatibility*, vol. 52, no. 4, pp. 1060–1062, 2010.

- [12] A. Orlandi, "Circuit Model for Bulk Current Injection Test on Shielded Coaxial Cables", *IEEE Transactions on Electromagnetic Compatibility*, vol. 45, no. 4, pp. 602–615, 2003.
- [13] T. Demeester and D. De Zutter, "Quasi-TM Transmission Line Parameters of Coupled Lossy Lines Based on the Dirichlet to Neumann Boundary Operator", *IEEE Transactions on Microwave Theory and Techniques*, vol. 56, no. 7, pp. 1649–1660, 2008.
- [14] L. Qi, X. Cui, and X. Gu, "A Simple Method for Measuring Complex Transfer Impedance and Admittance of Shielded Cable in Substations", in *2006 17th International Zurich Symposium on Electromagnetic Compatibility*, Singapore, Singapore, 2006, pp. 650–653.
- [15] C. R. Paul, *Analysis of Multiconductor Transmission Lines*. J. Wiley and Sons, New York and Sons, New York, 1994.
- [16] N. Lambrecht, C. Gazda, H. Pues, D. De Zutter, and D. Vande Ginste, "Efficient Circuit Modeling Technique for the Analysis and Optimization of ISO 10605 Field Coupled Electrostatic Discharge (ESD) Robustness of Nonlinear Devices", *IEEE Transactions on Electromagnetic Compatibility*, vol. 58, no. 4, pp. 971–980, 2016.
- [17] N. Lambrecht, H. Pues, D. De Zutter, and D. Vande Ginste, "Modeling of Contact Bounce in a Transient Electromagnetic Compatibility Test for the Analysis and Optimization of Nonlinear Devices", *IEEE Transactions on Electromagnetic Compatibility*, pp. 1–4, 2016.
- [18] *FMC1278, Electromagnetic Compatibility Specification for Electrical and Electronic Components and Subsystems*, www.fordemc.com/docs/download/FMC1278.pdf, Ford, Oct. 2016.

5

Modeling of Contact Bounce in a Transient Electromagnetic Compatibility Test for the Analysis and Optimization of Nonlinear Devices

Based on “Modeling of Contact Bounce in a Transient Electromagnetic Compatibility Test for the Analysis and Optimization of Nonlinear Devices,” N. Lambrecht, H. Pues, D. De Zutter, and D. Vande Ginste, *IEEE Transactions on Electromagnetic Compatibility*, vol. 59, no. 2, pp. 541 - 544, 2017.

★ ★ ★

In this chapter, we propose a methodology to include contact bounce, unavoidably occurring in a pulse generator, in the modeling of a transient electromagnetic compatibility (EMC) test. An example of such an EMC test is the RI-130 test, well-known in the automotive sector and used as case study in this chapter. First, a detailed study of contact bounce of an electromagnetic relay is performed, leading to a novel modeling approach. Next, a multiconductor transmission line (MTL) equivalent is developed for the electrically large RI-130 test bench and concatenated with models for the load box and the device under test (DUT). Then, to apply and validate the advocated model, the behavior of the nonlinear DUT is simulated and compared to measurements under the RI-130 test conditions, showing good agreement. Finally, it is also shown that the overall model can be used to efficiently optimize the design of the DUT, making it more robust.

5.1 Introduction

The EMC test discussed in this chapter is the RI-130 test [1], which is a broadband transient test. RI-130 is a typical EMC test where contact bounce of an electromagnetic relay plays a significant role during the disturbance of the device under test (DUT). We propose a new modeling technique for the contact bounce, which we consider as a stochastic process. Together with a multiconductor transmission line (MTL) model for the electrically large RI-130 test bench, this results in an overall equivalent circuit, able to deal with active nonlinear components and easily integrated with advanced optimization and troubleshooting techniques. The method is thoroughly validated by means of measurements and its appositeness for rapid EMC analysis of the DUT, here being a low drop-out voltage regulator (VR), and its subsequent optimization is illustrated. The remainder of this chapter is organized as follows. In Section 5.2, the modeling techniques for each part of the RI-130 test setup, including the relay that is affected by contact bounce, are explained. Section 5.3 deals with the validation of the developed circuit model, via comparison with measurements using the nonlinear active DUT. Finally, some concluding remarks are formulated in Section 5.4.

5.2 Methodology

In this section, we discuss the RI-130 standard test [1] and, as a case study, we develop a circuit model for it. Particular attention is devoted to the modeling of the generator, including its relay that is affected by contact bounce.

5.2.1 Description of the RI-130 test

Although the methodology described in this chapter is more generally applicable, as the RI-130 test is gaining importance, it is the focus of this chapter and we start with its rigorous description. The default RI-130 test setup is depicted in Fig. 5.1. The test bench itself consists of a large ground plane and a coupling test fixture, which rests on this ground plane. An aggressor wire is mounted in the coupling test fixture and a single wire of the wire harness is placed on top of the aggressor wire in the coupling test fixture, while the other wires of the wire harness are placed at least 200 mm away from the coupling test fixture, so that no direct field coupling can occur between the aggressor wire and the remainder of the wire harness. As always, the wire harness connects the DUT with a load simulator (aka load box). In this particular EMC test, every wire of the wire harness is tested by placing it on top of the aggressor wire. The aggressor wire is excited by a transient generator, of which the schematic is shown in Fig. 5.2. The transient generator comprises a passive charging circuit, which is triggered via an electromechanical relay. The required pulse sequence of 3.45 s, depicted in Fig. 5.3, is applied to node E , saturating the transistor and, consequently, activating the relay. The components of the transient generator have the following values: $R_{TG1}=39\Omega$, $C_{TG1}=100\text{nF}$,

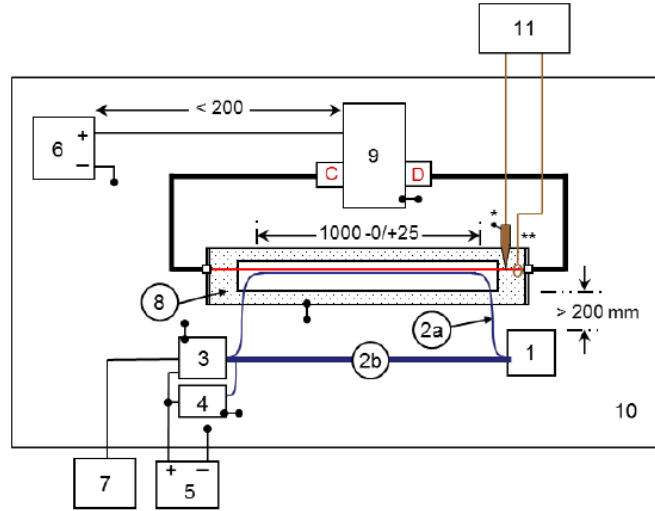


Figure 5.1: The default RI-130 test setup [1], where 1=DUT, 2a=DUT circuit wire to be tested, 2b=DUT wire harness, 3=load box, 4=artificial network, 5=power supply, 6=automotive battery, 7=DUT monitor, 8=coupling test fixture, 9=transient generator, 10=ground plane and 11=test point.

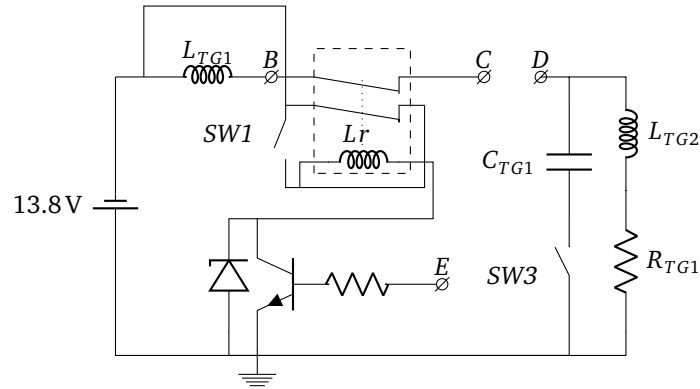


Figure 5.2: Schematic of the transient generator.

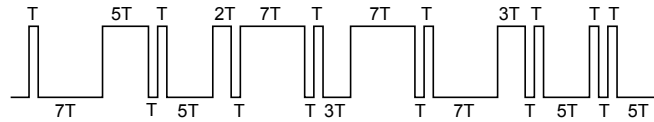


Figure 5.3: Pulse sequence ($T=50$ ms, total period of 3.45 s).

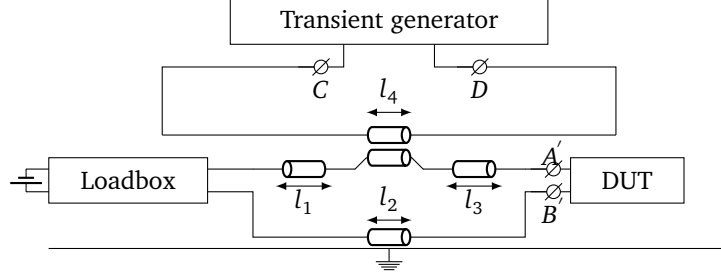


Figure 5.4: RI-130 test bench with MTLs.

$L_{TG1}=5\mu\text{H}$, $L_{TG2}=100\text{ mH}$. L_r represents the relay's coil. The transient generator can be operated in several modes, depending on the settings of the switches SW1 and SW3. RI-130 encompasses four different modes, depending on whether SW1 and SW3 are closed or open. In [1], much attention is devoted to the case where SW1 is left open, this case is called mode 3 in [1]. Therefore, in this chapter, we will apply our methodology to mode 3.

5.2.2 Modeling of the RI-130 test bench

To avoid time-consuming full-wave simulations, we propose a multiconductor transmission line (MTL) approach to model the test bench. Thereto, we apply the same method as in [2]. Without loss of generality but for conciseness, we consider a wire harness consisting of only two wires. The corresponding equivalent cascaded MTL circuit is shown in Fig. 5.4, where $l_1=0.3\text{ m}$, $l_2=1.2\text{ m}$, $l_3=0.15\text{ m}$ and $l_4=1\text{ m}$. The load box and the DUT are connected to the two ends of the wire harness. The load box is a passive impedance, readily characterized by means of S-parameter measurements or simulations, and it is described in the EMC test plan. At the other end of the wire harness, the DUT is connected. The two-terminal nonlinear DUT considered here, is described further in Section 5.3.

5.2.3 Modeling of the contact bounce

It is known that contact bounce of a relay is unavoidable. When contact is made, two objects collide and there will be a rebound. The corresponding displacement waveform is not a sinusoid, but it has a damped behavior. If one is able to measure or simulate the displacement of the relay contact, then one can, e.g., make use of Prony analysis to directly estimate the frequency and magnitude of all exponentially damped modes [3]. However, in our case and often in EMC tests, the relay is standardized and we cannot change or even measure the displacement of the relay contact. Hence, we have chosen to characterize the contact bounce by measuring the voltage waveform directly across the relay contact (between nodes B and C in Fig. 5.2). When the relay is activated in mode 3 by the transistor, the normal-closed

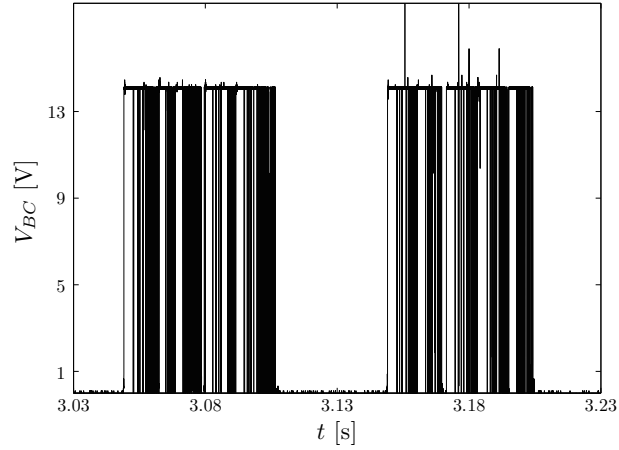


Figure 5.5: Typical voltage waveform between node B and C due to contact bounce of an electromagnetic relay in mode 3 when $L_{TG1} = L_{TG2} = C_{TG1} = 0$ and node C and D are short-circuited.

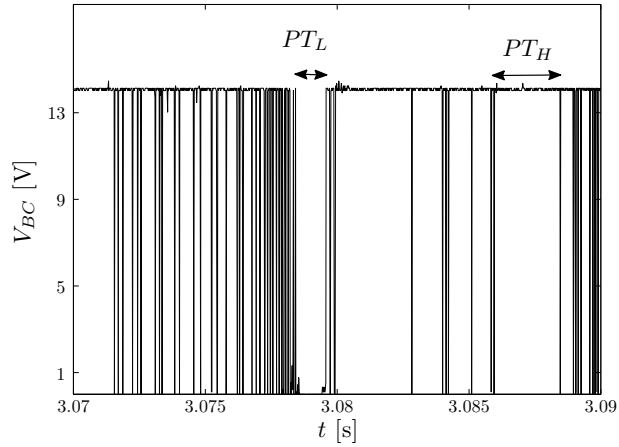


Figure 5.6: A zoom of the contact bounce Fig. 5.5.

(NC) relay contacts will open. So, the power supply will be disconnected from the relay's coil (L_r), by which the NC relay contact rapidly closes again. Owing to the (unpredictable) contact bounce of the mechanical parts, this repeatedly opening and closing of the relay does not happen in a periodical fashion, but typically leads to a waveform as depicted in Fig. 5.5, where the voltage waveform is shown for the last two pulses of the sequence shown in Fig. 5.3. When repeating the exper-

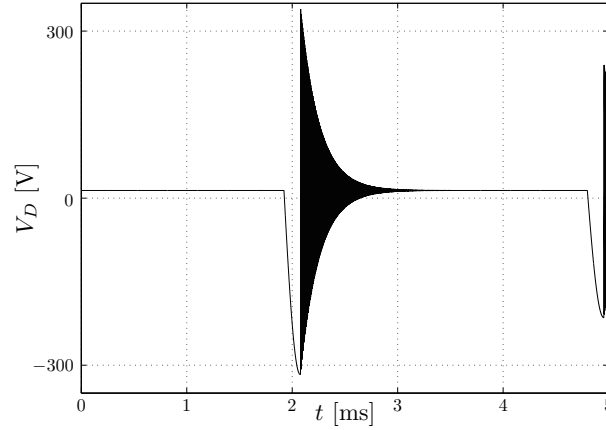


Figure 5.7: Simulation of waveforms appearing in the transient generator of Fig. 5.2, relevant to the contact bounce phenomenon: voltage at node D w.r.t. ground.

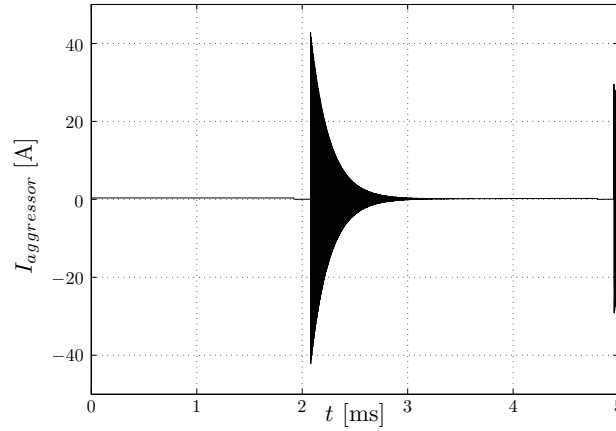


Figure 5.8: Simulation of waveforms appearing in the transient generator of Fig. 5.2, relevant to the contact bounce phenomenon: current through the aggressor wire for a worst case situation in mode 3, pulse A2-2.

iment many times, however, different waveforms with similar characteristics are obtained. Hence, these waveforms can be considered as a stochastic process. Recently in literature, polynomial chaos (PC) approaches [4], have been given a lot of attention to tackle variability in electronic design. Nonetheless, for the time-

variant system described in this chapter, PC becomes intractable (or even not feasible). Therefore, we adopt a more pragmatic approach to deal with the stochastic process. In particular, we provide a good estimation of the worst case situation, which is of course of importance to the EMC engineer or designer. Fig. 5.6 zooms in on a smaller portion of the waveform. When doing so, it appears that two parameters control the shape of this waveform. PT_L represents the time during which the relay contacts are closed during contact bounce and PT_H represents the time when the relay contacts are open. We now consider these two parameters, PT_H and PT_L , as random variables, defining the stochastic process. In case SW3 is closed, we are dealing with the so-called mode 3, pulse A2-2. In this mode, capacitor C_{TG1} is in parallel with the series coil (L_{TG2}) and resistance (R_{TG1}). We will further use mode 3, pulse A2-2 to apply our methodology. When all the relay contacts are at rest (e.g., during PT_L , see Fig. 5.6) L_{TG1} , L_{TG2} and C_{TG1} will be charged with a time constant $\tau = (L_{TG1} + L_{TG2})/R_{TG1} = 2.56$ ms. On the other hand, when the relay contact is open, the LC tank (L_{TG2} , C_{TG1} , R_{TG1}) oscillates at 1.6 kHz. As can be seen from Fig. 5.7, a maximum voltage will occur at a quarter of a period of the oscillating frequency ($=156.25 \mu\text{s}$) after the relay contact opened. When the relay contact closes, L_{TG1} also affects the oscillation frequency, which then becomes 225 kHz. When the maximum voltage at node D is reached, a maximum current will flow through the aggressor wire (see Fig. 5.8) with peak-to-peak values up to 80 A. This in turn gives rise to a great deal of crosstalk from the aggressor wire to the victim wire that lays on top of it. In our proposed worst case scenario, the current through the aggressor wire and voltage at node D should be as high as possible, as this leads to the worst crosstalk. Thereto, we choose $PT_H = 156.25 \mu\text{s}$, as we then close the relay contact when there is a maximum voltage at node D . The parameter PT_L should be large enough such that the inductors can be fully charged. Typically, one could choose $PT_L = 5\tau = 12.8$ ms. However, such a large time interval never really occurs during contact bounce. From measurements we derived that the maximum value for PT_L during contact bounce is 2.72 ms. So, we set $PT_L = 2.72$ ms.

To implement this behavior using a circuit simulator, we replace the relay by a voltage controlled switch (see Fig. 5.9). We apply the pulse sequence of Fig. 5.3 to this switch, where each individual pulse is now periodically switched on during a time interval PT_H and switched off during a time interval PT_L . This leads to the worst case scenario. A detail of this signal, that is applied to the voltage controlled switch, i.e. again the two last pulses of the entire sequence, is shown in Fig. 5.10.

5.3 Measurements and Results

To validate and illustrate the appositeness of our proposed model, we apply it to a nonlinear DUT and compare it with measurements. All measurement results are performed as described in [1], measuring the DUT during 60 s, from which we select and show the worst situation, i.e., the particular 3.45 s period yielding the worst case result.

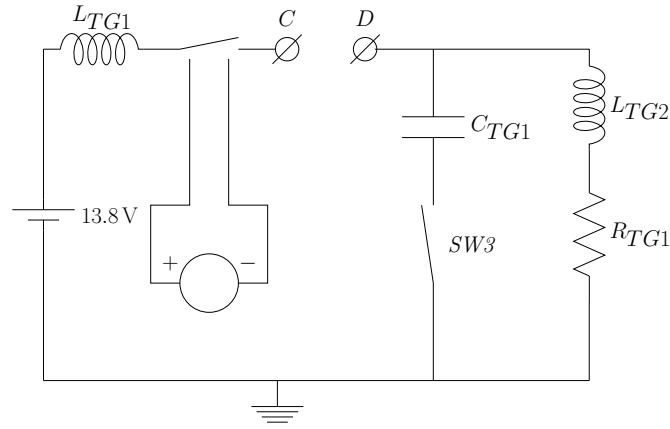


Figure 5.9: Proposed circuit model for the transient generator Fig. 5.2.

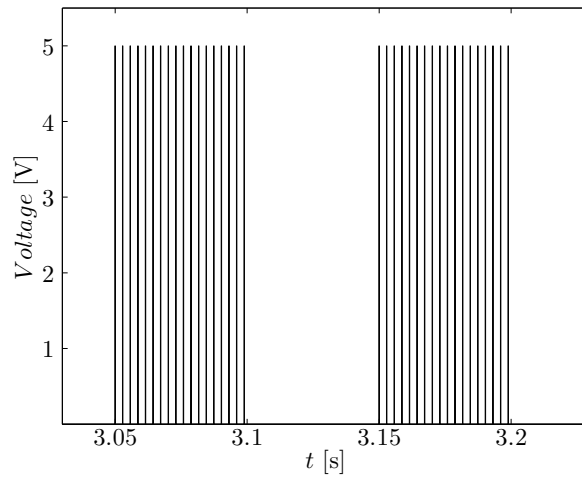


Figure 5.10: Detail of the signal applied to the voltage controlled switch of Fig. 5.9.

5.3.1 Validation of the model using a nonlinear DUT

The DUT is a low drop-out voltage regulator (VR) with schematic shown in Fig. 5.11. For clarity, the parasitics are not shown in the schematic, but they are included in the simulations, based on the datasheet of the components. In particular, the DUT is a controlled series regulator, converting an input voltage of 12V to an output voltage of 5V. Bipolar junction transistors (BJT), i.e., the BC846 by NXP Semiconductor, are used in this design. The zener diode is the BZX84C2V4 by NXP Semiconductors.

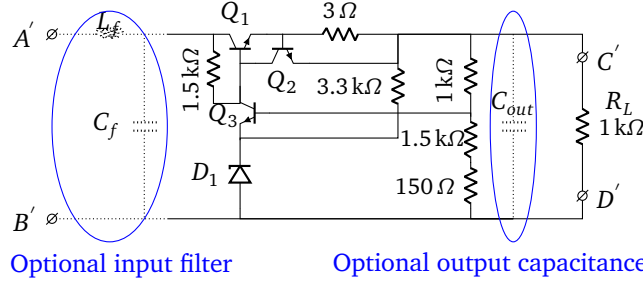


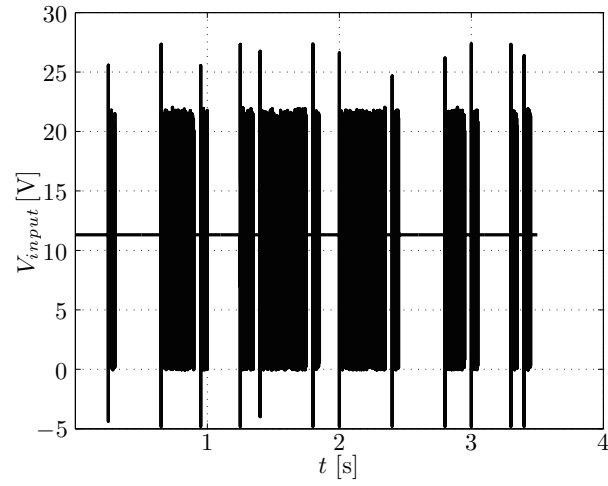
Figure 5.11: Schematic of the controlled series voltage regulator. The optional components (L_f , C_f , C_{out}) are omitted for the validation of Section 5.3.1 and their values are optimized in the application example of Section 5.3.2.

To validate our worst case model in concatenation with the proposed MTL model for the test bench, we measure the voltage at the *input* of the voltage regulator i.e., between nodes A' and B' , during the test in mode 3, pulse A2-2 (Fig. 5.12(b)). Compared to the simulation with our novel model (Fig. 5.12(a)), it is clear that the (worst case) maximum amplitudes are quite accurately predicted without too much overestimation. Of course, there is no exact agreement between simulation and measurement concerning the duration (time constant) since our advocated model is based on the worst case scenario, for the reason that, to decide whether the DUT fails or passes the test, the maximum amplitude is of critical importance. When measuring the *output* of the voltage regulator i.e., between nodes C' and D' , we get large negative peaks (Fig. 5.13). This is due to the fact that Q_1 is in cut off for negative input voltage, leading to a drop of the output voltage. During one full period of 3.45 s, simulations with the advocated model (Fig. 5.13(a)) are compared with the measurements (Fig. 5.13(b)), again leading to the conclusion that the model correctly predicts the worst case negative peaks. Due to the inherent unpredictability and complexity of the contact bounce, the tolerances on the components and their models provided by the vendors, one can of course not expect simulation and measurement results to coincide completely. In particular, tolerances on the zener diode cause a small discrepancy of the expected DC value. Also, the measurements show more fluctuations of the voltage levels, occurring to the random nature of the contact bounce, whereas our worst case model is purely deterministic.

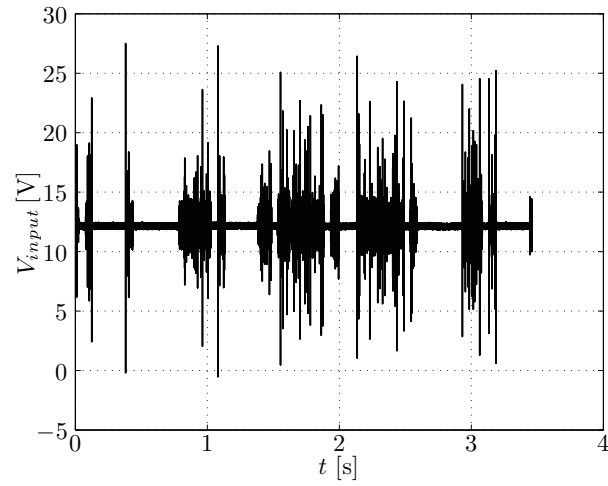
For completeness, we mention that similar results are obtained in the so-called mode 3, pulse A2-1, i.e. when switch SW3 is open during the test.

5.3.2 Optimization

Whereas the model itself was validated in the previous section, it is also clear that this DUT would never pass the RI-130 test, as typically, one does not want the output voltage to deviate from 5V by more than, say, 150 mV. To further illustrate

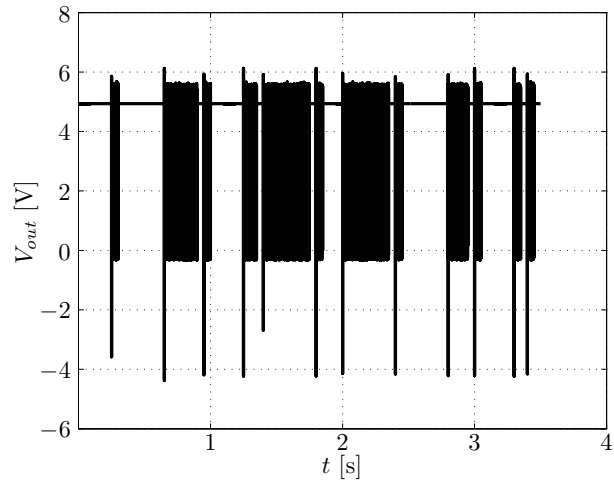


(a)

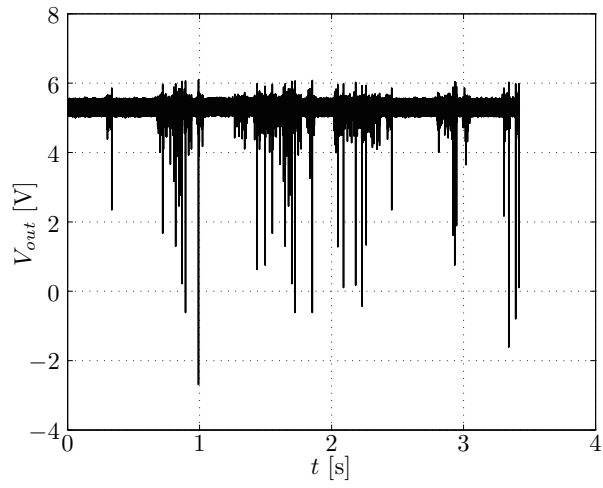


(b)

Figure 5.12: Input voltage of the voltage regulator shown in Fig. 5.11 during one full period of 3.45 s in mode 3, pulse A2-2. (a) Simulation. (b) Measurement.



(a)



(b)

Figure 5.13: The output voltage of the voltage regulator shown in Fig. 5.11 during one full period of 3.45 s in mode 3, pulse A2-2. (a) Simulation. (b) Measurement.

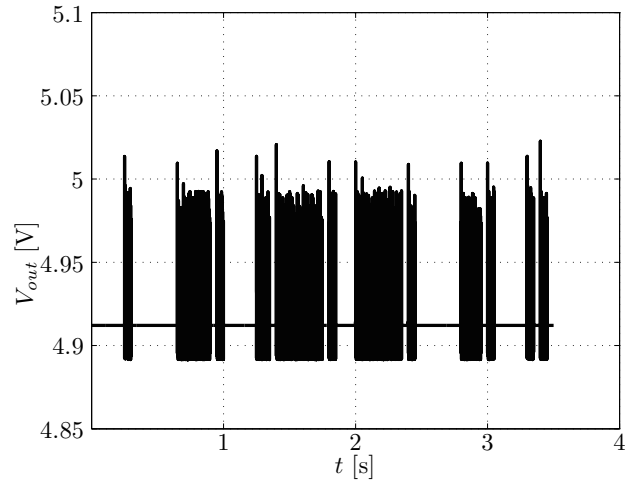
the benefits of the proposed model, we will now use it to make the VR more robust. Thereto, an LC low-pass filter (L_f and C_f) at the input, and a capacitor (C_{out}) at the output were added. Of course, for various reasons (parasitics, cost, mechanical, ...), we want the additional three components L_f , C_f and C_{out} to be as small as possible, whilst the output voltage remains with the interval $[4.85\text{V}, 5.15\text{V}]$. So, we are confronted with the following optimization problem:

$$\min(L_f, C_f, C_{out}) \text{ for } 4.85\text{V} < |V_C - V_D| < 5.15\text{V}$$

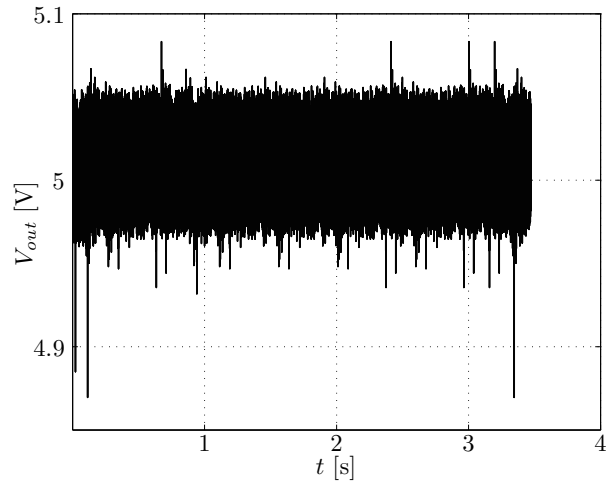
This optimization problem is solved with the gradient optimizer embedded in the ADS circuit simulation of Keysight Technologies. Leveraging our novel equivalent circuit model, the complete optimization process only takes 8 min 42 s of CPU time and yields the following values: $L_f = 40\mu\text{H}$, $C_f = 20\text{nF}$ and $C_{out} = 2\mu\text{F}$. To manufacture the optimized voltage regulator, the following commercially available values were selected: $L_f = 47\mu\text{H}$, $C_f = 22\text{nF}$ and $C_{out} = 2.2\mu\text{F}$. As can be seen from Fig. 5.14, both in measurement and in simulation, the maximum deviation is reduced to less than 150 mV.

5.4 Conclusion

In this chapter, we have proposed a solution for the efficient circuit modeling of the stochastic behavior of contact bounce, observed during the RI-130 test. Additionally, the electrically large RI-130 test has been modeled with a MTL model. The combination of the MTL model and our novel proposed model of the contact bounce leads to a complete circuit model of the RI-130 test. With a nonlinear VR as DUT, this model was extensively validated by means of measurements and it was shown that it allows to efficiently and accurately predict the behavior of the DUT in the design phase. Moreover, we demonstrated that our proposed circuit model may be advantageously used for the optimization of DUTs, making them more immune against the RI-130 test conditions. It can be concluded that the advocated approach is useful to effectively troubleshoot and solve problems when contact bounce has to be taken into account in a transient EMC test.



(a)



(b)

Figure 5.14: The output voltage of the optimized voltage regulator during one full period of 3.45 s in mode 3, pulse A2-2. (a) Simulation. (b) Measurement.

References

- [1] *FMC1278, Electromagnetic Compatibility Specification for Electrical and Electronic Components and Subsystems*, www.fordemc.com/docs/download/FMC1278.pdf, Ford, Oct. 2016.
- [2] N. Lambrecht, C. Gazda, H. Pues, D. De Zutter, and D. Vande Ginste, “Efficient Circuit Modeling Technique for the Analysis and Optimization of ISO 10605 Field Coupled Electrostatic Discharge (ESD) Robustness of Nonlinear Devices”, *IEEE Transactions on Electromagnetic Compatibility*, vol. 58, no. 4, pp. 971–980, 2016.
- [3] J. Xiong, J. He, C. Zang, C. Liu, and L. Wang, “Influence of Characteristic Parameters on Contact Bounce in Reed Systems of Relays”, *2008 Proceedings of the 54th IEEE Holm Conference on Electrical Contacts*, 2008.
- [4] P. Manfredi, D. Vande Ginste, D. De Zutter, and F. G. Canavero, “Stochastic Modeling of Nonlinear Circuits via SPICE-Compatible Spectral Equivalents”, *IEEE Transactions on Circuits and Systems I: Regular Papers*, vol. 61, no. 7, pp. 2057–2065, 2014.

6

Conclusions and Future Work

6.1 General Conclusions

For designers of electronic circuits and equipment, it is of the utmost importance that during the pre-compliance phase, i.e. early in the design phase, the EMC behavior of their novel devices and systems can be predicted efficiently. This avoids expensive iterations in later stages of the design cycle, costly and time-consuming measurements and troubleshooting. Hence, it reduces time to market, leading to a more cost-effective development. To accomplish this, modeling of EMC tests has become indispensable. However, there are many different types of EMC tests and almost every EMC test has to be modeled in a different way.

This Ph.D. dissertation focused on the modeling of transient field coupled EMC tests, which are becoming the biggest EMC challenge in the automotive industry. In this work, we presented a fast and reliable circuit modeling techniques of entire test setups. As circuit simulators are powerful design tools, able to deal with active nonlinear components and easily integrated with advanced optimization and troubleshooting techniques, our circuit modeling approach allows for a rapid analysis of the DUT and its subsequent optimization. The transient field coupled EMC tests discussed in this Ph.D. dissertation are:

- ultrafast plate-to-wire coupled electrostatic discharge (ESD-Rinne)
- slow magnetic-field coupled immunity (ICC)
- fast electric-field coupled immunity (CCC)
- wideband wire-to-wire coupled immunity (RI-130)

In Chapter 2 an in-depth analysis of the ultrafast plate-to-wire coupled ESD test was given. It was clear that in this test the ESD gun is a very important part of the whole test setup. Having made the appropriate circuit models for each part of the test, we observed that the FCP behaves as a transmission line that is shorted at one end and open at the other. When injecting the ESD current, waves will travel to both ends, will be reflected there and all (reflected) contributions eventually create disturbances in the DUT. Here, the dominant differential mode contribution stems from the asymmetry introduced by the load box. With our MTL model we take the inductive and capacitive coupling plus all delays from the FCP to the wire harness into account. Moreover, by including the inductance and transmission line effects of the large ground strap of the ESD gun, an accurate model is obtained. This proposed model was thoroughly validated, also leveraging a real industrial automotive IC as DUT. In Chapter 3, we focused on the modeling of the slow magnetic-field coupled immunity (ICC) test. We presented an equivalent circuit of the injection clamp plus the long wire harness by making use of transmission line theory. In Chapter 4 we made an equivalent circuit model of the fast electric-field coupled immunity (CCC) test again by making use of transmission line theory. However, in this chapter, we adapted the transmission line theory to model the capacitive coupled clamp as two transmission lines that are (partially) shielded from one another. Using distributed voltage and current sources allowed to transform this complex fixture into an equivalent circuit model. In Chapter 5 we have dealt with the RI-130 wideband wire-to-wire coupled immunity test. Due to the presence of the mechanical relay in the transient generator, this test is influenced by contact bounce. As contact bounce should be considered as a stochastic phenomenon, we presented a circuit model that can predict the worst case scenario.

In this Ph.D. dissertation all the proposed equivalent circuit models were validated by comparison to measurements using a nonlinear device as DUT, as all DUTs in the automotive industry are also nonlinear devices. Moreover, in case of the ESD-Rinne, ICC and CCC test, the models were validated at different test levels and polarities. In all studied EMC tests we applied transmission line theory, although many researchers are tempted to use solely capacitive or inductive coupling. Our approach allows to generate more generally applicable circuit equivalent models that can be used for a large range of DUTs. All in all this Ph.D. research proves that reliable circuit models for transient EMC tests can indeed be developed but that this is not possible without including coupled transmission lines as essential parts of the models.

6.2 Future Work

While the proposed models can handle many ICs, we always considered electrically small DUTs, i.e. with dimensions much smaller than the dimension of the test bench. When the dimensions of the DUT are comparable to those of the test setup, direct coupling to the DUT has to be taken into account. This is the case when dealing with very large printed circuit boards (PCBs) or DUTs that are shielded

and locally grounded to the test setup.

Another aspect to study further is the repeatability of the transient field coupled EMC tests. As shown in Chapter 2, the ground strap of the ESD gun in the ultra-fast plate-to-wire coupled ESD test has a great influence on the pulse shape of the injected ESD pulse. Actually, many EMC tests consist of several long wires. The spacing between these wires and the length of these wires will have an influence on the mutual coupling and the resonances that can occur due to the transmission line effects. To investigate the effect of the variability of the wire harness and/or the test setup, one could combine the developed multiconductor transmission line (MTL) based circuit equivalent models, presented in this dissertation, with polynomial chaos theory for MTLs [1]–[3]. Such an approach might lead to an accurate uncertainty quantification of the several parameters that influence EMC tests and might provide insight concerning sensitivity and repeatability of the tests.

When performing a long time-domain simulation or measurement, it is laborious to search for all the possible errors in the output data. Furthermore, it is hard to decide by means of visual analysis whether or not errors occur, what type of error, etc. Therefore, an efficient post-processing is needed to classify the potential errors and to assess the DUT's robustness. Novel machine learning based approaches for error detection in transient susceptibility tests have to be developed. First promising results for automatic error detection in transient susceptibility tests were recently obtained [4].

References

- [1] P. Manfredi, D. Vande Ginste, D. De Zutter, and F. G. Canavero, “Stochastic Modeling of Nonlinear Circuits via SPICE-Compatible Spectral Equivalents”, *IEEE Transactions on Circuits and Systems I: Regular Papers*, vol. 61, no. 7, pp. 2057–2065, 2014.
- [2] P. Manfredi, D. Vande Ginste, I. S. Stievano, D. De Zutter, and F. Canavero, “Stochastic Transmission Line Analysis via Polynomial Chaos Methods: An Overview”, *IEEE Electromagnetic Compatibility Magazine*, vol. 6, no. 3, pp. 77–84, 2017.
- [3] D. Vande Ginste, D. De Zutter, D. Deschrijver, T. Dhaene, P. Manfredi, and F. Canavero, “Stochastic Modeling-Based Variability Analysis of On-Chip Interconnects”, *IEEE Transactions on Components, Packaging and Manufacturing Technology*, vol. 2, no. 7, pp. 1182–1192, 2012.
- [4] R. Medico, N. Lambrecht, H. Pues, D. Vande Ginste, D. Deschrijver, T. Dhaene, and D. Spina, “Machine Learning-Based Error Detection in Transient Susceptibility Tests”, *IEEE Transactions on Electromagnetic Compatibility*, accepted for publication on March 28th, 2018.



Solution of the Multiconductor Transmission Line Equations

Transmission lines are distributed-parameter systems. When the electrical dimensions of a structure are small, it can be approximately modeled as a lumped element system. These lumped elements depend only on time, t . Lumped-parameter systems are characterized by ordinary differential equations, whereas distributed systems, such as transmission lines, are characterized by partial differential equations. If our interest is only the time harmonic regime, then using phasor quantities removes the time dependence. This leads to a direct analogy between the time harmonic transmission line equations and a lumped-parameter model.

Now, consider a lumped-parameter system. One way of representing such a system is via n coupled ordinary differential equations in state-variable form [1] as

$$\frac{d}{dt}\mathbf{X}(t) = \mathbf{A}\mathbf{X}(t) + \mathbf{B}\mathbf{W}(t) \quad (\text{A.1})$$

where

$$\mathbf{X}(t) = \begin{pmatrix} x_1(t) \\ x_2(t) \\ \vdots \\ x_n(t) \end{pmatrix}, \quad (\text{A.2})$$

$$\mathbf{W}(t) = \begin{pmatrix} w_1(t) \\ w_2(t) \\ \vdots \\ w_n(t) \end{pmatrix}, \quad (\text{A.3})$$

$$\mathbf{A} = \begin{pmatrix} a_{11} & \cdots & a_{1l} & \cdots & a_{1n} \\ \vdots & \ddots & \vdots & \ddots & \vdots \\ a_{l1} & \cdots & a_{ll} & \cdots & a_{ln} \\ \vdots & \ddots & \vdots & \ddots & \vdots \\ a_{n1} & \cdots & a_{nl} & \cdots & a_{nn} \end{pmatrix}, \quad (\text{A.4})$$

$$\mathbf{B} = \begin{pmatrix} b_{11} & \cdots & b_{1l} & \cdots & b_{1n} \\ \vdots & \ddots & \vdots & \ddots & \vdots \\ b_{l1} & \cdots & b_{ll} & \cdots & b_{ln} \\ \vdots & \ddots & \vdots & \ddots & \vdots \\ b_{n1} & \cdots & b_{nl} & \cdots & b_{nn} \end{pmatrix}. \quad (\text{A.5})$$

The matrices \mathbf{A} and \mathbf{B} are assumed to be independent of time t , in which case the system is said to be stationary, i.e., its parameters do not vary with time. As shown below, this property is analogous to an uniform transmission line where the corresponding matrix \mathbf{A} is assumed independent of z , i.e., the line cross-sectional dimension and medium properties are constant along the line.

Multiconductor transmission lines, are governed by the following Telegraphers equations (in time-harmonic regime).

$$\begin{aligned} \frac{d}{dz} \mathbf{V}(z) &= -\mathbf{Z}\mathbf{I}(z) + \mathbf{V}_{FT}(z) \\ \frac{d}{dz} \mathbf{I}(z) &= -\mathbf{Y}\mathbf{V}(z) + \mathbf{I}_{FT}(z) \end{aligned} \quad (\text{A.6})$$

or, omitting the argument z ,

$$\frac{d}{dz} \begin{pmatrix} \mathbf{V} \\ \mathbf{I} \end{pmatrix} = \begin{pmatrix} \mathbf{0} & -\mathbf{Z} \\ -\mathbf{Y} & \mathbf{0} \end{pmatrix} \begin{pmatrix} \mathbf{V} \\ \mathbf{I} \end{pmatrix} + \begin{pmatrix} \mathbf{V}_{FT} \\ \mathbf{I}_{FT} \end{pmatrix}, \quad (\text{A.7})$$

where \mathbf{V} are the voltages, \mathbf{I} the currents, \mathbf{V}_{FT} are the distributed voltage sources and \mathbf{I}_{FT} the distributed current sources along the multiconductor transmission line. The analogy between (A.1) and (A.7) is now readily seen when making the following substitution $(\mathbf{V}\mathbf{I})^T = \mathbf{X}(t)$, $(\mathbf{V}_{FT}\mathbf{I}_{FT})^T = \mathbf{B}\mathbf{W}(t)$ and

$$\begin{pmatrix} \mathbf{0} & -\mathbf{Z} \\ -\mathbf{Y} & \mathbf{0} \end{pmatrix} = \mathbf{A}. \quad (\text{A.8})$$

For $n = 1$, the state-variable equations reduce to a scalar equation

$$\frac{d}{dt} x(t) = ax(t) + b w(t). \quad (\text{A.9})$$

For a prescribed initial state, $x(t_0)$, the solution of the homogeneous equation (with $w(t) = 0$) is

$$x_h(t) = e^{a(t-t_0)}x(t_0) = \phi(t-t_0)x(t_0) \quad (\text{A.10})$$

By making use of the method of variation of parameter [2], the particular solution becomes

$$x_p(t) = e^{at}k(t). \quad (\text{A.11})$$

Substituting this into the original equation, gives

$$a e^{at}k(t) + e^{at} \frac{d}{dt}k(t) = a e^{at}k(t) + b w(t) \quad (\text{A.12})$$

or thus

$$\frac{d}{dt}k(t) = e^{-at}b w(t), \quad (\text{A.13})$$

which has the solution

$$k(t) = \int_{t_0}^t e^{-a\tau} b w(\tau) d\tau. \quad (\text{A.14})$$

Substituting (A.14) into (A.11) gives the particular solution as

$$x_p(t) = e^{at} \int_{t_0}^t e^{-a\tau} b w(\tau) d\tau = \int_{t_0}^t e^{a(t-\tau)} b w(\tau) d\tau. \quad (\text{A.15})$$

Together with the homogeneous solution, the total solution reads

$$x(t) = x_h(t) + x_p(t) = e^{a(t-t_0)}x(t_0) + \int_{t_0}^t e^{a(t-\tau)} b w(\tau) d\tau. \quad (\text{A.16})$$

For a n^{th} order system we obtain in a similar fashion

$$\mathbf{X}(t) = \Phi(t-t_0)\mathbf{X}(t_0) + \int_{t_0}^t \Phi(t-\tau) \mathbf{B} \mathbf{W}(\tau) d\tau \quad (\text{A.17})$$

with

$$\Phi = e^{\mathbf{A}t} = \mathbf{I} + \frac{t}{1!}\mathbf{A} + \frac{t^2}{2!}\mathbf{A}^2 + \dots \quad (\text{A.18})$$

Here, $e^{\mathbf{A}t}$ is often calculated by means of the eigenvalue decomposition $\mathbf{A} = \mathbf{M}\Omega\mathbf{M}^{-1}$, where Ω is a diagonal matrix containing the eigenvalues of \mathbf{A} and the columns of \mathbf{M} are the eigenvectors of \mathbf{A} . Then we get:

$$\begin{aligned} e^{\mathbf{A}t} &= \mathbf{I} + \frac{t}{1!}\mathbf{A} + \frac{t^2}{2!}\mathbf{A}^2 + \dots \\ &= \mathbf{I} + \frac{t}{1!}\mathbf{M}\Omega\mathbf{M}^{-1} + \frac{t^2}{2!}\mathbf{M}\Omega\mathbf{M}^{-1}\mathbf{M}\Omega\mathbf{M}^{-1} + \dots \\ &= \mathbf{M}\left[\mathbf{I} + \frac{t}{1!}\Omega + \frac{t^2}{2!}\Omega\Omega + \dots\right]\mathbf{M}^{-1} \\ &= \mathbf{M}e^{\Omega t}\mathbf{M}^{-1} \end{aligned} \quad (\text{A.19})$$

One can now easily calculate the voltages and currents along the transmission line as follows:

$$\begin{pmatrix} \mathbf{V}(z) \\ \mathbf{I}(z) \end{pmatrix} = \Phi(z - z_0) \begin{pmatrix} \mathbf{V}(z_0) \\ \mathbf{I}(z_0) \end{pmatrix} + \int_{z_0}^z \Phi(z - \tau) \begin{pmatrix} \mathbf{V}_{FT}(\tau) \\ \mathbf{I}_{FT}(\tau) \end{pmatrix} d\tau \quad (\text{A.20})$$

where

$$\Phi = e^{\mathbf{A}t} \quad (\text{A.21})$$

with

$$\mathbf{A} = \begin{pmatrix} \mathbf{0} & -\mathbf{Z} \\ -\mathbf{Y} & \mathbf{0} \end{pmatrix}. \quad (\text{A.22})$$

References

- [1] C. R. Paul, *Analysis of Multiconductor Transmission Lines*. J. Wiley and Sons, New York and Sons, New York, 1994.
- [2] D. A. McQuarri, *Mathematical Methods for Scientist and Engineers*. Sausalito, California: University Science Books, 2003.

B

Analysis of the p.u.l. Parameters of the CCC Fixture

When analyzing the p.u.l. parameters of the CCC fixture we notice that the mutual inductance/capacitance has nearly the same value as the self inductance/capacitance of one of the wires. For illustration, we assume here one wire inside the CCC fixture and consider that the CCC fixture is completely closed and perfectly electrically conducting (PEC) (see Fig. B.1). To further ease calculations, the closed CCC fixture is chosen to be the reference conductor 0, the enclosed wire is signal conductor 1 and the ground plane is signal conductor 2.

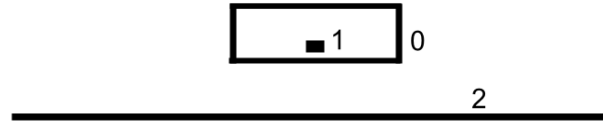


Figure B.1: Sketch of the cross-section of the closed CCC fixture.

The excitation of the signal conductor 1 is obtained by connecting a current source between this wire and signal conductor 2. The other end is shorted (see Fig. B.2).

Due to this type of excitation and choice of reference plane we find that $I_1 = -I_2$. Here I_1 is the current through signal conductor 1, and I_2 through the ground plane. In quasi-TEM regime, the following relations hold:

$$\Phi_1 = L_{11}I_1 + L_{12}I_2 \quad (\text{B.1})$$

$$\Phi_2 = L_{21}I_1 + L_{22}I_2. \quad (\text{B.2})$$

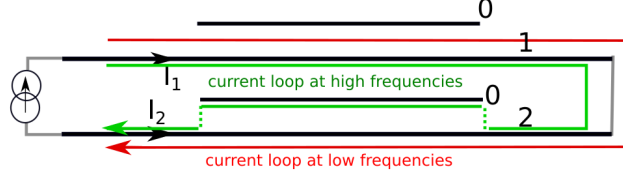


Figure B.2: Sketch of the side view of the closed CCC fixture, encompassing a wire harness consisting of one wire.

Due to reciprocity $L_{12} = L_{21}$. It is a well-known fact that a current will flow via the path of the least impedance. Writing an impedance as $Z = j\omega L + R$, at low frequencies for which $j\omega L \ll R$, the current will follow the path of least resistance. In the case of Fig. B.2, this corresponds to the red loop. At high frequencies the $j\omega L$ term will be dominant and the current will choose the path which will form the smallest inductance, hence the loop with the smallest area. This current loop is shown in green in Fig. B.2. This path can exist owing to displacement currents. Due to the fact that signal conductor 1 is completely enclosed and that at high frequencies the current loop will follow the green path, there is no magnetic field between conductor 0 and signal conductor 2. Hence, no magnetic flux will be present there ($\Phi_2 = 0$) and we obtain the following relations:

$$\Phi_1 = (L_{11} - L_{12})I_1 \quad (\text{B.3})$$

$$0 = (L_{12} - L_{22})I_1 \quad (\text{B.4})$$

from which we conclude that $L_{12} = L_{22}$. If we now neglect the dielectric material of signal conductor 1, the background medium can be considered as homogeneous free space, such that $\mathbf{CL} = \mathbf{I}\epsilon_0\mu_0$ holds, with ϵ_0 and μ_0 the permittivity and permeability of free space. Hence

$$\mathbf{C} = \begin{bmatrix} L_{22} & -L_{12} \\ -L_{21} & L_{11} \end{bmatrix} \frac{\epsilon_0\mu_0}{L_{11}L_{22} - L_{12}L_{21}} \quad (\text{B.5})$$

Consequently, for the capacitance matrix, we get $C_{11} = -C_{12} = -C_{21}$. This is in correspondence with the values obtained by simulation (see Table B.1).

Table B.1: p.u.l. parameters of CCC fixture

f [MHz]	C_{11} [$\frac{\text{pF}}{\text{m}}$]	C_{12} [$\frac{\text{pF}}{\text{m}}$]	C_{22} [$\frac{\text{pF}}{\text{m}}$]	L_{11} [$\frac{\text{nH}}{\text{m}}$]	L_{12} [$\frac{\text{nH}}{\text{m}}$]	L_{22} [$\frac{\text{nH}}{\text{m}}$]
1	35.6	-35.6	99.3	505.2	175.1	175.1
10	35.6	-35.6	99.3	492.6	174.7	174.7
30	35.6	-35.6	99.3	490.2	174.7	174.7
60	35.6	-35.6	99.3	489.2	174.7	174.7
100	35.6	-35.6	99.3	488.6	174.6	174.6

Table B.2: p.u.l. parameters of ESD test bench

f [MHz]	C_{11} [$\frac{\text{nF}}{\text{m}}$]	C_{12} [$\frac{\text{nF}}{\text{m}}$]	C_{22} [$\frac{\text{nF}}{\text{m}}$]	L_{11} [$\frac{\mu\text{H}}{\text{m}}$]	L_{12} [$\frac{\mu\text{H}}{\text{m}}$]	L_{22} [$\frac{\mu\text{H}}{\text{m}}$]
100	0.1004	-0.0386	0.0451	0.4575	0.4514	0.6987

For illustration we also investigate what the effect is when the CCC clamp is open, just like in the case of the wire harness on top of the FCP in the ESD Rinne test (see Fig. B.3). Here, the FCP is considered as the reference conductor 0, the wire on top of the FCP is signal conductor 1 and the ground plane is signal conductor 2.

Due to the fact that the wire harness lays on top of the FCP, we will have some shielding, albeit less than in the CCC test. This can easily be seen by looking at Table B.2, where the values of L_{11} and L_{12} (C_{12} and C_{22}) deviate from each other because the “enclosure” is not perfectly shielding the wires now. But still, they are of the same order of magnitude.

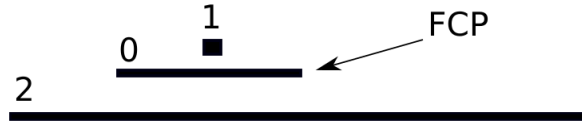


Figure B.3: Cross-section of the ESD fixture with one wire on top of the FCP



Description of the Electrical Fast Transient Pulse According to ISO 7637-3

In this appendix we describe the relationship between the physical parameters rise time t_r , pulse width t_d and maximum amplitude U_s and the mathematical formulation of an electrical fast transient [1]. The mathematical formulation is

$$U(t) = U_0(e^{-\alpha t} - e^{-\beta t}). \quad (\text{C.1})$$

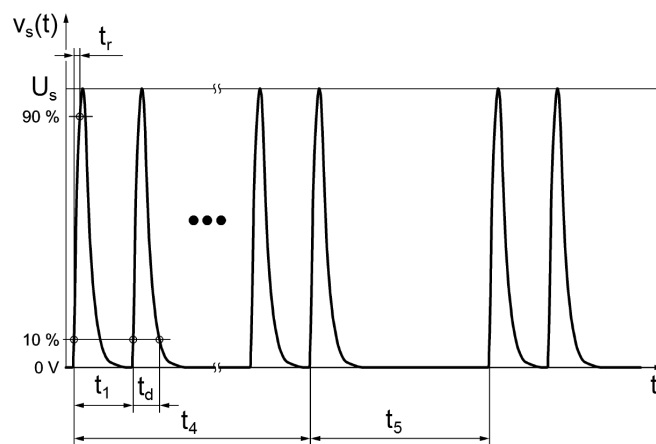


Figure C.1: Fast transient pulse 3b [1].

The physical parameters t_r , t_d and U_S , indicated in Fig. C.1, are easily related to α , β and $U0$ by using the following approximations [2].

$$\alpha_{approx} = \frac{1}{t_r} \frac{X1}{\left(\left(\frac{t_d}{t_r}\right)^{X2} - X3\right)^{X4}}, \quad (C.2)$$

$$\beta_{approx} = \frac{1}{t_r} \left[Y1 - Y2e^{-\frac{t_d}{t_r}Y3} - Y4e^{-\frac{t_d}{t_r}Y5} - Y6e^{-\frac{t_d}{t_r}Y7} \right], \quad (C.3)$$

Where $X1$ up to $X4$ are found in Table C.1 and $Y1$ up to $Y7$ are found in Table C.2.

Table C.1: Parameters for the approximation of α .

Parameter	value
X1	0.842411
X2	1.660852,
X3	8.887335
X4	0.624129

Table C.2: Parameters for the approximation of β .

Parameter	value
Y1	2.167370
Y2	0.360349
Y3	0.013289
Y4	1.358701
Y5	0.137057
Y6	122.802861
Y7	1.314850

$U0$ (C.1) is calculated from the maximum value of the pulse, U_S . By taking the derivative of (C.1) we deduce that the maximum is reached at time t_p given by

$$t_p = \frac{\ln\left(\frac{\beta}{\alpha}\right)}{\beta - \alpha}. \quad (C.4)$$

Substitution of t_p in (C.1) yields

$$U0 = \frac{U_S}{(e^{-\alpha t_p} - e^{-\beta t_p})}. \quad (C.5)$$

Hence, with these simple formulas an electrical fast transient with known physical parameters t_r , t_d and U_S can be cast into the form (C.1).

References

- [1] *ISO 7637-3 Road Vehicles, Electrical Disturbances from Conduction and Coupling, Part 3, Electrical Transient Transmission by Capacitive and Inductive Coupling via Lines Other than Supply Lines*, 2014.
- [2] M. Magdowski and R. Vick, "Estimation of the Mathematical Parameters of Double-Exponential Pulses Using the Nelder-Mead Algorithm", *IEEE Transactions on Electromagnetic Compatibility*, vol. 52, no. 4, pp. 1060–1062, 2010.

